# University of Alberta

## Burning Velocity of Methane/EGR/Air Mixtures with Reformer Gas Addition

by

Panfeng Han

A thesis submitted to the Faculty of Graduate Studies and Research in partial fulfillment of the requirements for the degree of Master of Science

Department of Mechanical Engineering

Edmonton, Alberta
Spring 2005

0-494-08073-6

Library and Archives Canada

Published Heritage Branch

395 Wellington Street
Ottawa ON K1A 0N4
Canada

Bibliothèque et Archives Canada

Direction du Patrimoine de l'édition

395, rue Wellington
Ottawa ON K1A 0N4
Canada

*Your file* *Votre référence*
*ISBN:*
*Our file* *Notre reference*
*ISBN:*

NOTICE:
The author has granted a non-exclusive license allowing Library and Archives Canada to reproduce, publish, archive, preserve, conserve, communicate to the public by telecommunication or on the Internet, loan, distribute and sell theses worldwide, for commercial or non-commercial purposes, in microform, paper, electronic and/or any other formats.

The author retains copyright ownership and moral rights in this thesis. Neither the thesis nor substantial extracts from it may be printed or otherwise reproduced without the author's permission.

AVIS:
L'auteur a accordé une licence non exclusive permettant à la Bibliothèque et Archives Canada de reproduire, publier, archiver, sauvegarder, conserver, transmettre au public par télécommunication ou par l'Internet, prêter, distribuer et vendre des thèses partout dans le monde, à des fins commerciales ou autres, sur support microforme, papier, électronique et/ou autres formats.

L'auteur conserve la propriété du droit d'auteur et des droits moraux qui protège cette thèse. Ni la thèse ni des extraits substantiels de celle-ci ne doivent être imprimés ou autrement reproduits sans son autorisation.

---

In compliance with the Canadian Privacy Act some supporting forms may have been removed from this thesis.

While these forms may be included in the document page count, their removal does not represent any loss of content from the thesis.

Conformément à la loi canadienne sur la protection de la vie privée, quelques formulaires secondaires ont été enlevés de cette thèse.

Bien que ces formulaires aient inclus dans la pagination, il n'y aura aucun contenu manquant.

Canada

# ABSTRACT

The motivation of this study is to explore the feasibility of extending the EGR (exhaust gas recirculation) diluent tolerance for methane/air mixtures with reformer gas (CO and $H_2$). A preheated cylindrical combustion chamber was used to measure the laminar burning velocity of methane/air mixture with variations of EGR diluent, reformer gas, temperature and pressure. The experiments were carried out at the range of initial temperature from 298 K to 498 K and initial pressure from 1 atm to 5 atm. Reformer gas was introduced to raise the burning velocity of methane/EGR mixture to undiluted level. The relationships of the burning velocity as functions of temperature, pressure, and percent of EGR diluent were derived from the experimental data. The theoretical nitric oxide equilibrium concentration and formation rate were calculated. The reformer gas has potential to improve the burning velocity while reducing the nitric oxide emission.

# ACKNOWLEDGMENT

I would like to thank the following people who have helped me during my whole study.

The deepest appreciation is given to my supervisors, Dr. M.D. Checkel and Dr. B.A. Fleck. They gave me the opportunity to come to Canada and study at the University of Alberta. These three years are the most memorable and valuable period in my life. I would like to thank them for their financial support and their academic guidance.

I would like to thank my lab mates, not only for their technical help, but also for the happy time we have spent together. They have showed me a whole new world and helped me explore it. We "share the moment and share the life". They have shared my happiness so my happiness has enlarged several times and they have shared my sadness so my sadness has diminished several times. I would like to list some of their names as the following, Dave Arthur, Matt Atkins, Ryan Chladny, Jason Hawirko, Travis Manchur, Jason Olfert, and Senthil Ponnusamy.

I would like to thank Bernie Faulkner, Terry Nord and other technicians for their great help.

Finally and most importantly, I would like to thank the unconditional support and love from my family. Without them, my achievement would be impossible.

# TABLE OF CONTENTS

CHAPTER

1 INTRODUCTION 1

1.1 BACKGROUND ..... 1

1.2 INTRODUCTION ..... 3

REFERENCES ..... 8

2 LITERATURE REVIEW AND BACKGROUND STUDY 12

2.1 BURNING VELOCITY ..... 12

2.1.1 Burner Method ..... 12

2.1.2 Effects of Mixture Composition ..... 13

2.1.3 Bomb Method ..... 14

2.2 STRETCH RATE ..... 22

2.3 NITRIC OXIDE ..... 25

REFERENCES ..... 29

3 EXPERIMENTAL APPARATUS AND METHODS 34

3.1 EXPERIMENTAL APPARATUS ..... 34

3.1.1 Cylinder Combustion Chamber ..... 34

3.1.2 Data Acquisition System ..... 35

3.2 EXPERIMENTAL MIXTURES ..... 35

3.3 EXPERIMENTAL PROCEDURE ..... 39

3.4 FLAME GROWTH MODEL ..... 40

3.4.1 Lewis and Von Elbe Model ..... 40

3.4.2 Multi-zone Thermodynamic Equilibrium Model ..... 41

3.5 EVALUATION OF BURNING VELOCITY ..... 43

3.5.1 Effects of Diluent, Temperature and Pressure on Stretch Rate .. 43
3.5.2 Evaluation of Burning Velocity ..... 43
3.5.3 Comparison of Previous Published Results ..... 49
REFERENCES ..... 53

4 RESULTS AND DISCUSSION 56
4.1 INTRODUCTION ..... 56
4.2 LAMINAR BURNING VELOCITY ..... 56
4.2.1 Effect of EGR ..... 56
4.2.2 Effect of Temperature ..... 62
4.2.3 Effect of Pressure ..... 68
4.2.4 Effect of Reformer Gas ..... 76
4.3 NITRIC OXIDE EMISSIONS ..... 82
4.3.1 Nitric Oxide Equilibrium Concentration ..... 82
4.3.2 Nitric Oxide Formation Rate ..... 85
REFERENCES ..... 93

5 CONCLUSIONS AND FUTURE WORK 97
5.1 CONCLUSIONS ..... 97
5.2 FUTURE WORK ..... 100
REFERENCES ..... 102

APPENDIX
A COMPARISON OF THERMAL EFFICIENCY AND ENERGY OF STEAM REFORMING AND PARTIAL OXIDATION ..... 103
B EGR SIMULATION ..... 105
C COMPARISON OF MULTI-ZONE MODEL AND STANJAN ..... 109
D ERROR ANALYSIS ..... 117

E BURNING VELOCITY ..... 119
F NITRIC OXIDE FORMATION ..... 124

# LISTS OF TABLES

Table 3-1 Composition of Experimental Mixtures ..... 36

Table 3-2 Burning Velocity of Stoichiometric Methane/Air Mixture at 1 atm and 298 K ..... 50

Table 4-1 Burning velocity of stoichiometric hydrogen/air mixtures ..... 76

Table 4-2 EGR and required reformer gas fractions to retain the undiluted burning velocity ..... 77

Table A-1 Thermal efficiency and thermal energy of steam reforming and partial oxidation ..... 104

Table B-1 Calculation of molar mass of mixtures ..... 106

Table E-1 Burning velocity of methane/EGR mixtures at elevated pressure and 298 K ..... 119

Table E-2 Burning velocity of methane/EGR mixtures at 1 atm ..... 120

Table E-3 Burning velocity of methane/EGR/RG mixtures at 1 atm ..... 121

Table E-4 Burning velocity at 5 atm ..... 122

Table E-5 Inaccurate burning velocity at 5 atm and 473 K ..... 123

Table F-1 Flame temperature (K) of methane/EGR mixtures at 1 atm ..... 124

Table F-2 Peak combustion pressure (kPa) of methane/EGR mixtures at 1 atm ..... 125

Table F-3 NO equilibrium concentration (ppm) of methane/EGR mixtures at 1 atm . 125

Table F-4 NO formation rate (ppm/sec) of methane/EGR mixtures at 1 atm ..... 125

Table F-5 Flame temperature (K) of methane/EGR/RG mixtures at 1 atm ..... 126

Table F-6 Peak combustion pressure (kPa) of methane/EGR/RG mixtures at 1 atm . 126

Table F-7 NO equilibrium concentration (ppm) of methane/EGR/RG mixtures at 1 atm ..... 126

Table F-8 NO formation rate (ppm/sec) of methane/EGR/RG mixtures at 1 atm .... 127

Table F-9 Flame temperature (K) of methane/EGR mixtures at 5 atm ..... 127

Table F-10 Peak combustion pressure (kPa) of methane/EGR mixtures at 5 atm .... 127

Table F-11 NO equilibrium concentration (ppm) of methane/EGR mixtures at 5 atm ..... 128

Table F-12 NO formation rate (ppm/sec) of methane/EGR mixtures at 5 atm ..... 128

# LIST OF FIGURES

Figure 2-1 Burning velocities of methane/air mixtures at 298 K and 1 atm ..... 21
Figure 2-2 Schematic diagram of NO concentration as a function of time after combustion. ..... 28
Figure 3-2 The schematic diagram of the total experimental system ..... 37
Figure 3-2 The schematic diagram of the cylindrical combustion chamber ..... 38
Figure 3-3 Comparison of unburnt gas temperature from Multizone and Lewis and Von Elbe models ..... 46
Figure 3-4 Comparison of flame radius from Multizone and Lewis and Von Elbe models ..... 46
Figure 3-5 Comparison of burnt mass fraction from Multizone and Lewis and Von Elbe models ..... 47
Figure 3-6 Comparison of stretch rates of methane/air and methane/10% EGR mixtures ..... 47
Figure 3-7 Initial temperature effects on stretch rate of methane/air mixture ..... 48
Figure 3-8 Initial pressure effects on stretch rates of methane/air mixtures ..... 48
Figure 3-9 Calculation of burning velocity of stoichiometric methane/air mixture at 298 K and 1 atm ..... 50
Figure 3-10 Comparison of burning velocities of stoichiometric methane/air mixtures at 1 atm and elevated initial temperature ..... 51
Figure 3-11 Comparison of burning velocities of methane/diluent mixtures at 1 atm and 298 K ..... 52
Figure 4-1 Peak combustion pressures and the occurring times of methane/EGR mixtures at 298 K and 1 atm ..... 58
Figure 4-2 Flame radius of methane/EGR mixtures at 298 K and 1 atm ..... 59
Figure 4-3 Burnt mass fraction of methane/EGR mixtures at 298 K and 1 atm ..... 59

Figure 4-4 Effects of initial temperature on burning velocities of methane/EGR mixtures at 1 atm ..... 60
Figure 4-5 Burning velocities of methane/air mixtures with various EGR percent at 1 atm and elevated initial temperature ..... 61
Figure 4-6 Flame radius of methane/air mixture at 1 atm and elevated initial temperature ..... 65
Figure 4-7 Burnt mass fraction of methane/air mixture at 1 atm and elevated initial temperature ..... 65
Figure 4-8 Burning velocity ratios as a function of initial temperature ..... 66
Figure 4-9 Burning velocity ratios as a function of EGR percent ..... 67
Figure 4-10 Flame radius of methane/air mixtures at elevated initial pressure and 298 K ..... 72
Figure 4-11 Burnt mass fraction of methane/air mixtures at elevated initial pressure and 298 K ..... 72
Figure 4-12 Burning velocities of methane/air and methane/15% EGR mixtures at elevated initial pressure and 298 K ..... 73
Figure 4-13 Initial pressure effects on burning velocities of methane/air mixtures at 298 K ..... 74
Figure 4-14 Burning velocity of methane/air mixture at 5 atm and elevated initial temperature ..... 75
Figure 4-17 Reformer gas effects on burning velocity of methane/5% EGR mixture at 1 atm ..... 79
Figure 4-18 Reformer gas effects on burning velocity of methane/10% EGR mixture at 1 atm ..... 80
Figure 4-19 Reformer gas effects on burning velocity of methane/15% EGR mixture at 1 atm ..... 80
Figure 4-20 Reformer gas effects on burning velocity of methane/20% EGR mixture at 1 atm ..... 81

Figure 4-21 Reformer gas effects on burning velocity of methane/40% EGR mixture at 5 atm ..... 81
Figure 4-20 Calculated flame temperature of methane/EGR mixture at 1 atm ... 86
Figure 4-21 Calculated peak combustion pressure of methane/EGR mixture at 1 atm . 87
Figure 4-22 Calculated NO equilibrium concentration of methane/EGR mixture at 1 atm ..... 87
Figure 4-23 Calculated NO equilibrium concentration of methane/air mixture at 298 K and various initial pressure ..... 88
Figure 4-24 Calculated flame temperature and peak combustion pressure of methane/air mixture ..... 88
Figure 4-25 Calculated flame temperature of methane/5% EGR mixture with reformer gas addition ..... 89
Figure 4-26 Calculated NO equilibrium concentration of methane/5% EGR mixture with reformer gas addition ..... 89
Figure 4-27 Calculated NO equilibrium concentration of methane/40% EGR mixture with reformer gas addition ..... 90
Figure 4-28 Calculated NO concentration ratio based on that of methane/air mixture at 5 atm ..... 90
Figure 4-29 Calculated NO formation rate of methane/EGR mixture at 1 atm ..... 91
Figure 4-30 Calculated NO formation rate of methane/air mixture at elevated initial pressure and 298 K ..... 91
Figure 4-31 Calculated NO formation rate of methane/5% EGR mixture with reformer gas addition ..... 92
Figure 4-32 Calculated ratio of NO formation rate based on that of methane/air mixture at 5 atm ..... 92
Figure B-1 Comparison of specific heat capacity of simulated and wet exhaust gases 107
Figure B-2 Comparison of specific heat capacity of simulated and dry exhaust gases 108

# LIST OF NOMENCLATURE

| | |
|---|---|
| atm | Atmospheric pressure |
| A | Surface area |
| D | EGR fraction |
| dt | Time interval |
| K | Stretch rate |
| $K_a$ | Karlovitz number |
| $k_{lf}$ | Rate coefficient, |
| L | Markstein length |
| $M_a$ | Markstein number |
| n | Burnt mass fraction |
| P | Instantaneous pressure |
| $P_e$ | Peak pressure |
| $P_i$ | Initial pressure |
| $P_0$ | Reference pressure, 1 atm |
| $R_{cell}$ | Radius of the combustion bomb |
| $R_i$ | Nominal radius of burned gases in their unburnt state |
| $R_b$ | Flame radius |
| RG | Reformer gas or reformer gas fraction |
| $T_i$ | Initial temperature |
| $T_0$ | Reference temperature, 298 K |
| $T_0$ | Reference unburnt gas temperature, 298 K; |
| $T_u$ | Unburnt gas temperature |
| STANJAN | A computer program to calculate chemical equilibrium properties (see reference 33 in Chapter 2 ) |
| $S_u$ | Laminar burning velocity |
| $S_{u\infty}$ | Unstretched laminar burning velocity |

| | |
|---|---|
| $S_{u0}$ | Laminar burning velocity at 298 K and 1 atm |
| V | Volumetric fraction |
| | |
| $\alpha$ | Temperature exponent |
| $\beta$ | Pressure exponent |
| $\delta_D$ | Characteristic flame thickness |
| $\gamma_u$ | Specific heat ratio of unburnt gases |

# CHAPTER 1

# INTRODUCTION

## 1.1 BACKGROUND

The automotive industry faces continuing pressure from the public and government to reduce vehicle emissions as vehicles are a significant source of urban pollution. Oxides of nitrogen ($NO_x$) produced by vehicles accounted for 49% of U.S. national $NO_x$ in 2002 [1]. As a valuable tool, EGR (exhaust gas recirculation) has been widely used to reduce the $NO_x$ emission by lowering the combustion temperature, a major factor of $NO_x$ formation [2-4]. EGR also reduces $NO_x$ emission by diluting oxygen concentration in combustion mixtures [3], 10~25% EGR is able to substantially reduce $NO_x$ concentrations [4]. Sasaki et al. [5] investigated the effects of EGR on a direct inject gasoline engine and a large volume EGR (above 30%) reduced $NO_x$ to a extremely low level to 1/20 of the base value under stable ignition. EGR also reduces heat transfer rate from the cylinder contents to the surrounding surface and lowers specific fuel consumption [4]. A large volume of EGR dramatically increases the exhaust gas temperature which accelerates warm up of catalysts and enables early activation.

However, EGR has a key drawback, slowing down the burning velocity. Lower burning velocity works against ideal combustion stability and leads to more heat loss, lower combustion efficiency

and more misfires. EGR clearly reduces the flame temperature and consequently causes lower chemical heat release rates and less maximum power of the engine [3, 6]. Selim et al. [7] found that the thermal efficiency and pressure rise rate declined with over 5% EGR in a dual fuel engine. Increasing EGR also harms fuel economy and Hydrocarbon emission due to occurrence of misfire [5]. These combustion problems restrict the tolerance of EGR and potential benefits of high volumes of EGR.

To overcome those problems, hydrogen with high burning velocity and wide flammability limits is considered as an ideal fuel to raise the burning velocity and to extend the EGR tolerance. In a natural gas engine, 20% hydrogen addition broadened the EGR tolerance from 8% to 25% while retaining the stable combustion and low emissions [8]. Swain et al. [9] indicated that a volumetric mixture of 20% hydrogen and 80% methane reduced both flame initiation and flame propagation problems. In addition, even a small amount of hydrogen significantly decreases hydrocarbon emissions and cycle-by-cycle variability [10]. Combining EGR and a three-way catalytic converter, a hydrogen-fuelled engine was able to reduce $NO_x$ emissions to as low as less than 1 ppm [11].

However, the demands of production, distribution and storage of hydrogen on a vehicle are challenging. Therefore, a promising technology on-board fuel reforming that converts hydrocarbon fuel to reformer gas, i.e., hydrogen and carbon monoxide, emerged to suit the demands. The effects of the reformer gas on a gasoline engine were tested by Tully et al. [12]. The peak net

indicated fuel conversion efficiency was raised 12% and $NO_x$ emission dropped 94% (165 ppm vs. 2800 ppm) at the peak efficiency point compared to data obtained from an engine operating stoichiometrically on gasoline only. In summary, reformer gas (CO and $H_2$) has potential to practically broaden the tolerance of EGR and reduce the $NO_x$ emission while retaining combustion stability.

## 1.2 INTRODUCTION

The motivation of this study was to experimentally explore the temperature and pressure effects of reformer gas addition on methane/EGR mixtures by measuring the laminar burning velocity. The experiments were carried out to investigate the amount of reformer gas required to raise the burning velocities of methane/EGR mixtures to the undiluted level for elevated initial temperature and pressure conditions. The laminar burning velocity is a fundamental parameter to understand the combustion process and flame propagation and a necessary input to model the turbulent combustion and pollutant formation. Precise values of laminar burning velocities are useful for practical applications on internal combustion engines, which operate at pressure range from 5 atm to 60 atm and unburnt gas temperature range from 500 K to 1100 K [13]. The effects of reformer gas on engine performance and characteristics at near diluent limit and lean mixture have been studied in past [12, 14]. The burning velocities and flammability limits of n-butane and iso-butane with reformer gas addition were analyzed at 300 K [15]. However, all of these studies [12, 14]

[15] were concentrated on gasoline or partial oxidation reactions, and the data of burning velocities of methane/EGR/reformer gas mixtures are scarce, especially at elevated temperature and pressure to simulate the real engine operation. The burning velocity at elevated temperature and pressure draws a better picture to understand the effects of diluents and reformer gas. Furthermore, an interesting question remains whether the methane/EGR/reformer gas mixture loses the potential of low NO emission as the mixture maintains the undiluted burning velocity.

Methane, a major component of natural gas, was used in this study for experimental practicality and potential application in natural gas engines. The high octane rating, low level of non-HC impurities and low carbon/hydrogen ratio of methane provide the natural gas engine fundamental emission advantages [7]. However, the natural gas engine has relatively undesirable high nitrogen oxide emission [8] despite thorough development [16, 17]. Thus, EGR is essential for a methane-fuelled engine. However, the tolerance of EGR was restricted by the methane characteristics in order to avoid unacceptable poor combustion problems. A natural gas engine operating at 2 atmospherical indicated mean effective pressure (I.M.E.P.) and 2000 rpm, could only tolerate maximum 8 percent EGR, and this amount of EGR only reduced at most half nitric oxide emission [8]. Reformer gas is, therefore, necessary to broaden the EGR tolerance and improve the combustion stability.

This study focused on the stoichiometric mixtures used with three-way catalyst systems. Lean mixture causes lower flame temperature and consequently reduces $NO_x$ emission. Meanwhile,

engines operating with lean mixture have an efficiency benefit [12]. However, low flame temperature leads to low chemical heat release rates and thus the loss of maximum power. Extra lean mixture also has problems of flame blowout and loss of efficiency in spite of extremely low $NO_x$ emission. Stoichiometric mixture is comparatively worse than lean or extra lean mixture in $NO_x$ emission, but 3-way catalytic converters require the exhaust gas of stoichiometric combustion for the best effectiveness and efficiency. When considering both $NO_x$ emission and torque output, stoichiometric mixtures with EGR produced nearly 30% more torque than lean-burn mixtures and low $NO_x$ emission (<10 ppm) in a hydrogen-fuelled engine [11]. Therefore, this study deals only with stoichiometric mixtures.

Houseman and Cerini demonstrated the technical feasibility of onboard steam reforming of gasoline or methanol to generate hydrogen for automobiles [18]. Steam reforming of methane has been developed and a catalyst, such as Ni-YSZ, was strongly recommended to reduce the reaction temperature [19, 20]. An improved novel membrane reformer [21] was able to generate a large volume of hydrogen by steam reforming of methane at relative low temperature. Jamal et al. [22] concluded that steam reforming generated the maximum quantity of hydrogen and no nitrogen was involved. On the other hand, partial oxidation produced less hydrogen than steam reforming in spite of an exothermic reaction. For example, the products of partial oxidation of gasoline were only composed of a quarter hydrogen, a quarter carbon monoxide and half nitrogen [12] [14]. Additional CO was slightly effective in improving combustion efficiency, emissions and stability [12]. Furthermore, steam reforming has higher thermal efficiency and potential energy output than

partial oxidation (the calculation is given in Appendix A). Steam reforming also has the economic benefits of a comparatively low cost and relatively high efficiency of hydrogen production [23]. Therefore, hydrogen-rich products of ideal steam reforming were used in present experiments. Reformer gas was simulated by a mixture of $H_2$ and CO with volumetric ratio of 3:1, which corresponded to the ideal products of steam reforming of methane:

$$CH_4 + H_2O = CO + 3H_2 \qquad (1\text{-}1)$$

Due to inability to introduce the real exhaust gas to the combustion chamber, a mixture of 18.5% $CO_2$ and 81.5% $N_2$ was chosen to simulate the EGR diluent by the same specific heat (the calculation of specific heat is give in Appendix B).

Chapter 2 reviews the past studies on the laminar burning velocity and theoretical background on stretch rate and $NO_x$ mechanisms. Burning velocities of methane/air mixture investigated with various methods by a number of authors are analyzed. The effects of temperature and pressure on burning velocity are discussed as well. Stretch rate, a considerable influence on burning velocity, is analyzed. In order to further explore the influence of EGR and reformer gas on the emission of nitric oxides, the last section of this chapter describes $NO_x$ mechanisms and equations for predicting NO equilibrium concentration and formation rate of NO.

Chapter 3 describes the experimental apparatus and mixtures. The experimental procedure is also presented in detail. The maximum initial experimental temperature and pressure were up to 473 K (200 °C) and 5 atmospheres, respectively. The maximum volumetric percent of EGR was 40%. A theoretical model, the Multi-zone Thermodynamic Equilibrium Model (MTEM) is described. The more basic Lewis and Von Elbe Model is briefly introduced to verify the Multizone Thermodynamic Equilibrium Model. The effects of dilution, temperature and pressure on stretch rate are evaluated in order to investigate its impact on burning velocity. Finally, evaluation of burning velocity from the experimental pressure traces is analyzed and two sets of burning velocities are compared with published results to verify the reliability of the experimental system and analysis method.

Chapter 4 presents experimental and calculated results. Burning velocities at elevated temperature and pressure are analyzed. The correlations of burning velocity at various temperature, pressure and dilution are derived. Finally, data of NO equilibrium concentration and formation rate of NO at all experimental initial conditions are illustrated.

Final conclusions are presented in Chapter 5. The major conclusions are summarized and future work and improvements are suggested.

## REFERENCES:


1. *Air qaulity data report - 2002*. 2003, Colorado Department of Pubilc Health and Environment: Denver.

2. Ladommatos, N., S. Abdelhalim, and H. Zhao, *Control of oxides of nitrogen from diesel engines using diluents while minimising the impact on particulate pollutants.* Applied Thermal Engineering, 1998. **18**(11): p. 963-980.

3. Zheng, M., G.T. Reader, and J.G. Hawley, *Diesel engine exhaust gas recirculation--a review on advanced and novel concepts.* Energy Conversion and Management, 2004. **45**(6): p. 883-900.

4. Abd-Alla, G.H., *Using exhaust gas recirculation in internal combustion engines: a review.* Energy Conversion and Management, 2002. **43**(8): p. 1027-1042.

5. Sasaki, S., D. Sawada, T. Ueda, and H. Sami, *Effects of EGR on direct injection gasoline engine.* Society of Automotive Engineers of Japan, 1998. **19**(3): p. 223-228.

6. Satoh, K., L. Zhang, H. Hatanaka, T. Takatsuki, and K. Yokota, *Relationship between NOx and SM emissions from DI diesel engine with EGR.* Society of Automotive Engineers of Japan, 1997. **18**(4): p. 369-375.

7. Selim, M.Y.E., *Effect of exhaust gas recirculation on some combustion characteristics of dual fuel engine.* Energy Conversion and Management, 2003. **44**(5): p. 709-723.

8. Allenby, S., W.C. Chang, A. Megaritis, and M.L. Wyszynski, *Hydrogen enrichment: a way to maintain combustion stability in a natural gas fuelled engine with exhaust gas recirculation, the potential of fuel reforming.* Proceedings of the Institution of Mechanical Engineers Part D-Journal of Automobile Engineering, 2001. **215**(D3): p. 405-418.

9. Swain, M.R., M.J. Yusuf, Z. Dülger, and M.N. Swain, *The effects of hydrogen addition on natural gas engine operation.* Society of Automotive Engineers, SAE paper, 1993. **932775**.

10. Apostolescu, N. and R. Chiriac, *A study of combustion of hydrogen-enriched gasoline in a spark ignition engine.* Society of Automotive Engineers, SAE paper, 1996. **960603**.

11. Heffel, J.W., *NOx emission and performance data for a hydrogen fueled internal combustion engine at 1500 rpm using exhaust gas recirculation.* International Journal of Hydrogen Energy, 2003. **28**(8): p. 901-908.

12. Tully, E.J. and J.B. Heywood, *Lean-burn characteristics of a gasoline engine enriched with hydrogen from a plasmatron fuel reformer.* Society of Automotive Engineers, SAE paper, 2003. **2003-01-0630**.

13. James, E.H., *Laminar burning velocities of iso-octane-air mixtures ~ a literature review.* Society of Automotive Engineers, SAE paper, 1987. **870170**.

14. Quader, A.A., J.E. Kirwan, and M.J. Grieve, *Engine performance and emissions near the dilute limit with hydrogen enrichment using an on-board reforming strategy.* Society of Automotive Engineers, SAE paper, 2003. **2003-01-1356**.

15. Sung, C.J., Y. Huang, and J.A. Eng, *Effects of reformer gas addition on the laminar flame speeds and flammability limits of n-butane and iso-butane flames.* Combustion and Flame, 2001. **126**(3): p. 1699-1713.

16. Weaver, C.S., *Natural gas vehicles~a review of the state of the art.* Society of Automotive Engineers, SAE paper, 1989. **892133**.

17. Kato, K., K. Igarashi, M. Masuda, K. Otsubo, A. Yasuda, K. Takeda, and T. Sato, *Development of engine for natural gas vehicle.* Society of Automotive Engineers, SAE paper, 1999. **1999-01-0574**.

18. Houseman, J. and D.J.Cerini. *Onboard hydrogen genration for automobiles.* in *Intersociety Energy Conversion Engineering Conference.* 1976.

19. Ahmed, K. and K. Foger, *Kinetics of internal steam reforming of methane on Ni/YSZ-based anodes for solid oxide fuel cells.* Catalysis Today, 2000. **63**(2-4): p. 479-487.

20. Takeguchi, T., Y. Kani, T. Yano, R. Kikuchi, K. Eguchi, K. Tsujimoto, Y. Uchida, A. Ueno, K. Omoshiki, and M. Aizawa, *Study on steam reforming of CH4 and C2 hydrocarbons and carbon deposition on Ni-YSZ cermets.* Journal of Power Sources, 2002. **112**(2): p. 588-595.

21. Chen, Z., P. Prasad, Y. Yan, and S. Elnashaie, *Simulation for steam reforming of natural gas with oxygen input in a novel membrane reformer.* Fuel Processing Technology, 2003. **83**(1-3): p. 235-252.

22. Jamal, Y. and M.L. Wyszynski, *On-board generation of hydrogen-rich gaseous fuels - a review.* International Journal of Hydrogen Energy, 1994. **19**(7): p. 557-572.

23. Kukkonen, C.A., *Hydrogen as an alternative automotive fuel.* Society of Automotive Engineers, SAE paper, 1981. **810349**.

# CHAPTER 2

# LITERATURE REVIEW AND BACKGROUND STUDY

This chapter describes prior research on burning velocity, flame stretch rate and nitrogen oxide ($NO_x$) emissions.

## 2.1 BURNING VELOCITY

A number of methods have been developed to determine laminar burning velocity, defined as the velocity of the flame wave with respect to unburnt gas [1]. Some of them, such as tube method, bomb method, and burner method, were summarized comprehensively by Andrews and Rallis [2-4].

### 2.1.1 Burner Method

The burner method measures the adiabatic burning velocity from a flat flame operating at atmospheric pressure. The typical idea is to measure burning velocity and heat loss to the burner as a function of inlet velocity. The adiabatic burning velocity is obtained after extrapolating the results to zero heat loss. Since extrapolation generally causes uncertainty, the heat flux method avoiding the extrapolation was introduced to calculate more accurate burning velocity.

Dyakov et al. [5] used the heat flux method to evaluate the stretch-free flat flame propagation by a detailed C/H/N/O reaction mechanism. Errors from experimental performance, including variation in the mass flow controller, gas velocities and temperature measurement, were carefully analyzed. Results were in good agreement with others obtained from a stretch-free or stretch correction flame. The burning velocity of stoichiometric methane/air mixture was 36 cm/s.

Bosschaart and de Goey [6] improved the heat flux method on the burner head and temperature measurement. The temperature and heat loss were measured and evaluated. The heat flux method was also utilized to measure the burning velocities of several hydrocarbon fuels [7]. A parabolic parameter relative to the temperature, $\alpha$, was calculated and the adiabatic burning velocity was obtained by interpolating the burning velocity to $\alpha = 0$.

### 2.1.2 Effects of Mixture Composition

Additional gas, diluent or fuel, influences the burning velocity. Diluent, most often referred to as $CO_2$, $N_2$ or steam, reduces the burning velocity. In contrast, another fuel addition increases burning velocity. Dlugogorski et al. [8] investigated the effect of steam on laminar burning velocity of methane/air mixture by a $C_1$-$C_2$ mechanism and concluded that a higher steam concentration resulted in lower burning velocity. Oostendrop and Levinsky [9] also studied the effects of various additions, from ethane, propane, nitrogen to carbon dioxide, on the burning velocities of methane/air mixtures by a burner method. As expected, ethane and propane increased the burning

velocity, while the amount of diluent, nitrogen or carbon dioxide, was inversely proportional to burning velocity. Moreover, carbon dioxide had more reductive impact on burning velocity than nitrogen, and the authors attributed the reason to the differences in transport properties between $CO_2$ and $N_2$.

### 2.1.3 Bomb Method

The bomb method is recommended to measure burning velocity at a wide range of temperatures, pressures and equivalence ratios. Lewis and Von Elbe [1] explained the laminar flame propagation and determination of burning velocity in a constant-volume bomb with a central spark. The flame begins to propagate from the spark point spherically after the ignition. Because of the restriction of the vessel wall, the pressure increases and so does the unburnt gas temperature according to the adiabatic compression law. As a result, the burning velocity rises.

Assumptions for spherical flame propagation were analyzed thoroughly by Rallis et al. [4] and Hill et al. [10], respectively. They are summarized as the following:

1. The flame front is thin, smooth and spherical, so that effects of flame curvature and instability are negligible;
2. The pressure is spatially uniform;
3. The unburnt and burnt gas mixtures behave as ideal gases;
4. Chemical equilibrium is achieved immediately behind the flame front, i.e., the

temperature of burnt gas mixture is spatially uniform and theoretical equilibrium adiabatic value at this point;

5. Unburnt gas mixture is compressed isentropically;
6. No dissociation or pre-flame reactions occur in the unburnt gas mixture and all dissociation products in the burnt gas region are in equilibrium;
7. Buoyancy effects are neglectable.

A number of studies on laminar burning velocity of methane/air mixture by the bomb method are summarized in the following. The summary provides a thorough review of the constant-volume bomb method on burning velocity study to compare with this study.

Sharma et al. [11] studied the pressure and temperature dependence on burning velocity of methane/air mixture by a bomb method. A high speed camera and a pressure transducer were both used to record the flame propagation. A correlation equation was derived for the experimental pressure from 0.5 to 4 atm and capable to extrapolate to as high as 20 atm. The authors also simply compared the equations of previous researches for burning velocity calculations and analyzed the difference. Burning velocity was determined from the flame radius-time record. A series of empirical equations of temperature, pressure and equivalence ratio dependence on burning velocities were derived. The laminar burning velocity of stoichiometric methane/air mixture at 1 atm and 298 K was determined as 33 cm/s.

Iijima and Takeno [12] briefly compared laminar burning velocities calculated by the spherical bomb, burner, double kernel and numerical calculation. The burning velocities of methane/air mixtures were measured in a 16.0 cm diameter spherical combustion chamber at an initial pressure from 0.5 to 30 atm and room temperature. The burning velocity was calculated from the pressure trace on the basis of the quasi-steady flame surface model. No stretch effect was considered here. The method reliability was discussed in detail and the conclusion was reached that the chemical equilibrium, heat loss, the flame thickness, the small scale flame wrinkling and the quenching in the vicinity of the electrodes were not important. This conclusion was consistent with what was drawn from Metghalchi et al. [13]. Finally, the effect of buoyancy attracted the authors' concern. In order to minimize the effect of buoyancy, the equivalence ratio was restricted from 0.8 to 1.3 so that the asymmetry of the propagating flame was remained in the tolerant range. The laminar burning velocity of stoichiometric methane/air mixture at 1 atm was 35 cm/s.

Tseng et al. [14] determined laminar burning velocities in a quasi-spherical test chamber by a shadowgraph motion picture photography. The measurements were limited to a flame radius of less than 60 mm, so that the effects of flame thickness, curvature and unsteadiness were minor and neglectable. The authors also discussed the effects of cold and hot flame boundaries on the burning velocity and concluded that the uncertainties were small and distinction was unnecessary. Finally, a hot flame boundary was used. The stretch rate, curvature and unsteadiness, and relating Markstein length and Karlovitz number were discussed thoroughly for outwardly propagating spherical flame.

However, Taylor and Smith [15] corrected Tseng et al.'s [14] results. Taylor et al. proved that the density ratios calculated by Tseng et al. had large errors and that the raw data used by Tseng et al. were wrong as well. Taylor et al. calculated the corrected data and compared them with the [16] previous data. These two sets of data showed agreement.

Later, Aung et al. [17] responded to Taylor and Smith's [15] comments and improved their previous results. Aung et al. listed the test conditions, such as density ratio, characteristic flame thickness, flame stretch, Karlovitz number and Markstein number. The revised stretched and unstretched burning velocities were given as well. The results agreed with Taylor's [16]. Aung et al. attributed the slight discrepancy in the burning velocities to the different analysis methods in spite of the same experimental data. Taylor simply applied the density ratio correction, while Aung et al. used a more complicated way to re-analyze the results. The revised burning velocity of stoichiometric mixture was 34 cm/s.

Clark et al. [18] measured the laminar burning velocity of methane/diluent/air mixtures in a spherical bomb with 15.0 cm diameter in a micro-gravity environment. Burning velocity were calculated by Lewis and Von Elbe's equations assuming a smooth spherical flame front. The authors indicated that the micro-gravity environment overcame the buoyancy effects that raised the centre of flame kernel and deviated spherical flame front. Meanwhile, micro-gravity environment retarded the time of the flame front to touch the chamber wall. The authors did not correct the results for stretch rate when arguing its minor effects. The burning velocity was evaluated by

normalized flame radius from 0.49 to 0.93 due to small stretch rate. The flame stretch was found to be sufficiently small after normalized flame radius of 0.66. Since methane/diluent mixtures had slow flame propagation, Clarke et al. further pointed out that the stretch rate was reduced for slow flame propagation and therefore had less impact on burning velocity. The correlation equations were extended to a large range of temperature and pressure later [19]. The burning velocity of a stoichiometric methane/air mixture at 298 K and 1 atm was 37 cm/s. The cellularity effect was discussed cautiously, since it changed the assumption of smooth spherical flame front. Fortunately, it seemed that the combustion flame of methane-air mixture had no evident cellularity, even though Bradley [20] showed that flame loss at the spark electrodes might develop into cellularity.

Elia et al. [21] constructed a spherical combustion chamber with a pressure transducer, ionization probes and a thermocouple to measure burning velocity of methane/diluent mixtures in the pressure range from 0.75 to 70 atm. The computational model determined the burnt mass fraction from thermodynamic properties and pressure trace. The model also considered the effects of temperature gradients in the burned gas and flame stretch. Finally, the unstretched burning velocity was corrected from the measured stretched burning velocity. The burning velocity of stoichiometric methane/air mixture was determined as 37.2 cm/s. The burning velocities calculated by authors were slightly higher than the results of Clarke et al. [18] and Iijima and Takeno [12] even though similar models were used. Elia et al believed that Clark and Iijima ignored the temperature gradients and stretch effect.

Hassan et al. [22] studied the outwardly spherically propagating premixed methane/air flame at a pressure range from 0.5 to 4 atm. Experimental measurements were strictly limited so that effects of flame curvature and transient were neglectable. Experiments were recorded by means of a motion picture shadowgraph. The test conditions, including the various equivalence ratios, the initial pressures and density ratios, burning velocities and Markstein numbers, were given as well. Authors eventually drew the conclusion that there was a substantial stretch effect on laminar burning velocity. The unstretched burning velocity of stoichiometric methane/air mixture at 1 atm was found to be 35 cm/s.

Gu et al. [23] used a 38.0 cm diameter spherical combustion chamber to measure the unstretched burning velocity at initial temperature between 300 K to 400 K, and at pressure between 1 atm and 10 atm. The burning velocity was measured by a photographic observation of the flame. Two computational models were utilized, one considering one-dimensional flame propagation with fully detailed kinetics for unstretched burning velocity, and the other considering spherically expanding stretched flame with a reduced scheme for stretched burning velocity. Authors indicated that photographic measurement observed the flame distortion and cellularity and those two effects increased the burning velocity. After being correlated, the unstretched burning velocity of stoichiometric methane/air mixture at 298 K and 1 atm was 35.8 cm/s.

Bradley et al. [24] computed the burning velocity of spherical flame propagation using the reduced kinetic $C_1$ scheme of Mauss and Peters. The relationship between the Markstein lengths and

burning velocity were discussed in detail. As extrapolated to a zero stretch rate, the burning velocity of a stoichiometric methane/air mixture was 37.8 cm/s.

In summary, all methods generally predict a peak burning velocity on the slightly rich stoichiometric. The bomb method has a average stoichiometric burning velocity 35.9 cm/s with a standard deviation 1.39 cm/s. The burner method has slightly higher values than bomb method. Laminar burning velocities of methane/air mixtures measured in a constant-volume bomb at 1 atm and 298±2 K from several previous reports are plotted in Figure 2-1. It is clear that all results agree well despite of the different measurement and calculation methods. This study also used a constant volume bomb to measure laminar burning velocity due to the measurement advantages on a wide range of temperature, pressure and equivalence ratio. The above references on the bomb method provide a complete comparison with this study. The results from this study and above studies will be compared in Chapter 3.

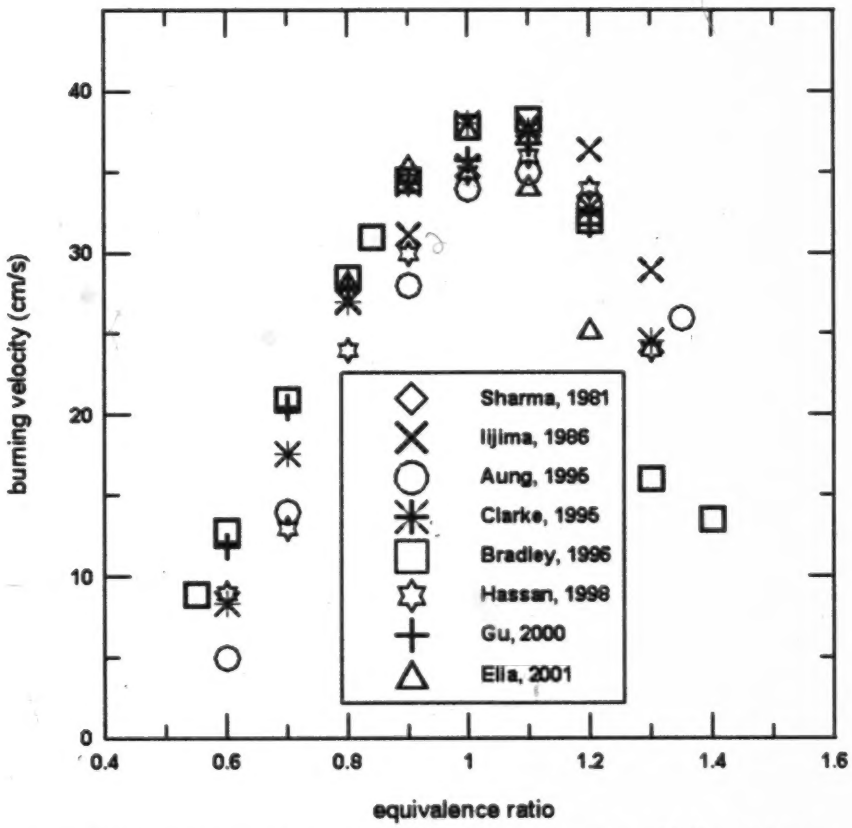


**Figure 2-1** Burning velocities of methane/air mixtures at 298 K and 1 atm

## 2.2 STRETCH RATE

The stretch rate has drawn considerable attention on the laminar burning velocity [14, 22-26]. The Markstein number and Karlovitz number are critical characteristics to represent the stretch rate. The unstretched laminar burning velocity can be derived from the stretched laminar burning velocity and stretch rate. For example, 45±2 cm/s was a general accepted burning velocity of stoichiometric methane/air mixture at 1 atm and 298 K in the past [2, 3]. However, Bosschaart et al. [6] demonstrated that this higher burning velocity was caused by ignoring stretch rate. As stretch rate was considered, recent experiments explored a lower burning velocity. A lower burning velocity was also obtained from the old experimental data as new methods considering the stretch rate were employed. In order to eliminate the stretch effect, some methods such as, the counterflow method [27], were developed to unambiguously determine the unstretched laminar burning velocity.

The stretch rate K on a flame surface is the time rate of change of the infinitesimal surface element of area, A, normalized by that area [24]:

$$K=\frac{1}{A}\frac{dA}{dt} \qquad (2\text{-}1)$$

Considering the geometry of a spherical flame front, the following expression is obtained from the above Equation 2-1:

$$K=\frac{2}{r_b}\frac{dr_b}{dt} \qquad (2\text{-}2)$$

where $r_b$ is the flame radius.

The positive stretch rate of outward propagating flame normally has a negative effect on laminar burning velocity. The stretch effects on burning velocity are correlated by the following equation [28]:

$$S_u = S_{u\infty} - LK \tag{2-3}$$

where,

$S_u$ is stretched laminar burning velocity;

$S_{u\infty}$ is unstretched laminar burning velocity;

L is Markstein length, a measure of the response of the flame to stretch;

K is the stretch rate.

The Markstein length is represented by a dimensionless Markstein number, $M_a$,

$$M_a = \frac{L}{\delta_D} \tag{2-4}$$

where,

$M_a$ is Markstein number;

$\delta_D$ is the characteristic flame thickness.

In general, positive Markstein number represents a stable flame while negative Markstein number represents a unstable flame [22]. Another dimensionless parameter, Karlovitz number, $K_a$, is also defined to describe the flame stretch.

$$K_a = \frac{K\delta_D}{S_u} \tag{2-5}$$

Therefore, the dimensionless relationship between burning velocity and stretch rate is shown as the

following:

$$\frac{S_u}{S_{u\infty}} = 1 - M_a K_a \qquad (2\text{-}6)$$

The Equations 2-3 to 2-6 are generally used to represent the relationship of burning velocities and stretch rate. A number of studies were carried out on stretch rate and Markstein number. For example, Mishra analyzed the stretch rate by a numerical model with detailed chemistry [29] and Davis et al. evaluated the stretch rate by a counterflow flame [30]. However, determination of the Marsktein number and stretch rate is still debated topics [30].

However, Elia et al. [21] pointed out that for a spherical flame the correction of burning velocity from flame stretch is less than 0.2 cm/s as the flame is close to the vessel wall (a spherical vessel with a diameter of 15.24 cm) and 1 cm/s at the smaller flame radius. A 10% increase of initial pressure promoted the flame radius by 50% and consequently reduced the stretch rate. They also illustrated that the stretch rate dropped significantly after normalized flame radius 0.5. Similarly, Clarke et al. [18] used a spherical combustion chamber with a diameter of 150 mm in a micro-gravity environment. Authors calculated burning velocity in a normalized flame radius from 0.49 to 0.93 corresponding to small stretch rate, and explained that the flame stretch was sufficiently small after a normalized flame radius of 0.66. Because of slow flame propagation of methane/diluent mixtures, Clarke et al. further demonstrated that slow flame propagation decreased the stretch rate and resulted in less effect on burning velocity of methane/diluent mixtures. Therefore, the stretch rate does not affect the results of this study as only larger flame radius was

used to analyze the burning velocity. Moreover, the stretch rate declines with additional dilution. In summary, the burning velocity does not corrected with stretch rate in this study.

## 2.3 NITRIC OXIDE

Oxides of nitrogen ($NO_x$) is one of the major pollutants from internal combustion engines and has strong adverse environmental effects. It forms nitric acid when it reacts with water vapor and forms ground level ozone when reacting with atmospheric hydrocarbon in the presence of solar radiation. Nitric oxide (NO) and nitrogen dioxide ($NO_2$) are two major components in oxides of nitrogen. Nitric oxide is the dominant component, contributing to over 90% in total oxides of nitrogen. For spark ignition engines, which burn near-stoichiometric mixture, the difference between NO and $NO_x$ measurement was negligible [31]. Therefore, only nitric oxide was studied in this research.

The primary source of NO is the oxidation of atmospheric nitrogen, while nitrogen contained in the fuel is another source. Because no nitrogen is presented in the currently used experimental fuels, nitric oxide is only formed by nitrogen from the air during combustion. There are three major chemical mechanisms, i.e., the Zeldovich or thermal mechanism, the Fenimore mechanism and $N_2O$-intermediate mechanism [32].

As generally accepted, the extended Zeldovich mechanism is the primary mechanism that governs NO formation in combustion of near stoichiometric fuel-air mixture [31]. The Zeldovich mechanism consists of two reactions:

$$O + N_2 \Leftrightarrow NO + N \tag{2-7}$$

$$N + O_2 \Leftrightarrow NO + O \tag{2-8}$$

It is called the extended Zeldovich Mechanism when one more reaction is added:

$$N + OH \Leftrightarrow NO + H \tag{2-9}$$

In extended Zeldovich mechanism, NO is formed in the burned gas region of high-temperature behind the flame front. The reaction of NO formation is strongly temperature dependent.

The derivation of formation rate of NO is simplified after assuming that NO formation begins with $N_2$,$O_2$,O and OH concentrations are at their post-combustion equilibrium values and N atoms are in steady state. Another assumption is that fuel combustion process and NO formation process are uncoupled [32] since the combustion process is much faster than NO formation. When no production begins, the reverse reactions are negligible as the NO concentrations are much less than their equilibrium values. Finally, the initial formation rate of NO is expressed as:

$$\frac{d[NO]}{dt} = 2k_{1f}[O][N_2] \tag{2-10}$$

where,

[] is species concentration in combustion products before any nitric oxide has been formed, kmol/m$^3$;

$k_{1f}$ is the rate coefficient, $1.8\times10^{11}\exp[-38370/T]$, $m^3$/kmol-s;

T is flame temperature, K;

As the unit of formation rate of NO in Equation 2-10 is changed from kmol/$m^3$-s to ppm/s, the Equation 2-10 becomes [32]:

$$\frac{d[NO]}{dt}=2k_{1f}\chi_O\chi_{N_2}\frac{P_e}{R_uT} \qquad (2\text{-}11)$$

where,

$P_e$ is peak combustion pressure, kPa;

T is flame temperature, K;

$R_u$ is universal gas constant, 8.31434 kPa-$m^3$/kmol-K;

$\chi_i$ is equilibrium post combustion molar fraction of component i in total combustion products.

Figure 2-2 demonstrates the rise of NO concentration as a function of time. NO concentration rises from effectively zero at the beginning and finally reaches the equilibrium post combustion value. This NO equilibrium concentration is strongly affected by flame temperature and atomic oxygen concentration in mixtures. The formation rate of NO is not only temperature dependent, but also combustion pressure and NO equilibrium concentration dependent.

In this study, the NO equilibrium concentration and formation rate of NO were calculated by the

above equations with the combustion properties from Stanjan [33] running as the constant-volume combustion at experimental initial temperature, pressure and components. The two parameters, NO equilibrium concentration and formation rate are also marked in Figure 2-2.

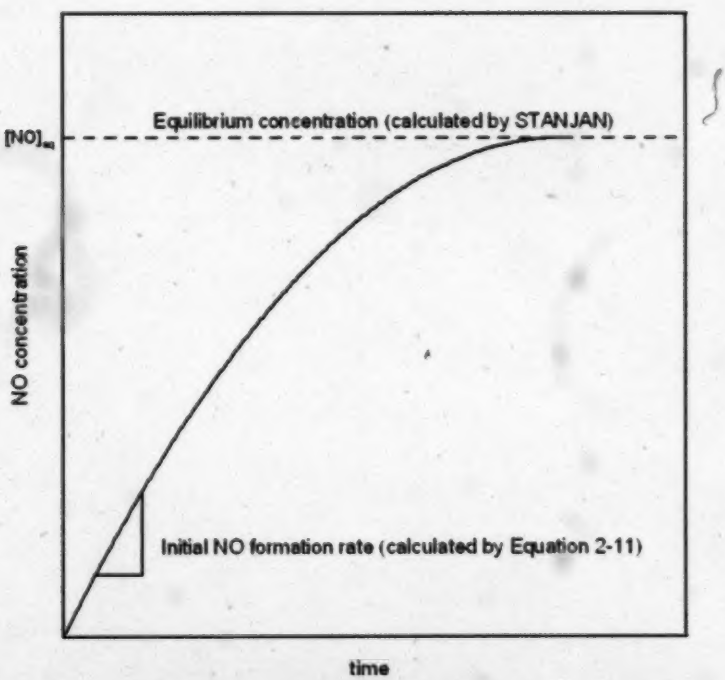


**Figure 2-2** Schematic diagram of NO concentration as a function of time after combustion. Diagram shows the two parameters calculated in Section 2-3

## REFERENCES:


1. Lewis, B. and G. Von Elbe, *Combustion, Flames, and Explosions of Gases*. 3rd ed. 1987, Orlando: Academic Press.

2. Andrews, G.E. and D. Bradley, *The burning velocity of methane-air mixtures.* Combustion and Flame, 1972. **19**: p. 275-288.

3. Andrews, G.E. and D. Bradley, *Determination of laminar burning velocity: a critical review.* Combustion and Flame, 1972. **18**: p. 133-153.

4. Rallis, C.J. and A.M. Garforth, *The determination of laminar burning velocity.* Progress in Energy and Combustion Science, 1980. **6**(4): p. 303-329.

5. Dyakov, I.V., A.A. Konnov, J. De Ruyck, K.J. Bosschaart, E.C.M. Brock, and L.P.H. De Goey, *Measurement of adiabatic burning velocity in methane-oxygen- nitrogen mixtures.* Combustion Science and Technology, 2001. **172**: p. 81-96.

6. Bosschaart, K.J. and L.P.H. de Goey, *Detailed analysis of the heat flux method for measuring burning velocities.* Combustion and Flame, 2003. **132**(1-2): p. 170-180.

7. Bosschaart, K.J., L.P.H. de Goey, and in collaboration with J.M. Burgers Center for Fluid Mechanics, *The laminar burning velocity of flames propagating in mixtures of hydrocarbons and air measured with the heat flux method.* Combustion and Flame, 2004. **136**(3): p. 261-269.

8. Dlugogorski, B.Z., R.K. Hichens, E.M. Kennedy, and J.W. Bozzelli, *Propagation of laminar flames in wet premixed natural gas-air mixtures.* Process Safety and

Environmental Protection, 1998. **76**(B2): p. 81-89.

9. Oostendrop, D.L.v. and H.B. Levinsky, *The effects of fuel and non-fuel gases on the laminar burning velocity of methane-air flames.* Journal of the Institute of Energy, 1990. **63**: p. 160-166.

10. Hill, P.G. and J. Hung, *Laminar burning velocities of stoichiometric mixtures of methane with propane and ethane additives.* Combustion Science and Technology, 1988. **60**(1-3): p. 7-30.

11. Sharma, S.P., D.D. Agrawal, and C.P. Gupta. *The pressure and temperature dependence of burning velocity in a spherical combustion bomb.* in *18th Symposium (International) on Combustion, the Combustion Institute.* 1981.

12. Iijima, T. and T. Takeno, *Effects of temperature and pressure on burning velocity.* Combustion and Flame, 1986. **65**(1): p. 35-43.

13. Metghalchi, M. and J.C. Keck, *Burning velocities of mixtures of air with methanol, isooctane, and indolene at high-pressure and temperature.* Combustion and Flame, 1982. **48**(2): p. 191-210.

14. Tseng, L.K., M.A. Ismail, and G.M. Faeth, *Laminar burning velocities and Markstein numbers of hydrocarbon/air flames.* Combustion and Flame, 1993. **95**(4): p. 410-426.

15. Taylor, S.C. and D.B. Smith, *Laminar burning velocities and Markstein numbers of hydrocarbon air flames - comment.* Combustion and Flame, 1995. **102**(4): p. 523-525.

16. Taylor, S.C., *Burning velocity and the influence of flame stretch*. 1991, University of Leeds.

17. Aung, K.T., L.K. Tseng, M.A. Ismail, and G.M. Faeth, *Laminar burning velocities and Markstein numbers of hydrocarbon air flames - response*. Combustion and Flame, 1995. **102**(4): p. 526-530.

18. Clarke, A., R. Stone, and P. Beckwith, *Measuring the laminar burning velocity of methane/diluent/air mixtures within a constant-volume combustion bomb in a microgravity environment*. Journal of the Institute of Energy, 1995. **68**(476): p. 130-136.

19. Stone, R., A. Clarke, and P. Beckwith, *Correlations for the laminar-burning velocity of methane/diluent/air mixtures obtained in free-fall experiments*. Combustion and Flame, 1998. **114**(3-4): p. 546-555.

20. Bradley, D. and C.M. Harper, *The Development of Instabilities in Laminar Explosion Flames*. Combustion and Flame, 1994. **99**(3-4): p. 562-572.

21. Elia, M., M. Ulinski, and M. Metghalchi, *Laminar burning velocity of methane-air-diluent mixtures*. Journal of Engineering for Gas Turbines and Power-Transactions of the Asme, 2001. **123**(1): p. 190-196.

22. Hassan, M.I., K.T. Aung, and G.M. Faeth, *Measured and predicted properties of laminar premixed methane/air flames at various pressures*. Combustion and Flame, 1998. **115**(4): p. 539-550.

23. Gu, X.J., M.Z. Haq, M. Lawes, and R. Woolley, *Laminar burning velocity and Markstein lengths of methane-air mixtures.* Combustion and Flame, 2000. **121**(1-2): p. 41-58.

24. Bradley, D., P.H. Gaskell, and X.J. Gu, *Burning velocities, Markstein lengths, and flame quenching for spherical methane-air flames: a computational study.* Combustion and Flame, 1996. **104**(1-2): p. 176-198.

25. Aung, K.T., M.I. Hassan, and G.M. Faeth, *Flame stretch interactions of laminar premixed hydrogen/air flames at normal temperature and pressure.* Combustion and Flame, 1997. **109**(1-2): p. 1-24.

26. Aung, K.T., M.I. Hassan, S. Kwon, L.K. Tseng, O.C. Kwon, and G.M. Faeth, *Flame/stretch interactions in laminar and turbulent premixed flames.* Combustion Science and Technology, 2002. **174**(1): p. 61-99.

27. Egolfopoulos, F.N., P. Cho, and C.K. Law, *Laminar flame speeds of methane air mixtures under reduced and elevated pressures.* Combustion and Flame, 1989. **76**(3-4): p. 375-391.

28. Markstein, G.H., *Nonsteady flame propagation.* 1964: Pergamon.

29. Mishra, D.P., P.J. Paul, and H.S. Mukunda, *Stretch effects extracted from propagating spherical premixed flames with detailed chemistry.* Combustion and Flame, 1994. **99**(2): p. 379-386.

30. Davis, S.G. and G. Searby, *The use of counterflow flames for the evaluation of*

*burning velocities and stretch effects in hydrogen/air mixtures.* Combustion Science and Technology, 2002. **174**(11-2): p. 93-110.

31. Heywood, J.B., *Internal Combustion Engine Fundamentals*. 1988.

32. Turns, S.R., *An Introduction to Combustion, Concepts and Applications*. 2nd edition ed. 2000.

33. Reynolds, W.C., *The element potentials method for chemical equilibrium analysis: implementation in the interactive program STANJAN*. 1986, Department of Mechanical Engineering, Stanford University.

# CHAPTER 3

# EXPERIMENTAL APPARATUS AND METHODS

## 3.1 EXPERIMENTAL APPARATUS

The experimental apparatus consists of a mixing chamber, a preheated high pressure cylinder combustion chamber and a data acquisition system. The schematic diagram of the system is shown in Figure 3-1.

### 3.1.1 Cylinder Combustion Chamber

A preheated high pressure cylinder combustion chamber with central spark ignition designed by Checkel [1] was reconstructed. The chamber was a thick-wall carbon steel cylinder capped by two steel flanges with O-ring seals. The chamber volume was 1.1 Liter with 114 mm equal diameter and length. The heavily insulated chamber was wrapped in electric heating elements capable of producing an initial temperature up to 498 K (225 °C) using a 1200 Watt AC power. Two K-type thermocouples were used to monitor the initial temperature of the cell exterior and inside chamber. The chamber was able to withstand peak combustion pressure up to 225 atm at 498 K. An extended-electrode spark plug was located along the axis of the chamber and insulated by heat shrink tubing to ensure central ignition. The spark gap was 2.5 mm. The ignition energy was provided by a spark generator mainly composed of a high voltage capacitor and an

ignition coil. A schematic diagram of the combustion chamber is shown in Figure 3-2.

### 3.1.2 Data Acquisition System

The data acquisition system consists of pressure transducers, and a National Instruments CB-68 LP Data Acquisition Card (68-Pin Digital and Trigger I/O Terminal Block) controlled by a Labview 6i program. Two channels were created on the Data Acquisition Card. One generated a pulse to trigger the spark box through a Digital Delay Generator – 201AR, and the other was an analog input channel to record the pressure trace from the pressure transducer. Two pressure transducers were utilized for different initial pressure. A Flush Diaphragm Pressure Transducer 7820 with 13.6atm (200 psi) pressure range was used for 1 atm pressure experiments and an Omega PX800-2KSV pressure transducer with 136 atm (2000 psi) pressure range was used for experiments at elevated initial pressure up to 5 atm.

## 3.2 EXPERIMENTAL MIXTURES

The experimental gases were methane, carbon dioxide, nitrogen, carbon monoxide, hydrogen, and compressed dry air. The purity of experimental gases except air was 99.9%. The experimental mixture was a stoichiometric blend of three gas mixtures: methane/air, simulated EGR and simulated reformer gas. The mixture composition is shown in Table 3-1, where $V_1$, $V_2$ and $V_3$ are volumetric percentage of methane-air mixture, EGR and reformer gas, respectively. Fraction

$V_1$ consists of 9.5% methane and 90.5% dry air; a stoichiometric methane/air mixture composition. The EGR percent, $V_2$, consists of 18.5% $CO_2$ and 81.5% $N_2$ to simulate the exhaust gases since it has almost the same molar mass and heat capacity of the real exhaust gases. This composition was slightly different from that used by others (14% $CO_2$ and 86% $N_2$ in [2] or 15% $CO_2$ and 85% $N_2$ in [3]), which only simulated the "dry" exhaust gas and ignored the significant water content of real exhaust gas. Appendix B demonstrates the calculation of EGR simulation. To keep the total mixture stoichiometric, reformer gas, $V_3$, includes 22.1% $H_2$, 7.4% CO, and 70.5% air by volume. The ratio of volume fraction of hydrogen to carbon monoxide is 3:1 in order to simulate the ideal steam reforming products of methane. Totally, $V_1 + V_2 + V_3 = 100\%$. The experimental initial pressure ranged from 1 atm to 5 atm and initial temperature varied from 298 K to 473 K. There are two definitions of EGR percent. One is defined as a mass ratio and the other is defined as a volumetric ratio [4]. In this thesis, the volumetric ratio has been used. It is the ratio of the volumetric percent of EGR to total mixture. The maximum percent of EGR is 40% in this study.

**Table 3-1** Composition of Experimental Mixtures

| | | | |
|---|---|---|---|
| $V_1$ | Methane-air mixture | $0.095V_1$ $CH_4$ | $0.905V_1$ air |
| $V_2$ | EGR | $0.185V_2$ $CO_2$ | $0.815V_2$ $N_2$ |
| $V_3$ | Reformer gas | $0.221V_3$ $H_2$ + $0.074V_3$ CO | $0.705V_3$ air |

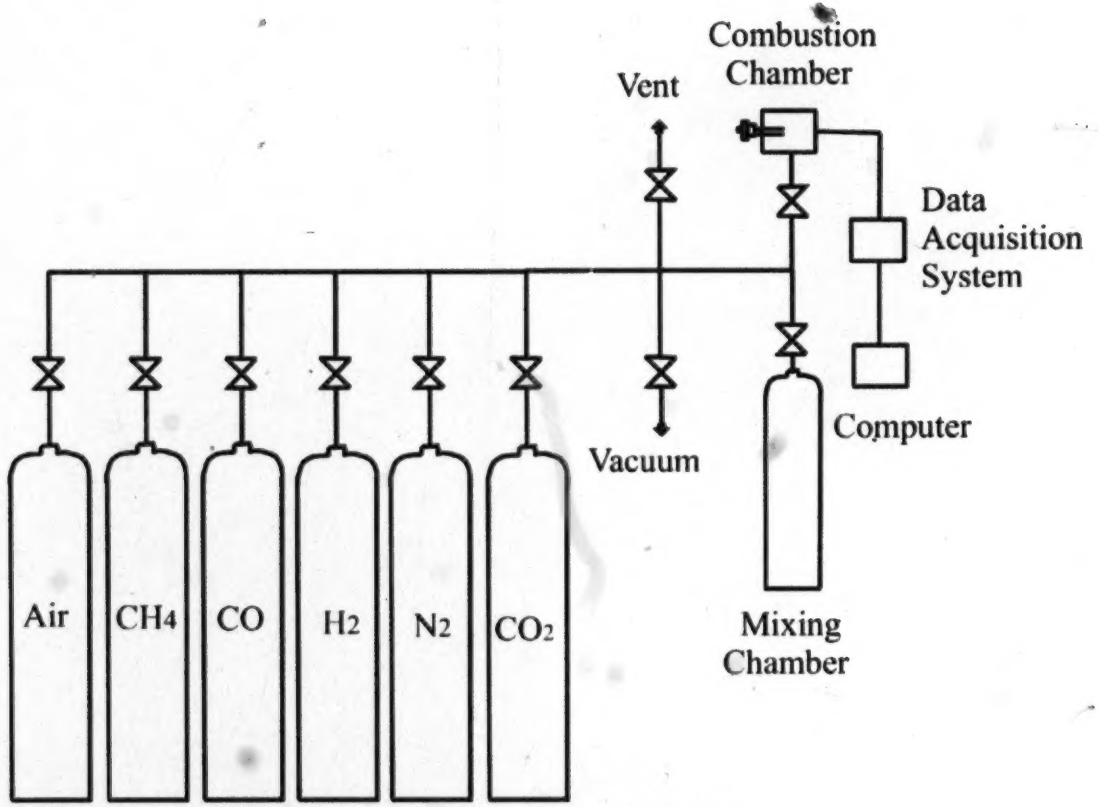


**Figure 3-1** The Schematic diagram of total experimental apparatus

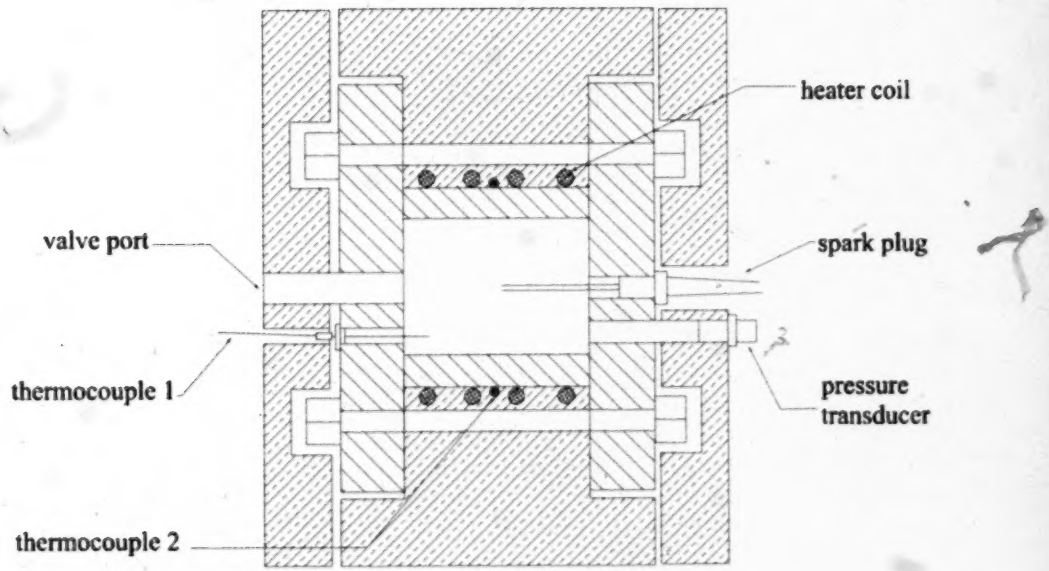


**Figure 3-2** The schematic diagram of the cylindrical combustion chamber

## 3.3 EXPERIMENTAL PROCEDURE

The mixture with desired components was initially prepared by the partial pressure method in a 7 Liter stainless steel mixing chamber at ambient-temperature to ensure that each experimental series had a consistent mixture. One experimental series included experiments from 298 K to 473 K at a certain pressure with the same composition mixture. The mixing chamber was evacuated and filled with air several times before each series of experiments to purge the residual gases.

After the evacuated combustion chamber (Figure 3-2) was heated to the desired temperature, the mixture was fed to the combustion chamber and allowed to stabilize for 5 to 8 minutes before ignition. Wierzba et al. [5, 6] argued that such short time had neglectable effects on flammability limits of hydrogen at the initial temperature up to 473 K and ambient pressure. Therefore, it is reliable to conclude that experimental results were not changed by the short residence time (time before ignition). The combustion chamber was vacuumed during preheating to avoid soot formation from the exhaust gases of the last run, especially at high temperature and pressure. Goethals et al. [7] tested soot formation from the rich flammability limits of methane at elevated temperature and pressure. Soot was found at 10 atm and room temperature and at 5 atm and 473 K, respectively. Because current experimental mixtures and initial conditions were far away from the above limits (equivalence ratio and initial conditions), soot formation was neglected at this study. The initial experimental temperature inside the combustion chamber was cautiously

controlled to an accuracy of ± 1 K by a type K thermocouple probe (thermocouple 1). Because the probe junction directly contacted the mixture that was heated by the surrounding chamber wall, the thermocouple read the mixture temperature accurately within the 5~8 minute stabilization period. After ignition, the combustion pressure was measured by the pressure transducer. The pressure data were collected instantaneously at 5 KHz by a National Instruments CB-68 LP data acquisition board.

## 3.4 FLAME GROWTH MODEL

### 3.4.1 Lewis and Von Elbe Model

Lewis and Von Elbe [8] studied the burning velocity in a constant-volume combustion bomb. A series of equations was derived to calculate essential properties, such as, unburnt gas temperature, burnt mass fraction and flame radius.

Unburnt gas temperature:

$$T_u = T_i\left(\frac{P}{P_i}\right)^{(\gamma_u-1)/\gamma_u} \tag{3-1}$$

burnt mass fraction:

$$n=\frac{P-P_i}{P_e-P_i} \tag{3-2}$$

flame radius:

$$R_b=R_{cell}\left(1-\frac{P_i\,T_u\,P_e-P}{P\,T_i\,P_e-P_i}\right)^{\frac{1}{3}} \tag{3-3}$$

Finally, the burning velocity was derived as:

$$S_u = \frac{dR_i}{dt}\left(\frac{R_i}{R_b}\right)^2\left(\frac{P_0}{P}\right)^{1/\gamma_u} \tag{3-4}$$

where,

$S_u$ is the laminar burning velocity;

$P_i$ and $T_i$ are initial pressure and temperature, respectively;

$R_i$ is nominal radius of burned gases in their unburnt state;

$R_{cell}$ is the radius of the combustion bomb;

$\gamma_u$ is the specific heat ratio of unburnt gases;

P is instantaneous pressure.

### 3.4.2 Multi-zone Thermodynamic Equilibrium Model

A multi-zone thermodynamic equilibrium model described previously [9-11] was developed to calculate the laminar burning velocity from the pressure trace. This model divided a mixture into 1500 elements with equal mass fraction and assumed isotropic, adiabatic flame propagation in the radial direction from the spark point. Each element was treated as a spherical shell which reacted to equilibrium to produce a pressure rise. Unburnt and burnt gas mixtures were assumed to behave as ideal gas. The temperature and pressure were assumed to be uniform in each element but vary among different elements. Two dissociation reactions, carbon dioxide dissociation and water gas reaction were considered.

$$CO_2 \Leftrightarrow CO + \frac{1}{2}O_2 \quad (3\text{-}5)$$

$$CO + H_2O \Leftrightarrow H_2 + CO_2 \quad (3\text{-}6)$$

Consequently, six species (CO, $CO_2$, $O_2$, $N_2$, $H_2$, and $H_2O$) represented the burnt gas.

After a combustion pressure was estimated for each given element, the volume and energy properties for all burnt and unburnt elements were evaluated. As energy balance and equilibrium calculation were performed, and the pressure iteration was carried out until the calculated sum of all element volumes was equal to the total combustion chamber volume. Eventually, a series of theoretic data from pressure, unburnt gas temperature, burnt gas temperature to relative flame radius, etc. were evaluated. Appendix C presents a comparison of results from multi-zone model and Stanjan that was set up as a standard. The results agree surprisingly well with a maximum error of 2.5%. After the theoretic data were interpolated with recorded experimental pressure, burning velocity was obtained as:

$$Su = \frac{dr}{dt} \quad (3\text{-}7)$$

where *dr* is radial consumption rate of unburnt gas during the time interval *dt*.

Unburnt gas temperature, flame radius and burnt mass fraction obtained from multi-zone model were compared with corresponding results from Lewis and Von Elbe's equations in Figures 3-3, 3-4 and 3-5. Except that the burnt mass fraction differs by maximum 14% because of different assumptions, the flame radius and unburnt gas temperature agree extremely well with less than

0.5% difference. Lewis and Von Elbe assumed that burnt mass fraction is a function of pressure gradient, while multi-zone model accounts for changing thermodynamic properties during combustion

## 3.5 EVALUATION OF BURNING VELOCITY

### 3.5.1 Effects of Diluent, Temperature and Pressure on Stretch Rate

The stretch rates of stoichiometric methane/air and methane/10% EGR mixtures are plotted in Figure 3-6. It is clear that adding diluent reduces the stretch rate because of the slow flame propagation. For example, at 45 mm flame radius, the stretch rate decreases from around 100 $s^{-1}$ to 60 $s^{-1}$ with 10% EGR addition. Temperature and pressure influence stretch rate slightly. Elevated initial temperature increases stretch rate but elevated pressure decreases stretch rate. The stretch rates of stoichiometric methane/air mixture at elevated initial temperature and pressure are illustrated in Figure 3-7 and Figure 3-8. The stretch rate increases from about 100 $s^{-1}$ to 135 $s^{-1}$ as initial temperature raises from 298 K to 373 K and decreases from around 100 $s^{-1}$ to 60 $s^{-1}$ as pressure increases from 1 atm to 5 atm.

### 3.5.2 Evaluation of Burning Velocity

In this study, the flame radius over which burning velocity was calculated was chosen due to small correction by stretch rate. Figures 3-6,3-7 and 3-8 illustrate that the stretch rate is small enough

after 45 mm flame radius. In order to minimize the stretch effect, only the burning velocities from a flame radius 45 to 57 mm were analyzed. Elia et al. [2] and Clarke et al. [3] showed that stretch rate of 80 $s^{-1}$ is a significant indicator which only has 1 cm/s correction on burning velocity of stoichiometric methane/air mixture. As described in Section 2.2, the stretch effect would be sufficiently small during this range, especially with reductive effects of diluent and elevated pressure. Additionally, the incremental effect of temperature on stretch rate decays significantly during this range.

An ignition energy above the minimum ignition energy leads to a high apparent initial flame speed, but it has the advantage to overcome quenching effects and establish the early flame propagation. Bradley et al. [12] showed that the enhancement of flame propagation has been observed at the radii up to 10 mm with a very high ignition energy of 1 J. As the ignition energy just above the minimum requirement, this radii was only 6 mm. The ignition energy during the whole current experiments was much less than 1 J, so the effects of spark energy on enhancement of flame speed were sufficiently neglectable after the flame radius 45 mm.

In this chamber, the flame does not contact the chamber wall ideally until the flame radius reaches 57 mm. Flame instability changes the assumption of a smooth spherical flame front. The development of instability leads to cellularity which increases the surface area and consequent flame speed. However, Stone and Clarke [13] argued that cellularity does not occur for a methane flame. Therefore, this study ignored the flame instability impact on burning velocity.

Eventually, the measured burning velocities from a flame radius 45 ~ 57 mm were fitted by equation 3-8 and then extrapolated to initial experimental pressure to obtain the burning velocity:

$$S_u = S_{u0}\left(\frac{T_u}{T_0}\right)^{\alpha}\left(\frac{P}{P_0}\right)^{\beta} \qquad (3\text{-}8)$$

where,

$T_0$ is reference unburnt gas temperature, 298 K;

$P_0$ is reference pressure, 1 atm;

$S_{u0}$ is laminar burning velocity at reference temperature and pressure;

$\alpha$, $\beta$ are exponents dependent on equivalent ratio and fuel properties.

Gülder [14] compared laminar burning velocities of methane/air mixture from a number of authors and concluded that the proper values of $\alpha$ and $\beta$ are 2 and -0.145, respectively. Figure 3-9 shows a typical calculated burning velocity trace of stoichiometric methane/air mixture as a function of combustion pressure at 1 atm and 298 K. Burning velocity increases during the combustion process due to rising unburnt gas temperature caused by adiabatic compression of the mixture. The solid line indicates the portion of the trace where burning velocity is fitted by above equation 3-8 and the dotted line indicates the extrapolation back to initial pressure, 1 atm.

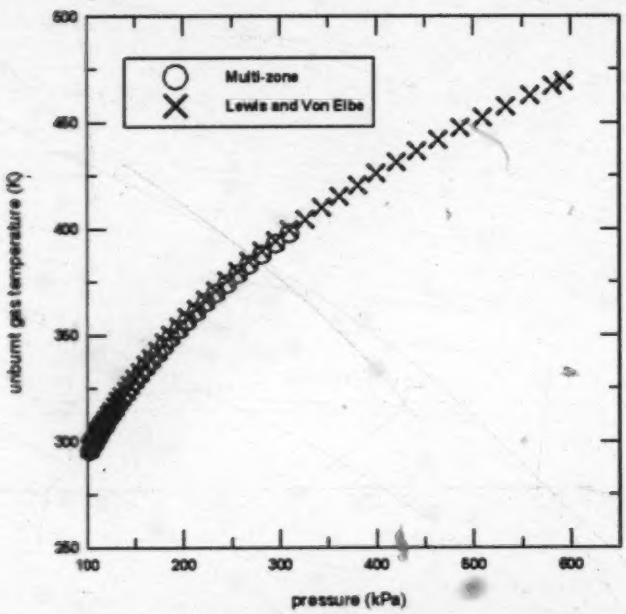


**Figure 3-3** Comparison of unburnt gas temperature from Multizone and Lewis and Von Elbe models

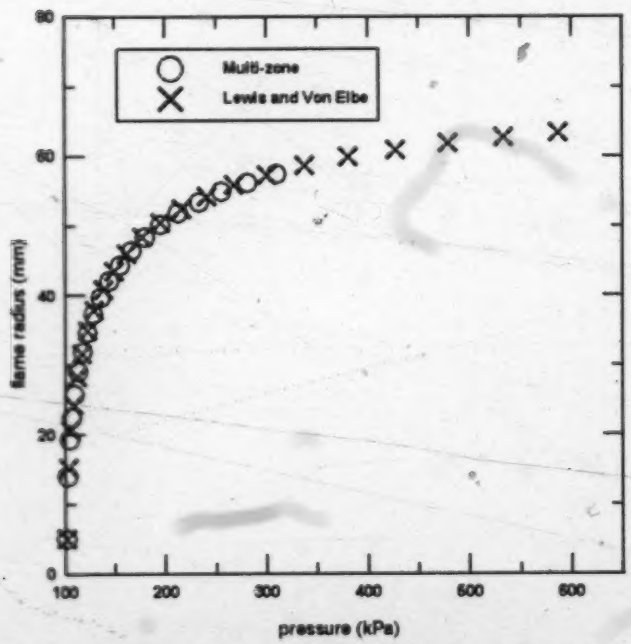


**Figure 3-4** Comparison of flame radius from Multizone and Lewis and Von Elbe models

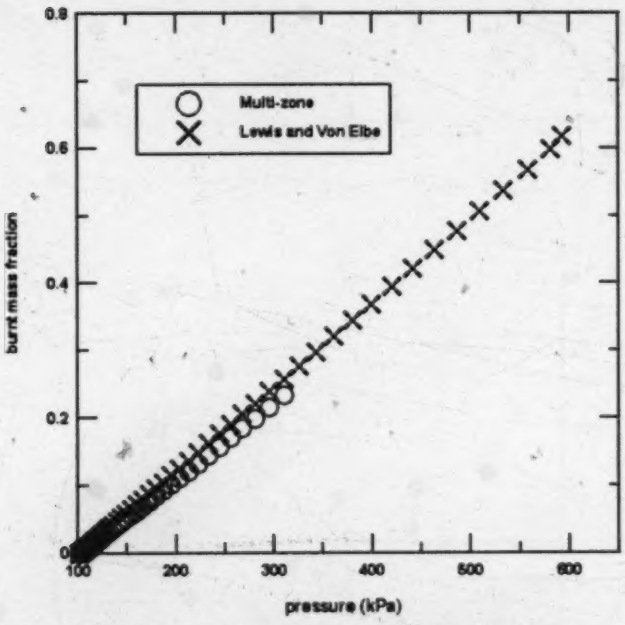


**Figure 3-5** Comparison of burnt mass fraction from Multizone and Lewis and Von Elbe models

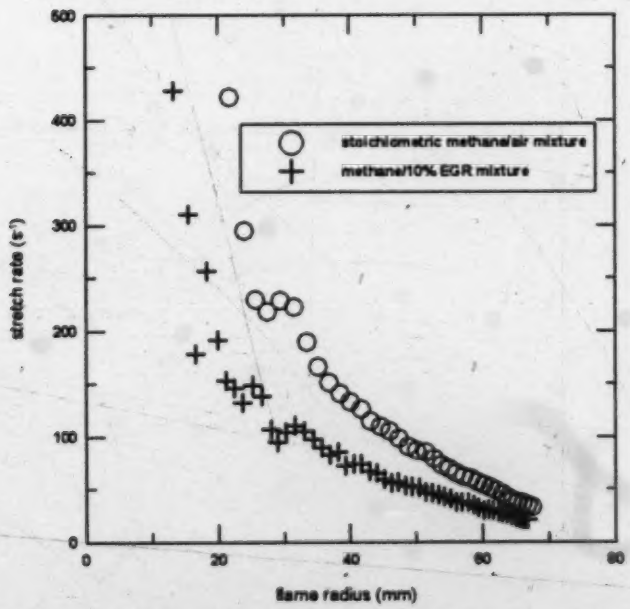


**Figure 3-6** Comparison of stretch rates of methane/air and methane/10% EGR mixtures

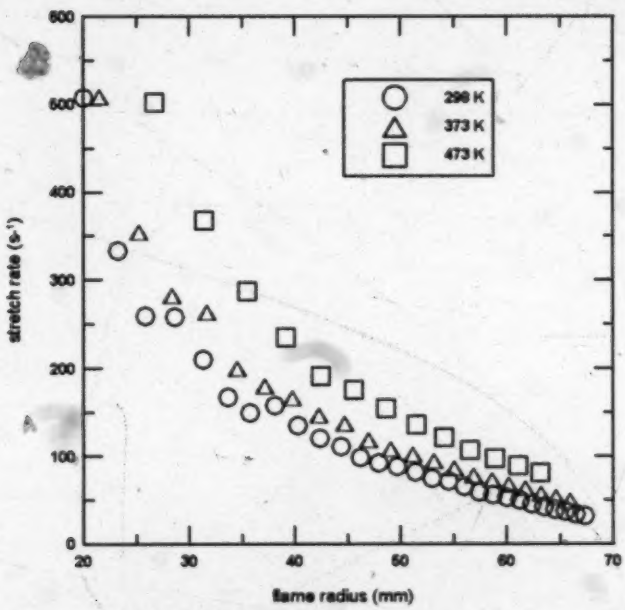


**Figure 3-7** Initial temperature effects on stretch rate of methane/air mixture

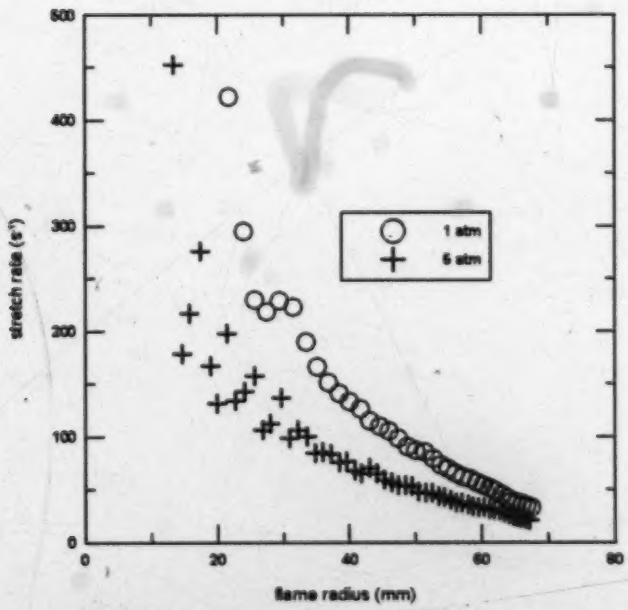


**Figure 3-8** Initial pressure effects on stretch rates of methane/air mixtures

### 3.5.3 Comparison of Previous Published Results

The burning velocities of stoichiometric methane/air mixture at 1 atm and 298 K from various resources, including this study, are displayed in Table 3-2. All results agree well, even though Aung et al. [15], Hassan et al. [16] and Gu et al. [17] corrected their results for stretch rate. The average burning velocity of all other resources is 35.2 cm/s with the standard deviation 0.79 cm/s. This burning velocity value agree very well with 35.3 cm/s in this study.

Gu et al. [17] and Sharma et al. [18] measured the burning velocity of a methane/air mixture in a constant-volume combustion chamber at elevated initial temperature and pressure. Mishra [19] investigated the initial temperature effect on burning velocity of methane/air mixtures by a numerical model of flame structure and propagation. Current burning velocities of methane/air mixtures at elevated initial temperature are compared with results from the above studies in Figure 3-10. It should be noted that the burning velocity in this study without stretch rate adjustment agrees well with Gu's unstretched burning velocity. The data of burning velocities of methane/diluent mixture at specific diluent composition are scarce. Elia et al. [2] measured the burning velocity of methane/diluent mixtures in a spherical combustion chamber. The diluent was composed of 86% nitrogen and 14% carbon dioxide. Clarke et al. [3] determined the burning velocity of methane/diluent mixture in a spherical bomb in a micro-gravity environment with 85% nitrogen and 15% carbon dioxide as a diluent. The burning velocities of methane/diluent mixtures at 298 K and 1 atm measured here are compared with results of Elia and Clarke in Figure 3-11. The diluent in

this study consisted of 18.5% carbon dioxide and 81.5% nitrogen. All results fit well despite the minor difference in diluent composition. The agreement of present results with other published results readily supports current measurement and analysis.

**Table 3-2** Burning Velocity of Stoichiometric Methane/Air Mixture at 1 atm and 298 K

| No. | Resources | Method | $S_u$ (cm/s) |
|---|---|---|---|
| 1 | Iijima (1986) | Bomb Method | 35 |
| 2 | Aung (1995) | Bomb Method | 34 |
| 3 | Hassan (1998) | Bomb Method | 35 |
| 4 | Gu (2000) | Bomb Method | 35.8 |
| 5 | Bosschaart (2003) | Burner Method | 36 |
| 6 | This Study | Bomb Method | 35.3 |

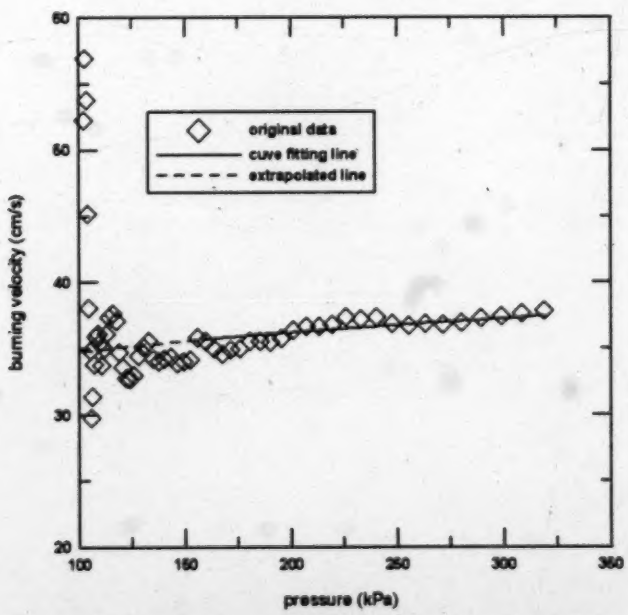


**Figure 3-9** Calculation of burning velocity of stoichiometric methane/air mixture at 298 K and 1 atm

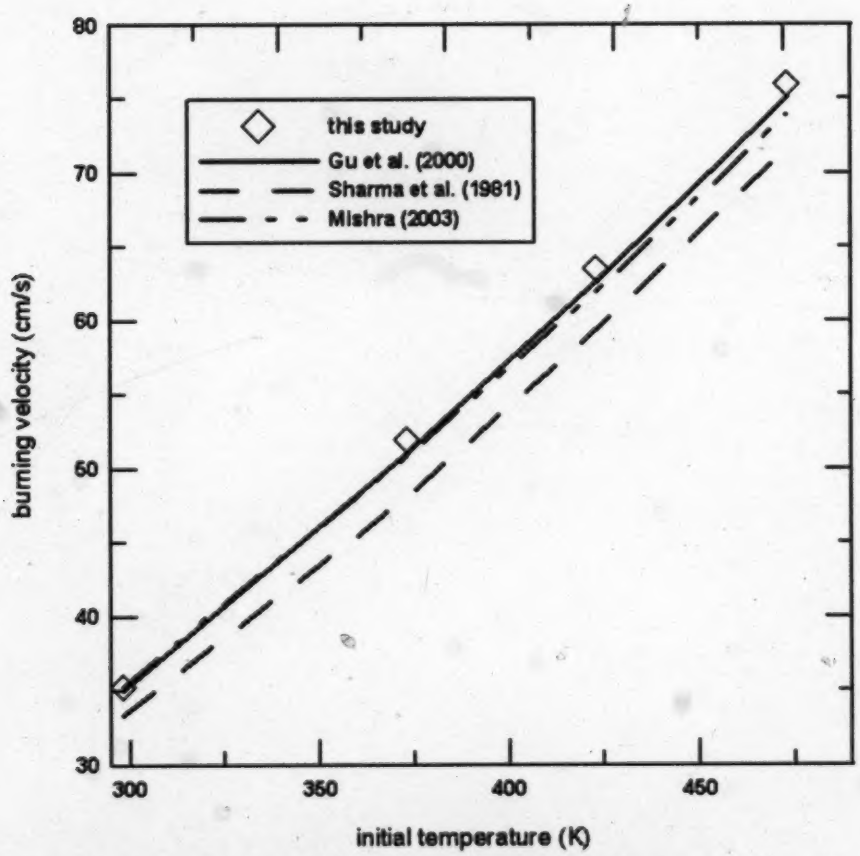


**Figure 3-10** Comparison of burning velocities of stoichiometric methane/air mixtures at 1 atm and elevated initial temperature

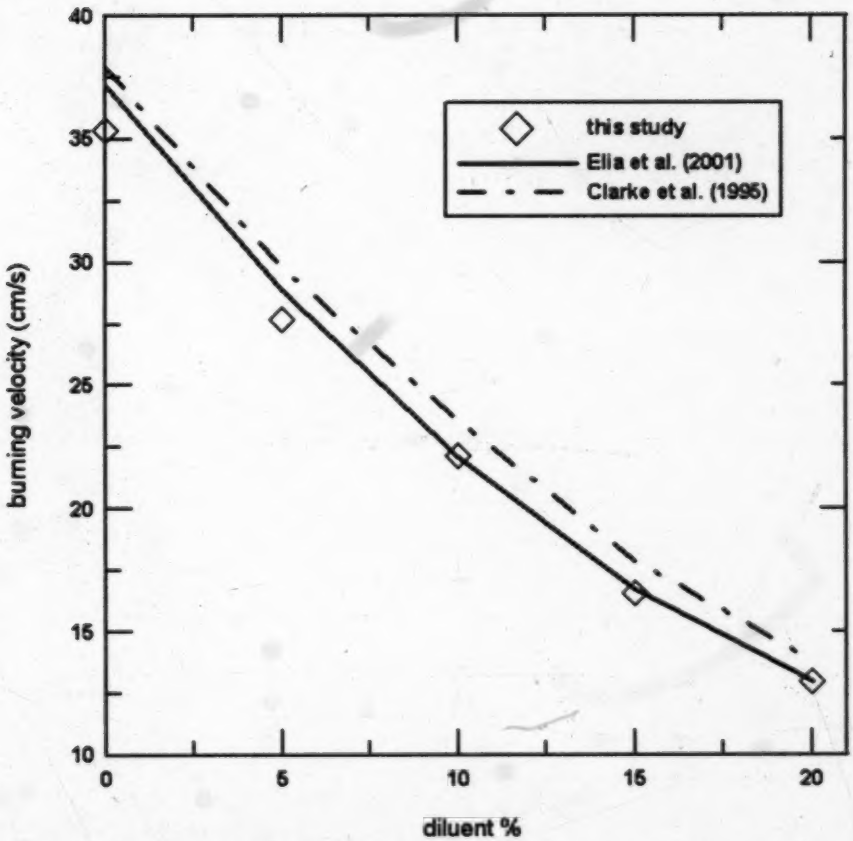


**Figure 3-11** Comparison of burning velocities of methane/diluent mixtures at 1 atm and 298 K

## REFERENCES:


1. Checkel, M.D., D.S.K. Ting, and W.K. Bushe, *Flammability limits and burning velocities of ammonia nitric- oxide mixtures.* Journal of Loss Prevention in the Process Industries, 1995. **8**(4): p. 215-220.

2. Elia, M., M. Ulinski, and M. Metghalchi, *Laminar burning velocity of methane-air-diluent mixtures.* Journal of Engineering for Gas Turbines and Power-Transactions of the Asme, 2001. **123**(1): p. 190-196.

3. Clarke, A., R. Stone, and P. Beckwith, *Measuring the laminar burning velocity of methane/diluent/air mixtures within a constant-volume combustion bomb in a microgravity environment.* Journal of the Institute of Energy, 1995. **68**(476): p. 130-136.

4. Abd-Alla, G.H., *Using exhaust gas recirculation in internal combustion engines: a review.* Energy Conversion and Management, 2002. **43**(8): p. 1027-1042.

5. Wierzba, I. and B.B. Ale, *Effects of temperature and time of exposure on the flammability limits of hydrogen-air mixtures.* International Journal of Hydrogen Energy, 1998. **23**(12): p. 1197-1202.

6. Wierzba, I. and V. Kilchyk, *Flammability limits of hydrogen-carbon monoxide mixtures at moderately elevated temperatures.* International Journal of Hydrogen Energy, 2001. **26**(6): p. 639-643.

7. Goethals, M., B. Vanderstraeten, J. Berghmans, G. De Smedt, S. Vliegen, and E. Van't Oost, *Experimental study of the flammability limits of toluene-air mixtures at*

*elevated pressure and temperature.* Journal of Hazardous Materials, 1999. **70**(3): p. 93-104.

8. Lewis, B. and G. Von Elbe, *Combustion, Flames, and Explosions of Gases*. 3rd ed. 1987, Orlando: Academic Press.

9. Modien, R.M., *The effects of enhanced ignition systems and turbulence on flame development*, in *Department of Mechanical Engineering.,*. 1991, University of Alberta.: Edmonton.

10. Ting, D.S.-K., *Turbulent flame growth in a combustion chamber with homogeneous decaying turbulence*, in *Department of Mechanical Engineering*. 1992, University of Alberta: Edmonton.

11. Ting, D.S.-K. and M.D. Checkel, *The effects of turbulence on spark-ignited, ultra lean, premixed methane-air flame growth in a combustion chamber.* Society of Automotive Engineers, SAE paper, 1995. **952410**.

12. Bradley, D., R.A. Hicks, M. Lawes, C.G.W. Sheppard, and R. Woolley, *The measurement of laminar burning velocities and Markstein numbers for iso-octane-air and iso-octane-n-heptane-air mixtures at elevated temperatures and pressures in an explosion bomb.* Combustion and Flame, 1998. **115**(1-2): p. 126-144.

13. Stone, R., A. Clarke, and P. Beckwith, *Correlations for the laminar-burning velocity of methane/diluent/air mixtures obtained in free-fall experiments.* Combustion and Flame, 1998. **114**(3-4): p. 546-555.

14. Gülder, Ö.L., *Correlations of laminar combustion data for alternative S.I. engine fuels.* Society of Automotive Engineers, SAE paper, 1984. **841000**.

15. Aung, K.T., L.K. Tseng, M.A. Ismail, and G.M. Faeth, *Laminar burning velocities and Markstein numbers of hydrocarbon air flames - response.* Combustion and Flame, 1995. **102**(4): p. 526-530.

16. Hassan, M.I., K.T. Aung, and G.M. Faeth, *Measured and predicted properties of laminar premixed methane/air flames at various pressures.* Combustion and Flame, 1998. **115**(4): p. 539-550.

17. Gu, X.J., M.Z. Haq, M. Lawes, and R. Woolley, *Laminar burning velocity and Markstein lengths of methane-air mixtures.* Combustion and Flame, 2000. **121**(1-2): p. 41-58.

18. Sharma, S.P., D.D. Agrawal, and C.P. Gupta. *The pressure and temperature dependence of burning velocity in a spherical combustion bomb.* in *18th Symposium (International) on Combustion, the Combustion Institute.* 1981.

19. Mishra, D.P., *Effects of initial temperature on the structure of laminar CH4-air premixed flames.* Fuel, 2003. **82**(12): p. 1471-1475.

# CHAPTER 4

# RESULTS AND DISCUSSION

## 4.1 INTRODUCTION

Measurements of the burning velocities of methane/air mixtures were made as functions of diluent, reformer gas, pressure and temperature. The equivalence ratios of all experimental mixtures were unity and mixture compositions are expressed as volume percentage. Experiments were carried out at the range of initial temperature from 298 K to 473 K and initial pressure from 1 to 5 atm. The experimental results at 1 atm and elevated initial temperature with maximum 20% diluent are analyzed in Section 4.2.1 and 4.2.2. Burning velocities of methane/15% diluent mixtures were measured for a range of pressure and ambient temperature. Another set of experiments with 40% diluent was carried out at 5 atm and elevated initial temperature. Section 4.2.3 includes those high pressure results. The effects of reformer gas are discussed at Section 4.2.4. Finally nitric oxide emissions at the experimental initial conditions are presented in Section 4.3.

## 4.2 LAMINAR BURNING VELOCITY

### 4.2.1 Effect of EGR

EGR (exhaust gas recirculation) dilution was simulated by mixtures consisting of 18.5% carbon

dioxide and 81.5% nitrogen in this study. Here after, the term "EGR" is replaced by "diluent" to refer to this specified components. The peak combustion pressure and the time of peak pressure for methane/EGR mixtures at 298 K and 1 atm are shown in Figure 4-1. The systematic uncertainty of the pressure trace is 1% according to the pressure transducer's output tolerance. The systematical uncertainty of the measured burning velocity caused by the pressure trace is 1.5% [1]. The flame radius is the radius of the spherical volume occupied by the burnt mixture. The burnt mass fraction is the fraction of burnt mass compared with the total burnt and unburnt mixture mass. Those two important parameters of flame propagation are shown in Figures 4-2 and 4-3. It is readily seen from Figures 4-1 to 4-3 that EGR lowers the peak combustion pressure and slows down the flame propagation. For example, 10% EGR reduces the peak combustion pressure 9.3% and slows down the combustion time 43%.

Figure 4-4 illustrates the effect of initial temperature on burning velocity of methane/EGR mixtures. The standard deviations of mean are also marked in Figure 4-4. The maximum standard deviation of mean of all results in this study is less than 1.5 cm/s. The effects of EGR on burning velocities of methane/air mixtures at elevated initial temperature are shown in Figure 4-5. As expected, EGR fraction is inversely proportional to burning velocity at all range of initial temperature. Shrestha et al. [2] analyzed the thermodynamic effects of diluents, $CO_2$ and $N_2$, on burning velocities of methane/air mixtures. The diluent reduces the effective heating value of the mixture resulting in a lower flame temperature and leading to a decreasing burning velocity.

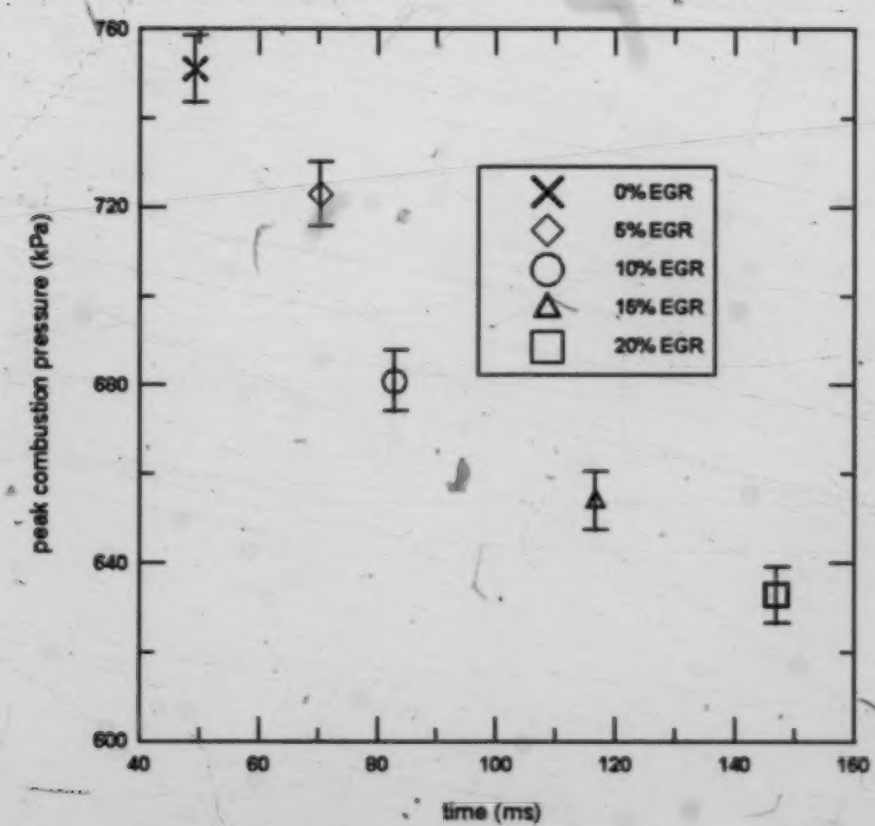


**Figure 4-1** Peak combustion pressures and the occurring times of methane/EGR mixtures at 298 K and 1 atm

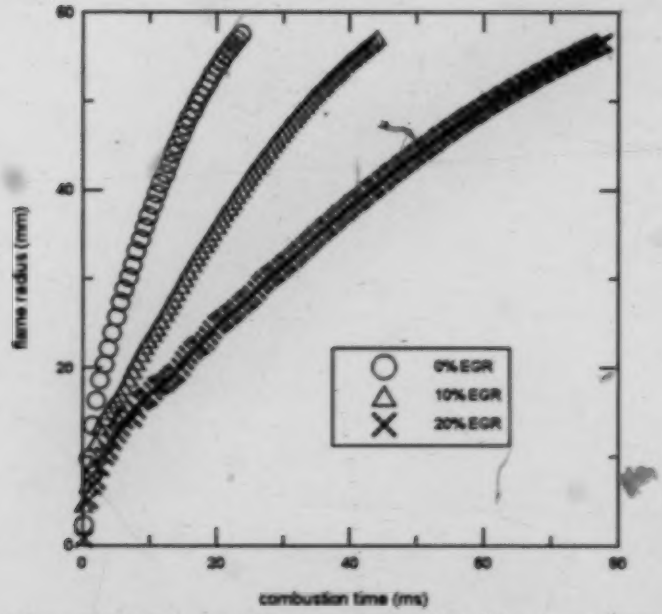


**Figure 4-2** Flame radius of methane/EGR mixtures at 298 K and 1 atm

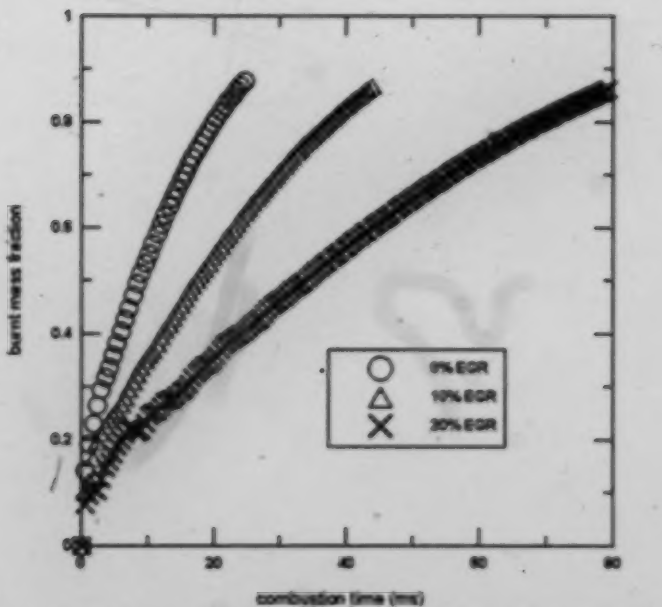


**Figure 4-3** Burnt mass fraction of methane/EGR mixtures at 298 K and 1 atm

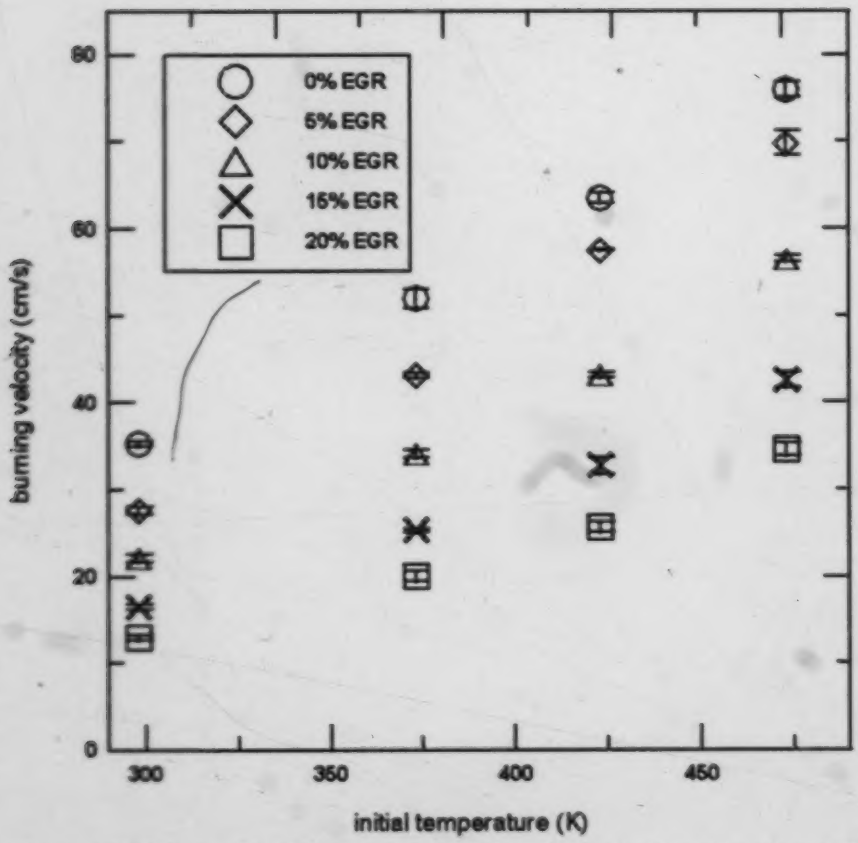


**Figure 4-4** Effects of initial temperature on burning velocities of methane/EGR mixtures at 1 atm

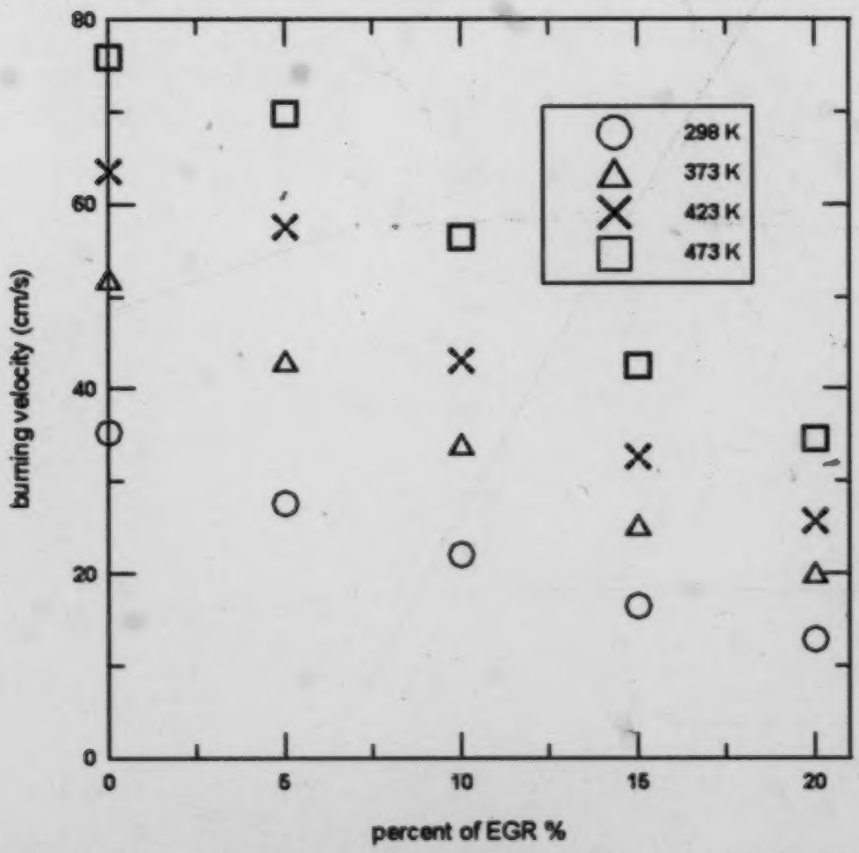


**Figure 4-5** Burning velocities of methane/air mixtures with various EGR percent at 1 atm and elevated initial temperature

### 4.2.2 Effect of Temperature

In general, initial temperature plays an important role on burning velocity of all kinds of fuels. The flame radius and burnt mass fraction of methane/air mixtures at 1 atm and elevated initial temperature are shown in Figures 4-6 and 4-7. Initial temperature dramatically promotes the flame propagation which leads to an increasing burning velocity. Mishra [3] analyzed the flame structure of stoichiometric methane/air mixtures at elevated initial temperature by a numerical model. The elevated initial temperature resulted in growing mass fraction of combustion species, such as $H_2$, $CH_3$, H and CHO, which contributed to the escalating heat release rate. On the other hand, the elevated initial temperature promoted total energy release. As a result, the increase of heat release rate and total energy release improved the burning velocity.

To better understand the effects of EGR and initial temperature on burning velocity, Figure 4-8 illustrates the burning velocity ratio as a function of initial temperature. It is the ratio of burning velocity at a given temperature to that at 298 K with the same EGR percent. The burning velocity ratios converge below 373 K but diverge above that temperature. Neglecting the methane/air mixtures, burning velocity ratios of methane/EGR mixtures converge remarkably well in full range of temperature. It may show the consistent effect of temperature on the burning velocity of methane/air mixtures regardless of the percent. A certain temperature increases burning velocity of methane/EGR mixture by nearly the same ratio. Figure 4-9 shows the burning velocity ratio against the EGR percent. It is the ratio of burning velocity of methane/EGR mixture to that of

methane/air mixture at the same initial temperature. The burning velocity ratio declines with EGR. For example, the methane/20% EGR mixture only has around 40% burning velocity of the methane/air mixture. The initial temperature is effective to raise the burning velocity and the effect becomes stronger at higher temperature. The mixtures at 473 K have the highest burning velocity ratios at the full range of EGR percent. That indicates the hot EGR mixture has faster burning velocity than the cold EGR mixture. The exhaust gas temperature in internal combustion engines was able to reach roughly around 773~873 K [4]. The high temperature is very helpful to reduce the hydrocarbon emission [4] and accelerate the catalyst converter. Therefore, hot EGR is more desirable to internal combustion engines in terms of high burning velocity and low hydrocarbon emission.

An empirical Equation 4-1 was derived to fit the burning velocity of methane/EGR mixtures at 1 atm and elevated initial temperature,

$$S_u = S_{u0}\left(\frac{T_i}{298}\right)^{2.006} \qquad (4\text{-}1)$$

$$S_{u0} = 2808D^3 - 864D^2 - 28.27D + 30.58$$

where $T_i$ is initial temperature in K and D is a volumetric fraction of EGR. Although this equation was derived from experimental EGR fraction between 0.05 and 0.2, it is possible to extend to the full EGR range at 1 atmospheric pressure. Without methane/air mixture included, the maximum error of Equation 4-1 is 5.1%.

Burning velocities of stoichiometric methane/air mixtures at 1 atm were correlated well by the Equation 4-2 with a maximum error 0.5%, where $T_i$ is initial temperature.

$$S_u = 35.33\left(\frac{T_i}{298}\right)^{1.653} \tag{4-2}$$

The power equation such as Equations 4-1 and 4-2 is a generally accepted expression to fit the burning velocity. The temperature exponent for methane/air mixtures varied in different studies. One early study by Andrews and Bradley [5] showed the exponent as 2. Babkin et al. [6] and Rallis et al. [7] both showed experimentally that the temperature exponent was pressure dependent. Babkin et al. [6] also pointed out that the temperature exponent increased with the lean mixture. Gulder [8] summarized that the temperature exponent ranged from 1.37 to 2.33 with the various pressures and equivalence ratios. Sharma et al. [9] and Elia et al. [10]obtained different temperature exponents as 1.68 and 1.857, respectively despite the similar bomb method. The exponent varied slightly as only stoichiometric methane/air mixture was considered. Iijima et al. [11] and Gu et al. [12] showed a close temperature exponent, 1.6 and 1.612, respectively. Stone et al. [13] gave a lower temperature exponent 1.42 with a micro-gravity environment measurement. Mishra [3] constructed a chemical model to obtain a temperature exponent 1.575. Liao et al. [14] measured the laminar burning velocity of natural gas and air mixture in a cubical chamber. The temperature exponent for the stoichiometric mixture was determined as 1.58. In this study, the larger exponent of methane/EGR mixtures indicates that initial temperature has more significant impact on methane/EGR mixtures than methane/air mixtures.

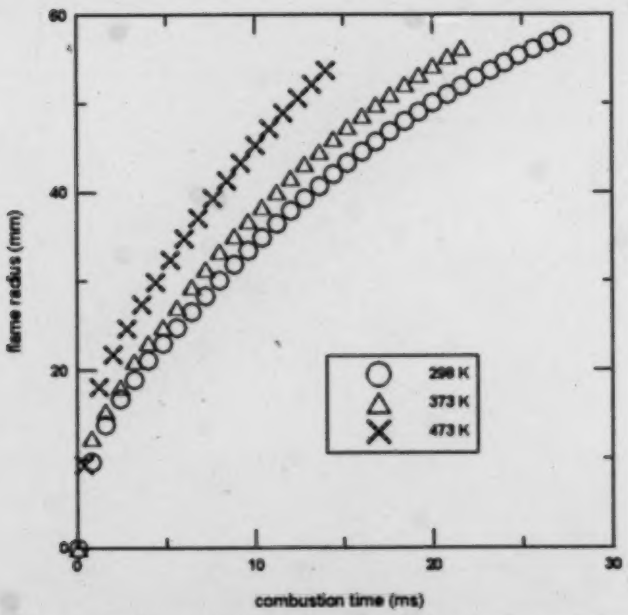


**Figure 4-6** Flame radius of methane/air mixture at 1 atm and elevated initial temperature

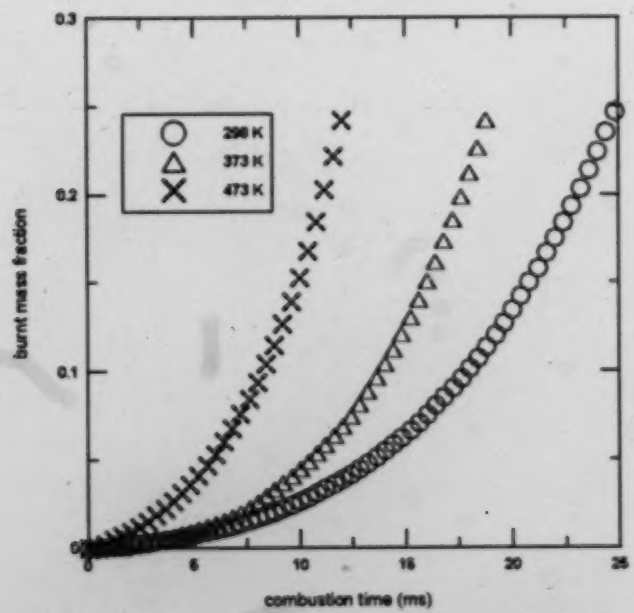


**Figure 4-7** Burnt mass fraction of methane/air mixture at 1 atm and elevated initial temperature

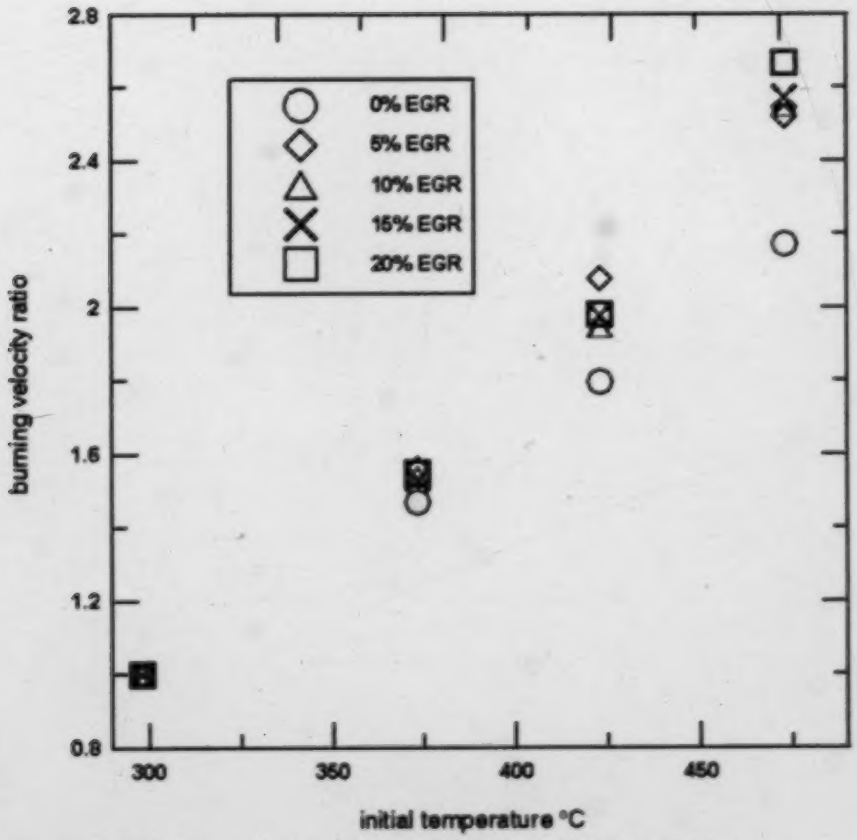


**Figure 4-8** Burning velocity ratios as a function of initial temperature

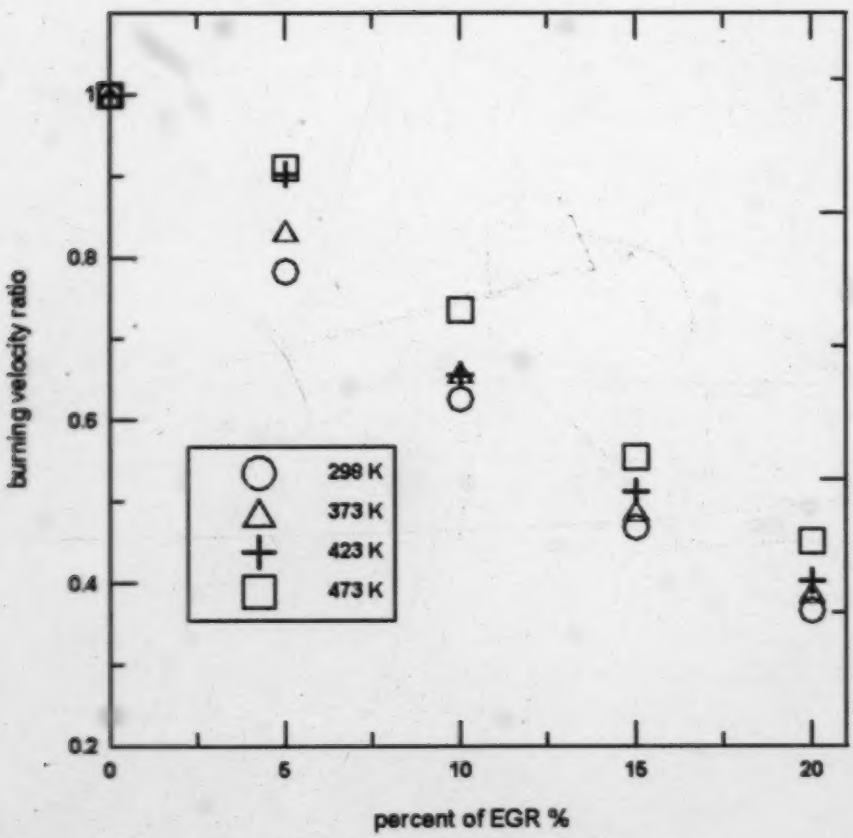


**Figure 4-9** Burning velocity ratios as a function of EGR percent

### 4.2.3 Effect of Pressure

High pressure restricts the flame propagation of methane/air and methane/diluent mixtures and consequently results in low burning velocity. Figures 4-10 and 4-11 show the flame radius and burnt mass fraction of stoichiometric methane/air mixture at elevated initial pressure and 298 K. The pressure dependence on burning velocity is caused by dissociation equilibrium and chemical reactions [15]. Pressure change affects reaction rates more than dissociation for methane/air mixture. Hence, increasing pressure decreases the concentrations of free radicals in the reaction zone and consequent burning velocity. Figure 4-12 illustrates the burning velocities of stoichiometric methane/air mixtures and methane/15% EGR mixtures at initial pressures up to 5 atm and 298 K. Clearly, the pressure has an inverse proportional impact on burning velocity. At 5 atmospheric pressure, even a moderate 15% EGR drops down the burning velocity to an extremely low level. Furthermore, due to the unstable combustion a large amount of EGR is not applicable to methane-fuelled engines despite its low NO emission. The burning velocities from other studies are also plotted in Figure 4-12. The burning velocities of methane/15% EGR mixtures are in good agreement with Elia's [10] results with less than 1 cm/s difference and a maximum 2 cm/s lower than Stone's [13] data. The discrepancy may be attributed to the micro-gravity method and small difference diluent components used by Stone. Comparing the burning velocities of stoichiometric methane/air mixtures with those from Gu et al. [12], Sharma et al. [9], Elia et al. [10] and Stone et al. [13], all results agree well with a maximum 2 cm/s difference including the higher burning velocities of Sharma et al. and Stone et al. at 4 and 5 atm. Bradley

et al. [16] and Gu et al. [12] argued that the pressure record above atmospheric pressure masked the flame distortion and cellularity which enhanced the burning velocity. The authors believed that visual observation overcame the problems. However, Gu's recent results from photographic measurement show good agreement with present results from pressure measurement.

An empirical equation derived from the burning velocity of stoichiometric methane/air mixtures at elevated pressure and 298 K is:

$$S_u = 36.11 \left( \frac{P_i}{P_0} \right)^{-0.37} \qquad (4\text{-}3)$$

where, $P_i$ is initial pressure, atm and $P_0$ is reference pressure, 1 atm. The maximum error equals to 4%. The burning velocities of methane/air mixtures at elevated pressure and 298 K with the curve fitting by Equation 4-3 are shown in Figure 4-13.

Different studies have given the various pressure exponents as the data of burning velocities were fitted by the power equation. Andrew and Bradely [5] reported the pressure exponent as −0.5, while Babkin et al. [6] gave a higher exponent, −0.3. However, some studies indicated that the pressure exponent was pressure dependent. Rallis and Garforth [7] summarized that pressure exponent was −0.51 at 3~10 atm pressure and −0.265 at 0.6~3 atm pressure. Gulder [8] found the pressure exponent as −0.5 or −0.145. Elia et al. [10] suggested pressure exponent as −0.435. As to stoichiometric methane/air mixture, Gu et al. [12] and Liao et al. [14] found similar pressure exponents; −0.374 and −0.398, respectively. Stone et al. [13] obtained a larger

pressure exponent −0.297.

The burning velocities of methane/air mixtures at 5 atm and initial temperature from 298 K to 473 k are compared with results from other studies [7, 9] in Figure 4-14. The burning velocities of methane/air mixtures at 1 atm are also plotted in Figure 4-14 for comparison. The burning velocities agree well at most temperature range but are clearly unacceptable high at 473 K. The reasons have been carefully explored and the problem was linked to the pressure transducer. At 473 K the temperature of the pressure transducer was over the operating temperature range. Appendix D has the detailed error analysis on the burning velocities at 473 K. Hence, the data at 473 K were ignored at later analysis.

A correlation relationship of stoichiometric methane/air mixtures at 5 atmospheric pressure and elevated temperature up to 423 K was derived with a maximum error 1.8%:

$$S_u = 19.23\left(\frac{T_i}{298}\right)^{2.119} \qquad (4\text{-}4)$$

where $T_i$ is initial temperature in K. A curve fitting of the burning velocity ratios by Equation 4-4 from 298 K to 423 K was plotted and extrapolated to 473 K. The original experimental result at 473 K was neglected in the curve fitting. The correlated burning velocities are in reasonable agreement with published data with a maximum 2.5 cm/s difference, as shown in figure 4-14.

Finally, an empirical Equation 4-5 for burning velocity of stoichiometric methane/air mixtures with temperature and pressure was derived. The temperature ranges from 298 K to 700 K corresponding to initial temperature range from 298 K to 473 K. The maximum error is 5.4% and the other errors are less than 3%.

$$S_u = 36.11\left(\frac{P_i}{P_0}\right)^{-0.37}\left(\frac{T_u}{298}\right)^{\alpha} \qquad (4\text{-}5)$$

$$\alpha = 1.566 + 0.087 P_i$$

where,

$P_i$ is initial pressure, atm;

$P_0$ is reference pressure, 1 atm;

$T_u$ is unburnt gas temperature, K;

$\alpha$ is the temperature exponent as a function of initial pressure.

The temperature exponent is pressure dependent. The temperature exponent increases with pressure. Babkin et al. [6] also found the pressure effect on temperature exponent and attributed it to decrease in dissociation with increase in pressure. But authors did not derive a relationship between the exponent and pressure. The unburnt gas temperature $T_u$ in Equation 4-5 ranges from 298 K to 700 K as corresponding to initial temperature between 298 K and 473 K.

Appendix E gives all data of measured burning velocities in this study.

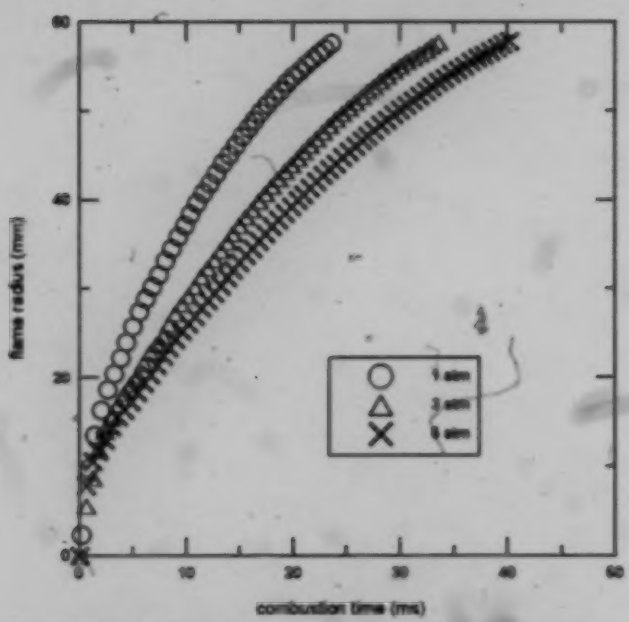


**Figure 4-10** Flame radius of methane/air mixtures at elevated initial pressure and 298 K

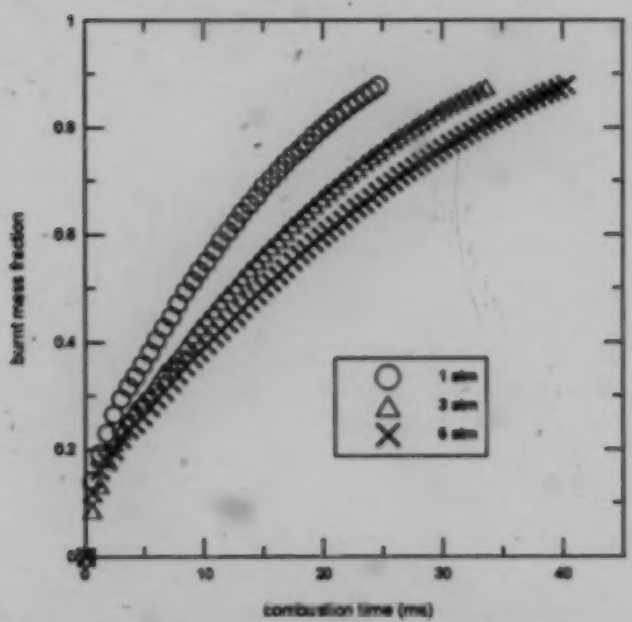


**Figure 4-11** Burnt mass fraction of methane/air mixtures at elevated initial pressure and 298 K

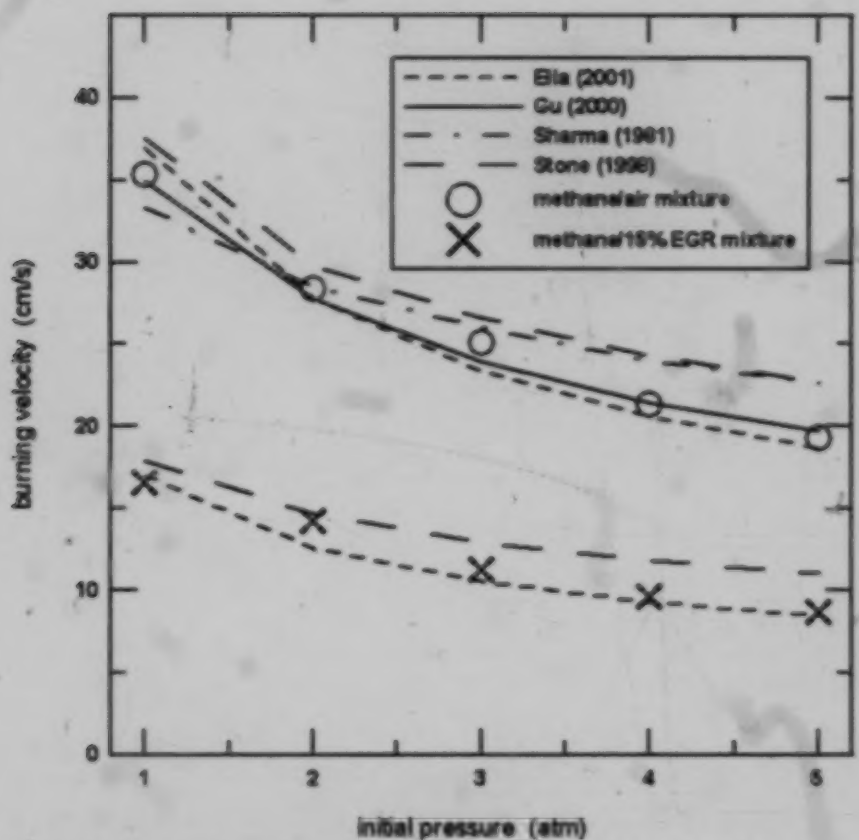


**Figure 4-12** Burning velocities of methane/air and methane/15% EGR mixtures at elevated initial pressure and 298 K

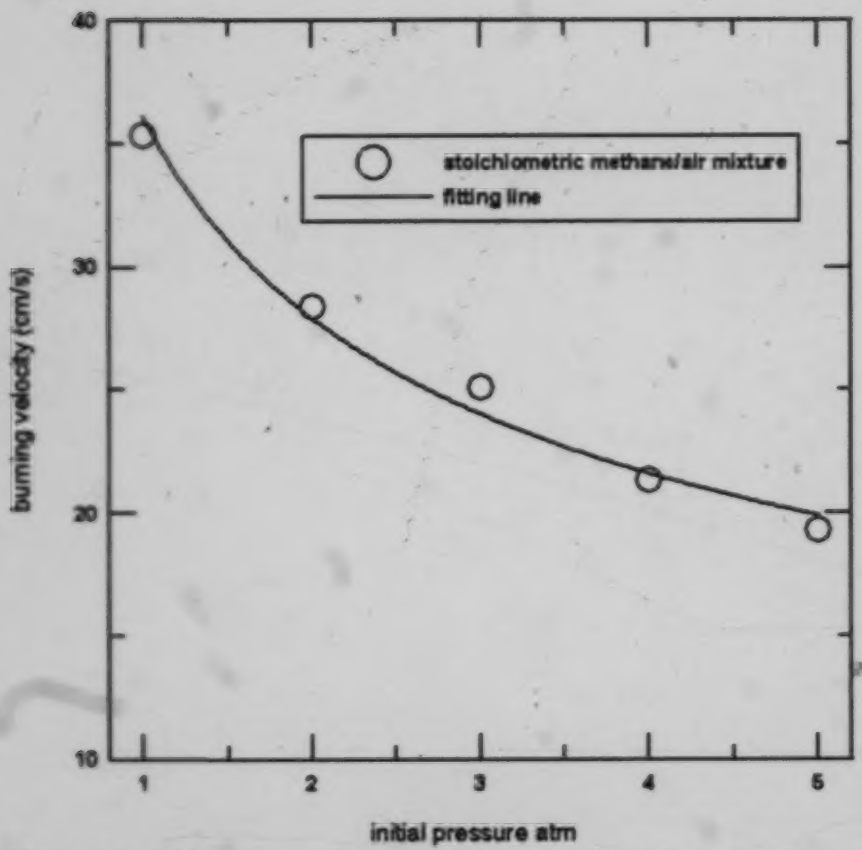


**Figure 4-13** Initial pressure effects on burning velocities of methane/air mixtures at 298 K

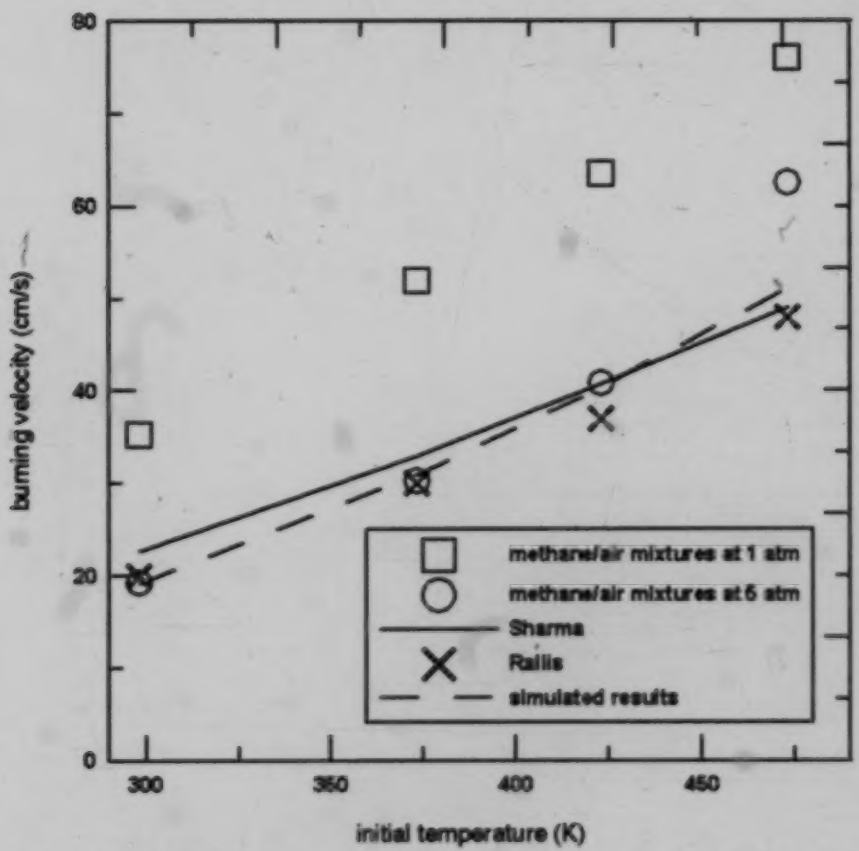


**Figure 4-14** Burning velocity of methane/air mixture at 5 atm and elevated initial temperature

### 4.2.4 Effect of Reformer Gas

Hydrogen has a high burning velocity. Heimel [17] measured the burning velocity of hydrogen/air mixtures at elevated temperature, and Iijima and Takeno [11] measured that at elevated pressure. The burning velocities of stoichiometric hydrogen/air mixture from above two studies are displayed in the Table 4-1. The reformer gas in this study consisted of 22.1% $H_2$, 7.4% CO and 70.5% air by volume to simulate the ideal steam reforming products of methane. McLean et al. [18] determined that the burning velocity with the similar consistent at 1 atm and 298 K was 156.7 cm/s, much higher than the burning velocity of methane/air mixture at the same conditions. Evidently, reformer gas has the potential to enhance the combustion of methane/diluent mixtures due to its high burning velocity. The abbreviation RG refers to reformer gas in this thesis.

**Table 4-1** Burning velocity of stoichiometric hydrogen/air mixtures

| Initial Pressure | 1 atm[17] | | | | 5 atm [11] |
|---|---|---|---|---|---|
| Initial Temperature ℃ | 23 | 100 | 150 | 200 | 23 |
| $S_u$ (cm/s) | 181.1 | 269.6 | 334.7 | 405.7 | 439.8 |

At each diluent level, the repeated experiments were run with varying percent of reformer gas in order to identify the required amount to return the burning velocity to the desirably undiluted value. Table 4-2 displays the fractions of EGR corresponding fractions of reformer gas and the ratios of fractions of reformer gas to EGR. The reformer gas effects on burning velocities of methane/EGR

mixtures at 1 atm are plotted from Figures 4-15 to 4-18. It is interesting to note that reformer gas raises the burning velocity at the full range of initial temperatures. In other words, the percent of reformer gas is temperature independent, but pressure and percent of EGR dependent. The ratio of fractions of reformer gas to EGR at high pressure drastically decreases. The increase of the burning velocity of hydrogen/air mixtures with pressure might be the reason. The burning velocity of stoichiometric hydrogen/air mixture at 5 atm is about 2.4 times of that at 1 atm from the Table 4-1. The ratio of fractions of reformer gas to EGR declines with EGR fraction. That indicates the rising effect on burning velocity with reformer gas. The increasing burning velocity by reformer gas is caused by the increases of H atom and the chain branching reaction $O_2 + H \leftrightarrow O + HO$ [19].

**Table 4-2** EGR and required reformer gas fractions to retain the undiluted burning velocity

| Initial Pressure | 1 atm | | | | 5 atm |
|---|---|---|---|---|---|
| EGR dilution | 0.05 | 0.1 | 0.15 | 0.2 | 0.4 |
| RG required | 0.11 | 0.19 | 0.28 | 0.34 | 0.53 |
| RG / EGR | 2.2 | 1.9 | 1.867 | 1.7 | 1.325 |
| correlated RG | 0.1095 | 0.1942 | 0.2716 | 0.3445 | 0.53 |

It can be readily found from Figure 4-12 that the methane/15% EGR mixture is close to the flammability limit at 5 atm and 298 K. Hence, greater than 15% EGR undermines the stability of

methane combustion at 5 atm. As a matter of fact, methane/30% EGR mixture failed to be ignited at 5 atm in the experiment. In order to take advantage of the desirable fuel-economy and low emission with high EGR, the reformer gas was used with methane/40% EGR mixtures to achieve the target of undiluted burning velocity. After repeated experiments, it was found that 53% reformer gas suits the demand for methane/40% EGR mixture at 5 atm. In other words, methane/40% EGR/53% reformer gas mixture has the same burning velocity as stoichiometric methane/air mixture at 5 atm. Therefore, the reformer gas widens the flammability limits of methane/EGR mixtures and broadens the tolerance of EGR use in methane-fuelled engines. The burning velocities of methane/air mixtures and methane/40% EGR/53% reformer gas mixtures at 5 atm and elevated initial temperature are compared in Figure 4-19. The burning velocities of methane/air mixtures at 1 atm are also shown in Figure 4-19. The scattered data at temperature 200 °C with a large standard deviation 2.6 cm/s (see appendix E for the data) may be attributed to the large uncertainty in the combustion reaction rate of the $CO/H_2$ mixture at high temperature. The uncertainty raised 5 times as the temperature rose from room temperature to 473 K [18]. However, due to a large number of sample number on 473 K experiments, the mean of standard deviation is less than 1 cm/s.

In order to find a relationship between fractions of EGR and reformer gas which produces the same burning velocity, several empirical equations were tried. Equation 4-6 provided the best fitting with a 3% maximum error. The correlated fractions of reformer gas are also given in Table 4-2.

$$RG=\exp(0.8269\log D+0.2652)\left(\frac{P_i}{P_0}\right)^{-0.0885} \quad (4\text{-}6)$$

where,

D and RG are volumetric fractions of EGR and reformer gas, respectively;

$P_i$ is initial pressure, atm;

$P_0$ is reference pressure, 1 atm.

This study has experimentally investigated the reformer gas effects and obtained the desirable reformer gas percent. However, no theoretical model is available to explain the experimental results in the Table 4-2 due to the limited knowledge on chemical effect on flame structure of $CH_4$/EGR/RG mixtures [20].

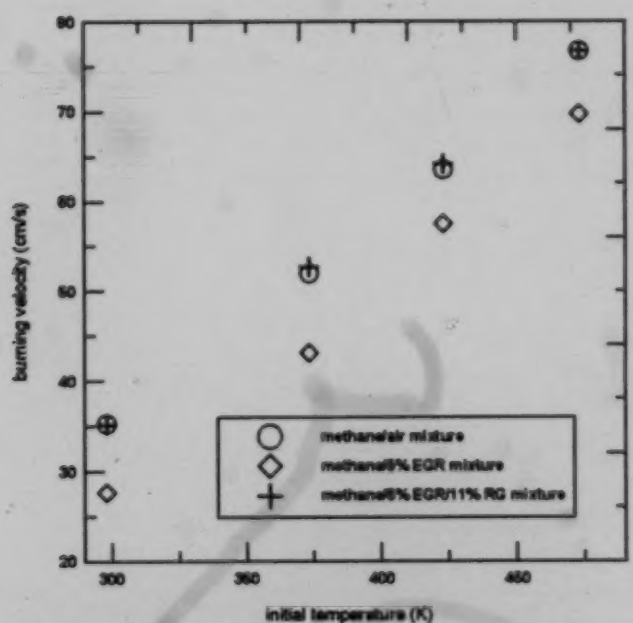


**Figure 4-17** Reformer gas effects on burning velocity of methane/5% EGR mixture at 1 atm

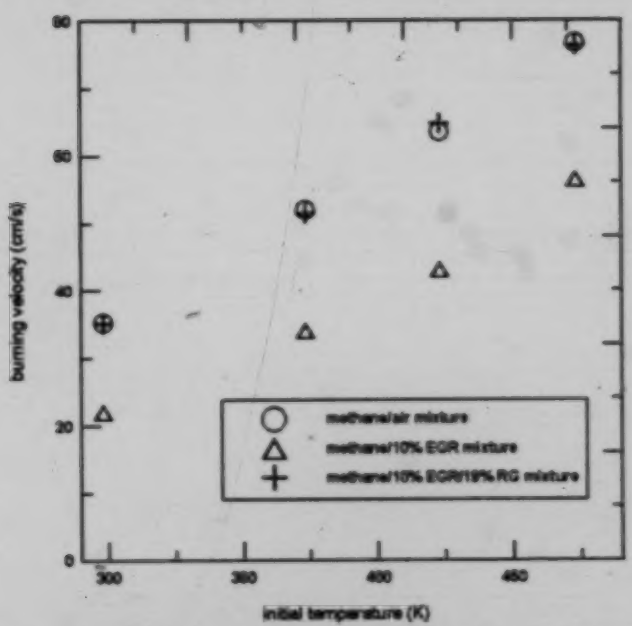


**Figure 4-18** Reformer gas effects on burning velocity of methane/10% EGR mixture at 1 atm

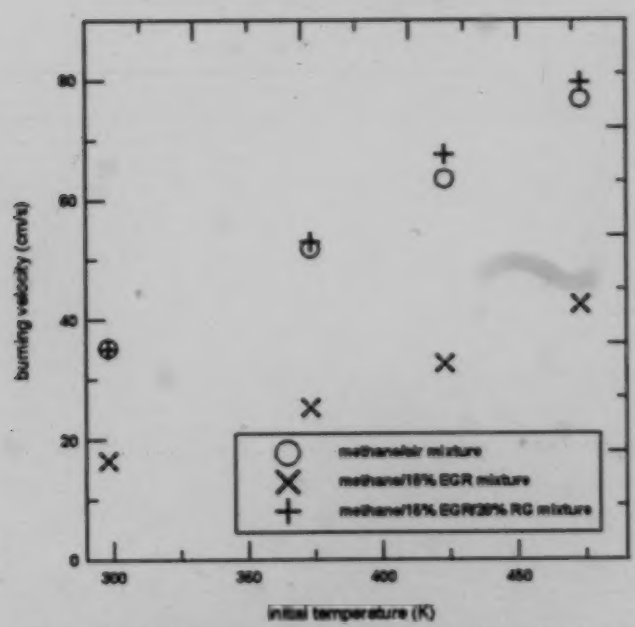


**Figure 4-19** Reformer gas effects on burning velocity of methane/15% EGR mixture at 1 atm

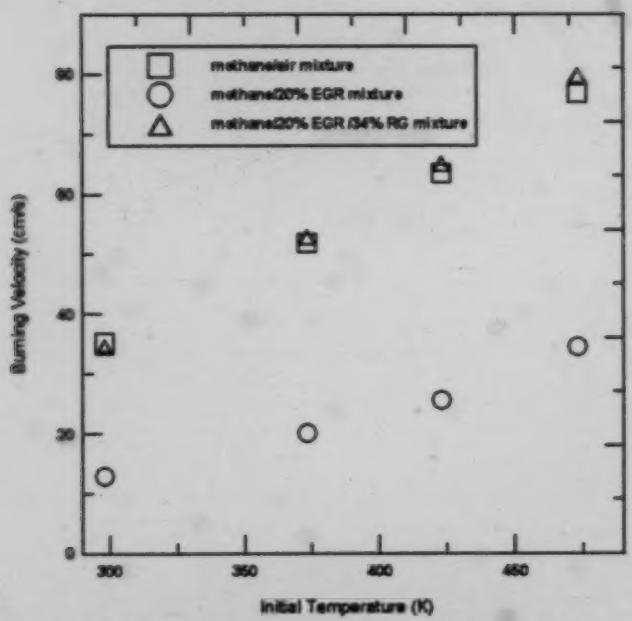


**Figure 4-20** Reformer gas effects on burning velocity of methane/20% EGR mixture at 1 atm

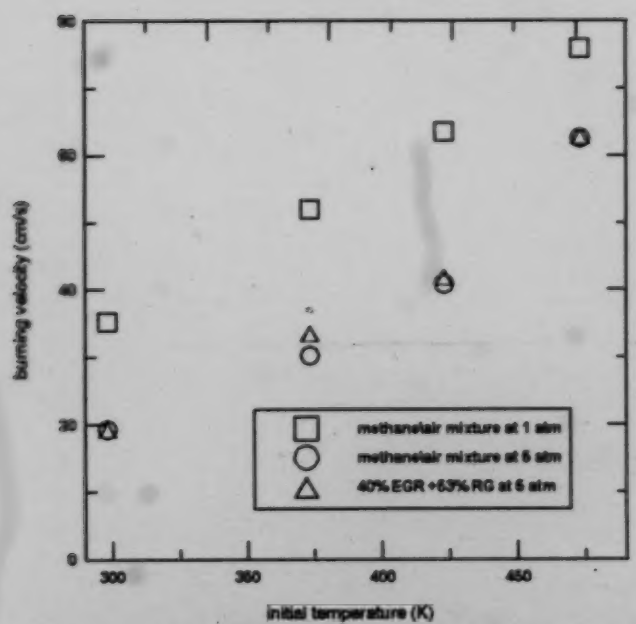


**Figure 4-21** Reformer gas effects on burning velocity of methane/40% EGR mixture at 5 atm

## 4.3 NITRIC OXIDE EMISSIONS

Stanjan was run as the constant-volume combustion with all dissociation products at experimental initial temperature, pressure and components. The combustion properties, such as the flame temperature, peak combustion pressure and equilibrium concentrations of combustion products, were obtained. The initial NO (nitric oxide) concentration was assumed as zero and all nitrogen came from the air. The NO equilibrium concentration and formation rate of NO were calculated with the combustion properties from Stanjan. The calculation equation shown in Chapter 2 was derived from the equilibrium assumption and extended Zeldovich mechanism. The results, including the flame temperature, peak combustion pressure, NO equilibrium concentration and NO formation rate are given in Appendix F. The same theoretical model was used by other researchers to calculate the NO concentrations. Ryan et al. [21] measured the experimental NO equilibrium concentration of the isooctane and n-heptane mixture combustion products in a bomb by a REM chemiluminescent detector. The combustion products were collected in Tedlar bags at atmospheric pressure. Shahed and Newhall measured the NO concentration of stoichiometric $H_2$/air mixture combustion behind a planar flames propagating axially in a cylinder bomb by $q$-band absorption technique [22, 23]. Both of the measured NO concentrations agreed very well with the theoretical values.

### 4.3.1 Nitric Oxide Equilibrium Concentration

The theoretical flame temperatures and peak combustion pressures of methane/EGR mixtures at

elevated initial temperature and 1 atm are shown in Figures 4-20 and 4-21, respectively. EGR clearly declines the flame temperature and peak combustion pressure. $CO_2$ and $N_2$ as diluent reduced the thermal enthalpy of the mixture and then resulted in reduction of flame temperature [20]. Since flame temperature plays a decisive role in NO formation, EGR dramatically decreases the NO concentration. Figure 4-22 illustrates the EGR effects on NO equilibrium concentration at 1 atm.

The elevated initial temperature increases NO concentration by increasing the flame temperature and decreasing the peak pressure. Both of changes on flame temperature and peak pressure promotes the carbon dioxide dissociation and therefore produces more oxygen. As a result, nitric oxide concentration increases.

Elevated pressure slightly decreases the nitric oxide concentration as shown in Figure 4-23. Drake and Richard showed the same descending trend of NO equilibrium concentration in a stoichiometric methane/air mixture [24]. The reasons are contributed to the significant increase of peak combustion pressure with pressure. The peak combustion pressure and flame temperature of methane/air mixtures at elevated initial pressure are plotted in Figure 4-24. The higher pressure prohibits the carbon dioxide dissociation and results in a less oxygen in combustion products which leads to a decreasing nitric oxide concentration.

This study has successfully introduced reformer gas to methane/EGR mixtures to remain the

burning velocity as the undiluted level. It is well known that $H_2$ addition on $CH_4$/air mixture decreases the NO species but CO addition increases the NO species [19]. However, it is unknown if the reformer gas drastically damages the low NO emission of methane/EGR mixtures. Since NO concentration is strongly dependent on flame temperature, the change of flame temperature of methane/EGR mixtures due to the additional reformer gas becomes important. Figure 4-25 gives one example of the effects of reformer gas on flame temperature of methane/5% EGR mixture at elevated initial temperature. Obviously, the flame temperature is only raised by the reformer gas a little but still lower than that of methane/air in spite of the same burning velocities. Therefore, it is possible to draw the conclusion that the NO concentration of methane/EGR/RG mixture is lower than that of methane/air mixture but higher than that of methane/EGR mixture. Figure 4-26 proves this conclusion showing the effects of reformer gas on NO equilibrium concentration of methane/5% EGR mixture.

Figure 4-27 shows the effects of 53% reformer gas on NO equilibrium concentration of methane/40% EGR mixtures at 5 atm and elevated initial temperature. Figure 4-28 plots the ratios of NO equilibrium concentration of methane/40% EGR and methane/40% EGR/53% RG mixtures to that of methane/air mixtures at 5 atm. The significant advantage of large amount of EGR and EGR/reformer gas mixture is easily seen from those two figures. The methane/40% EGR mixture only has less than 10% nitric oxide emission compared with the methane/air mixture. With an additional 53% reformer gas, the nitric oxide emission is still less than 12% based on the NO emission of the methane/air mixture. The methane/40% EGR is out of the flammability limit at

experiments, but with 53% reformer gas addition, the mixture has the same burning velocity with the methane/air mixture. It is now known that the methane/40% EGR/53% reformer gas also has significant advantage at lowering NO emission. In summary, reformer gas is effective to improve the combustion stability and reduce the nitric oxide emission for the large amounts of EGR.

### 4.3.2 Nitric Oxide Formation Rate

The formation rate of NO is temperature dependent. That means the formation rate of NO rises rapidly with increasing temperature. Figure 4-29 shows the EGR effect on formation rate of NO. As EGR reduces the flame temperature, the formation rate declines as well. The formation rate is also pressure dependent. That indicates that the formation rate of NO reduces with decreasing pressure. The formation rate is NO concentration dependent as well, i.e., high NO concentration accelerates the formation rate. The elevated initial temperature increases formation rate slightly. The elevated initial pressure greatly increases formation rate as shown in Figure 4-30. The reasons are attributed to higher flame temperature and peak combustion pressure.

As reformer gas was added, the formation rate slightly increases. One example of the reformer gas effects on formation rate of NO of methane/5% EGR mixture at elevated initial temperature and 1 atm are shown in Figure 4-31. The methane/5% EGR mixture has only less than 50% formation rate compared with methane/air mixture and 11% reformer gas raises the formation rate to less than 60%. Similar to the NO concentration at 5 atm, the large amount of EGR drastically reduces the formation rate of NO. The formation rate is slightly raised by reformer gas compared

with that of methane/EGR mixtures but still lower than that of methane/air mixtures. Figure 4-32 plots the ratios of NO formation rate of methane/40% EGR and methane/40% EGR/53% reformer gas mixtures to that of methane/air mixtures at 5 atm. It shows that with a large reformer gas the formation rate reduces to a extremely low level to 0.02% compared with methane/air mixture.

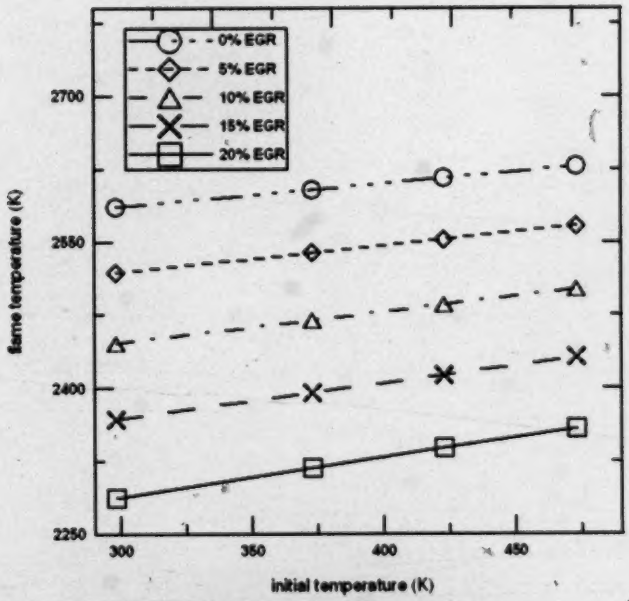


**Figure 4-20** Calculated flame temperature of methane/EGR mixture at 1 atm

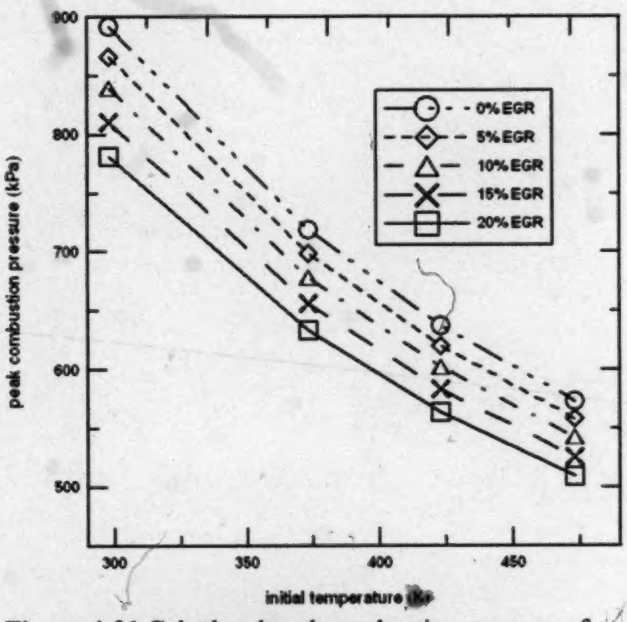


**Figure 4-21** Calculated peak combustion pressure of methane/EGR mixture at 1 atm

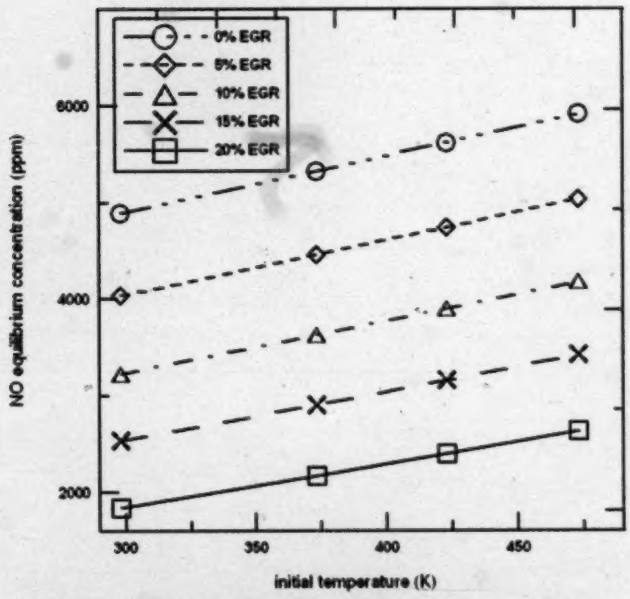


**Figure 4-22** Calculated NO equilibrium concentration of methane/EGR mixture at 1 atm

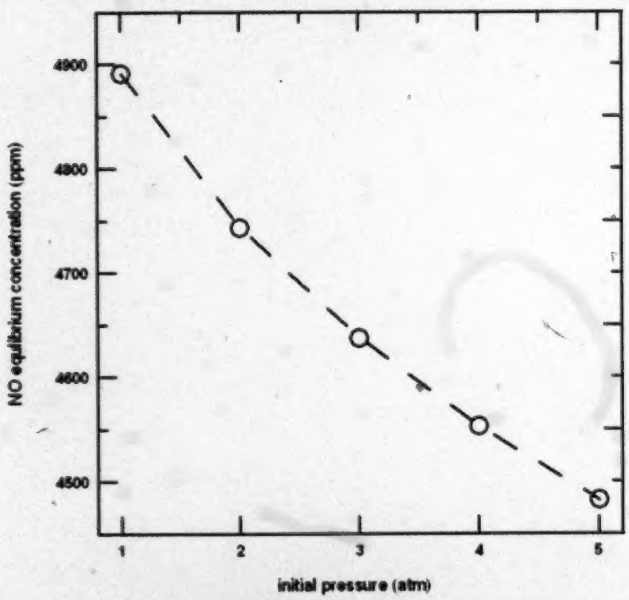


**Figure 4-23** Calculated NO equilibrium concentration of methane/air mixture at 298 K and various initial pressure

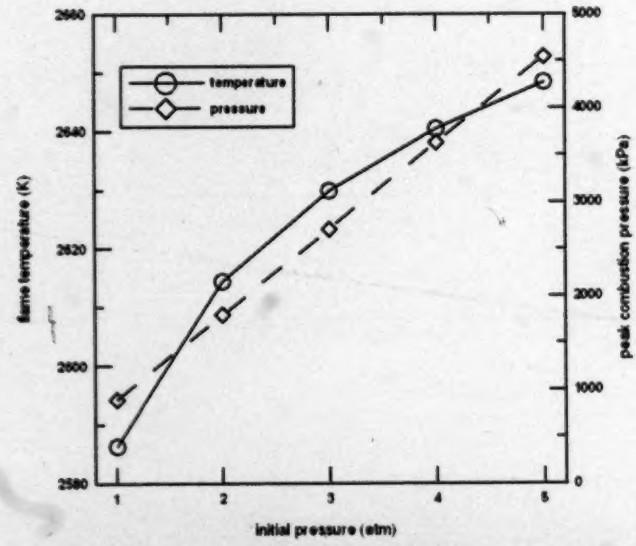


**Figure 4-24** Calculated flame temperature and peak combustion pressure of methane/air mixture

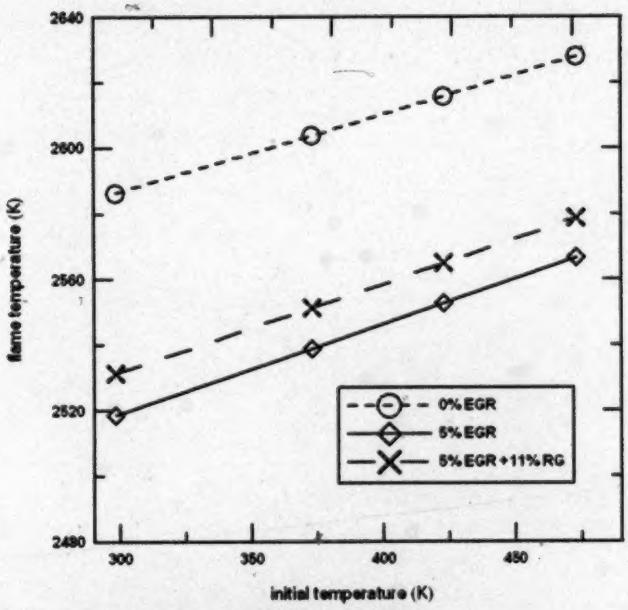


**Figure 4-25** Calculated flame temperature of methane/5% EGR mixture with reformer gas addition

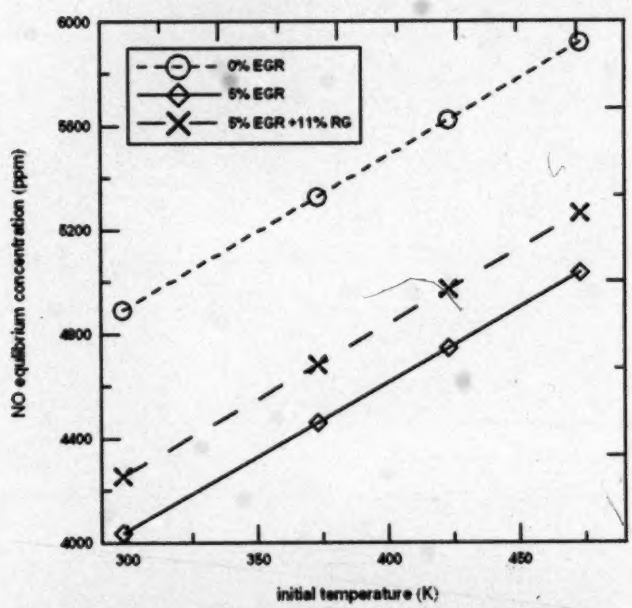


**Figure 4-26** Calculated NO equilibrium concentration of methane/5% EGR mixture with reformer gas addition

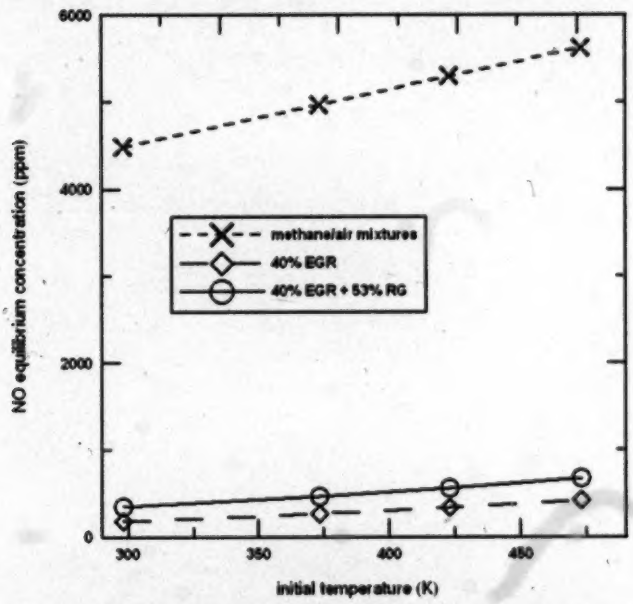


**Figure 4-27** Calculated NO equilibrium concentration of methane/40% EGR mixture with reformer gas addition

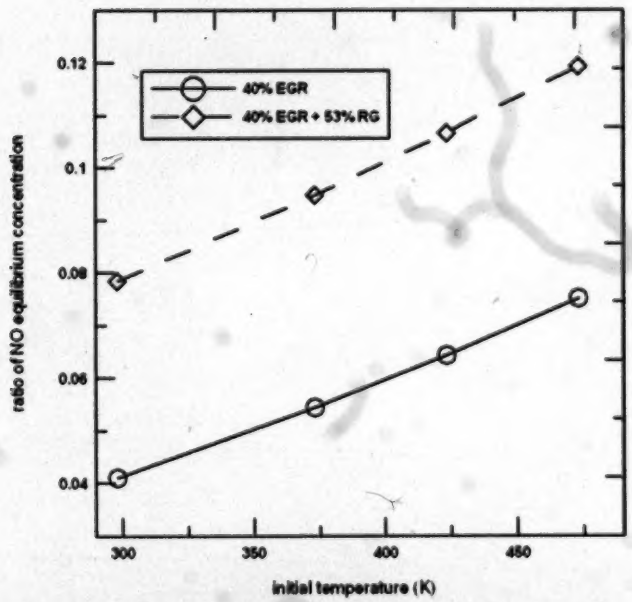


**Figure 4-28** Calculated NO concentration ratio based on that of methane/air mixture at 5 atm

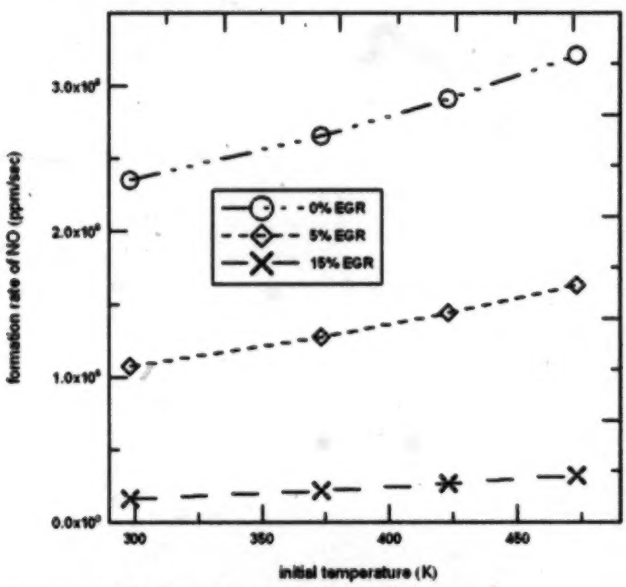


**Figure 4-29** Calculated NO formation rate of methane/EGR mixture at 1 atm

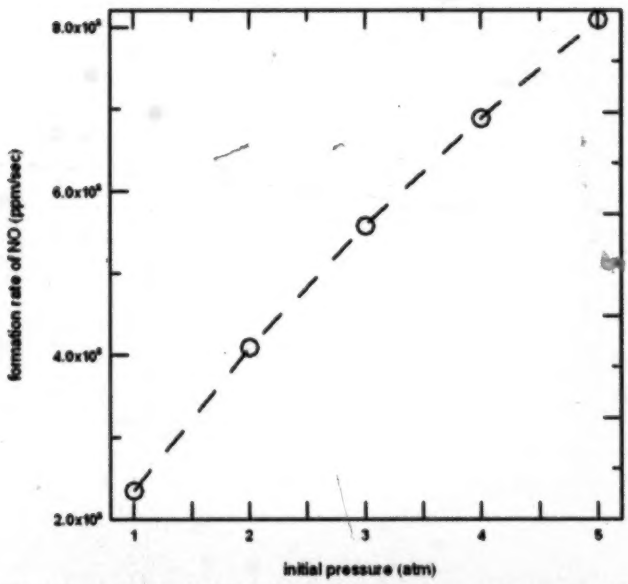


**Figure 4-30** Calculated NO formation rate of methane/air mixture at elevated initial pressure and 298 K

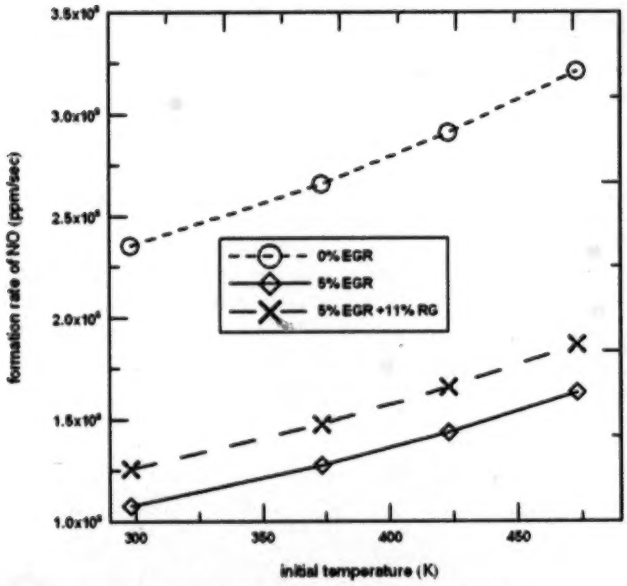


**Figure 4-31** Calculated NO formation rate of methane/5% EGR mixture with reformer gas addition

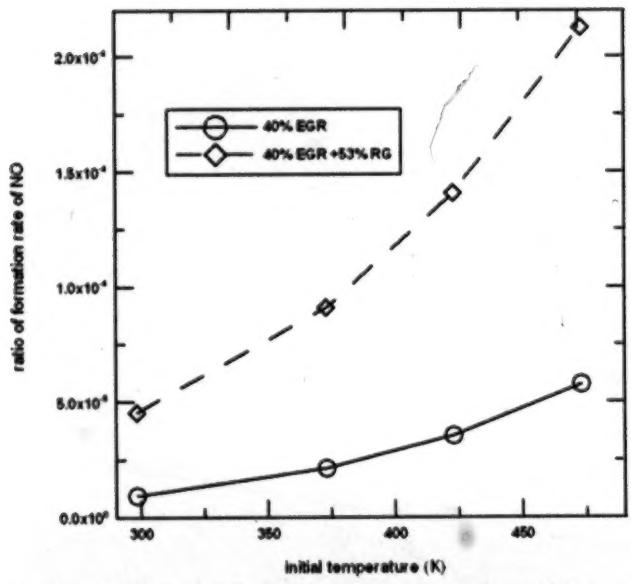


**Figure 4-32** Calculated ratio of NO formation rate based on that of methane/air mixture at 5 atm

## REFERENCES:


1. Holman, J.P., *Experimental Methods for Engineers*. 7th ed. 2001, New York: McGraw-Hill.

2. Shrestha, S.O.B. and G.A. Karim, *Predicting the effects of the presence of diluents with methane on spark ignition engine performance.* Applied Thermal Engineering, 2001. **21**(3): p. 331-342.

3. Mishra, D.P., *Effects of initial temperature on the structure of laminar CH4-air premixed flames.* Fuel, 2003. **82**(12): p. 1471-1475.

4. Allenby, S., W.C. Chang, A. Megaritis, and M.L. Wyszynski, *Hydrogen enrichment: a way to maintain combustion stability in a natural gas fuelled engine with exhaust gas recirculation, the potential of fuel reforming.* Proceedings of the Institution of Mechanical Engineers - Journal of Automobile Engineering, 2001. **215**(D3): p. 405-418.

5. Andrews, G.E. and D. Bradley, *The burning velocity of methane-air mixtures.* Combustion and Flame, 1972. **19**: p. 275-288.

6. Babkin, V.S. and L.S. Kozachenko, *Study of normal burning velocity in methane-air mixtures.* Fizika Goreniya i Vzryva, 1966. **2**(3): p. 77-86.

7. Rallis, C.J. and A.M. Garforth, *The determination of laminar burning velocity.* Progress in Energy and Combustion Science, 1980. **6**(4): p. 303-329.

8. Gülder, Ö.L., *Correlations of laminar combustion data for alternative S.I. engine fuels.* Society of Automotive Engineers, SAE paper, 1984. **841000**.

9. Sharma, S.P., D.D. Agrawal, and C.P. Gupta. *The pressure and temperature dependence of burning velocity in a spherical combustion bomb.* in 18th Symposium (International) on Combustion, the Combustion Institute. 1981.

10. Elia, M., M. Ulinski, and M. Metghalchi, *Laminar burning velocity of methane-air-diluent mixtures.* Journal of Engineering for Gas Turbines and Power-Transactions of the Asme, 2001. **123**(1): p. 190-196.

11. Iijima, T. and T. Takeno, *Effects of temperature and pressure on burning velocity.* Combustion and Flame, 1986. **65**(1): p. 35-43.

12. Gu, X.J., M.Z. Haq, M. Lawes, and R. Woolley, *Laminar burning velocity and Markstein lengths of methane-air mixtures.* Combustion and Flame, 2000. **121**(1-2): p. 41-58.

13. Stone, R., A. Clarke, and P. Beckwith, *Correlations for the laminar-burning velocity of methane/diluent/air mixtures obtained in free-fall experiments.* Combustion and Flame, 1998. **114**(3-4): p. 546-555.

14. Liao, S.Y., D.M. Jiang, and Q. Cheng, *Determination of laminar burning velocities for natural gas.* Fuel, 2004. **83**(9): p. 1247-1250.

15. Lewis, B. and G. Von Elbe, *Combustion, Flames, and Explosions of Gases.* 3rd ed. 1987, Orlando: Academic Press.

16. Bradley, D., R.A. Hicks, M. Lawes, C.G.W. Sheppard, and R. Woolley, *The measurement of laminar burning velocities and Markstein numbers for iso-octane-*

*air and iso-octane-n-heptane-air mixtures at elevated temperatures and pressures in an explosion bomb.* Combustion and Flame, 1998. **115**(1-2): p. 126-144.

17. Heimel, S., *Effect of initial temperature on burning velocity of hydrogen-air mixtures with preheating and simulated preburning*. 1957, National Advisory Committee for Aeronautics: Washington. p. 1-24.

18. McLean, I.C., D.B. Smith, and S.C. Taylor, *The use of carbon monoxide/hydrogen burning velocities to examine the rate of the CO + OH reaction.* Twenty Fifth Symposium (International) on Combustion/The Combustion Institute, 1994: p. 749-757.

19. El-Sherif, A.S., *Control of emissions by gaseous additives in methane-air and carbon monoxide-air flames.* Fuel, 2000. **79**(5): p. 567-575.

20. Park, J., S.G. Kim, K.M. Lee, and T.K. Kim, *Chemical effect of diluents on flame structure and NO emission characteristic in methane-air counterflow diffusion flame.* International Journal of Energy Research, 2002. **26**(13): p. 1141-1160.

21. Ryan, T.W.I. and S.S. Lestz, *The laminar burning velocity of issooctane, n-heptane, methanol, methane, and propane at elevated temperature and pressures in the presence of a diluent.* Society of Automotive Engineers, SAE paper, 1980. **800103**.

22. Shahed, S.M. and H.K. Newhall, *Kinetics of nitric-oxide formation in propane-air and hydrogen-air diluent flames.* Combustion and Flame, 1971. **17**(2):

23. Heywood, J.B., *Internal Combustion Engine Fundamentals*. 1988.

24. Drake, M.C. and R.J. Blint, *Calculations of Nox formation pathways in propagating laminar, high-pressure premixed CH4/air flames.* Combustion Science and Technology, 1991. **75**(4-6): p. 261-285.

# CHAPTER 5

# CONCLUSIONS AND FUTURE WORK

## 5.1 CONCLUSIONS

The effects of temperature, pressure, EGR and reformer gas on the burning velocities of methane/air mixtures have been studied in this thesis. The measurements were made in a preheated cylindrical combustion chamber at the range of initial temperature from 298 K to 473 K and initial pressure from 1 to 5 atm. EGR diluent was simulated by 18.5% $CO_2$ and 81.5% $N_2$ and the reformer gas was simulated by 22.1% $H_2$, 7.4% CO, and 70.5% air. The methane/air mixture consisted of 9.5% methane and 90.5% air. The maximum EGR percent was 20% for experiments at 1 atmosphere and 40% at 5 atmospheres. All percentages were shown in volume and the equivalence ratios of all mixtures were unity. The combustion pressure was recorded by a pressure transducer. The burning velocity was calculated by a Multi-zone Thermodynamic Equilibrium Model. The following conclusions were reached:

1. Initial temperature plays an important role in the burning velocity. Elevated initial temperature dramatically increases the burning velocity of all kinds of fuel/air mixtures.

2. Elevated initial pressure decreases the burning velocities of methane/air and methane/diluent mixtures but raises the burning velocities of hydrogen/air mixtures.

3. Diluent, simulated as EGR in this thesis, is inversely proportional to burning velocities of methane/air mixtures. At 5 atm, 40% EGR .

4. Reformer gas has a promising effect on improving combustion. The certain percent of reformer gas was found to maintain the burning velocity of methane/EGR mixtures at undiluted level. The percent of reformer gas is temperature independent but EGR percent and initial pressure dependent. A correlation relationship between fractions of reformer gas and EGR was derived.

5. A series of empirical power equations of effects of temperature, pressure and EGR on burning velocity of methane/air mixtures was derived. All equations fitted the data of burning velocities reasonably well. The initial temperature ranges from 298 K to 473 K and unburnt gas temperature ranges from 298 K to 700 K. Burning velocity of methane/EGR mixtures at 1 atm was fitted as:

$$S_u = S_{u0}\left(\frac{T_i}{298}\right)^{2.006}$$

$$S_{u0} = 2808D^3 - 864D^2 - 28.27D + 30.58$$

Burning velocity of stoichiometric methane/air mixtures at 1 atm was fitted as:

$$S_u = 35.33\left(\frac{T_i}{298}\right)^{1.653}$$

Burning velocity of stoichiometric methane/air mixtures at elevated pressure and 298 K was fitted as the following equation,

$$S_u = 36.11\left(\frac{P_i}{P_0}\right)^{-0.37}$$

Burning velocity of stoichiometric methane/air mixtures was finally derived as:

$$S_u = 36.11\left(\frac{P_i}{P_0}\right)^{-0.37}\left(\frac{T_u}{298}\right)^{\alpha}$$

$$\alpha = 1.566 + 0.087 P_i$$

Fractions of EGR and reformer gas which produces the same burning velocity were fitted as:

$$RG = \exp(0.8269 \log D + 0.2652)\left(\frac{P_i}{P_0}\right)^{-0.0885}$$

Nomenclature is summarized here,

D and RG are volumetric fractions of EGR and reformer gas, respectively;

$T_u$ is unburnt gas temperature, K;

$T_i$ is initial temperature, K;

$P_i$ is initial pressure, atm;

$P_0$ is reference pressure, 1 atm.

$\alpha$ is the temperature exponent as a function of initial pressure.

6. Experimental measured burning velocities at 5 atm and 473 K were determined to be inaccurate. The reason was linked to the pressure transducer. The temperature of the pressure transducer at 473 K was over the operating temperature range. The data at this condition were eliminated for further analysis (see appendix D for details).

7. Stanjan was run as constant-volume combustion with all dissociation reactions at experimental initial conditions. The peak combustion pressure, flame temperature, and equilibrium concentrations of products were obtained. Formation rate of nitric oxide was evaluated by Extend Zeldovich mechanism and equilibrium assumption. It was found that EGR dramatically reduces equilibrium NO concentration, especially at high pressure. The NO equilibrium concentration of methane/40% EGR mixture at 5 atm is only less than 10% based on that of methane/air mixture. Using sufficient reformer gas to raise the burning velocity to undiluted level also increases NO concentration a little but the NO concentration is still much lower than that of methane/air mixtures, especially at high pressure. In summary, reformer gas has the potential to improve the combustion and reduce the oxides of nitrogen emissions of methane/air mixtures.

## 5.2 FUTURE WORK

1. More data at high pressure and temperature

Due to the operating temperature range of the pressure transducer, the measured burning velocities were limited at the temperature range of 298 K to 423 K at 5 atm. The data at 473 K and 5 atm were not accurate for analysis. Further experiments are required to investigate the burning velocity at extended high temperature and pressure range to verify the correlation equation.

## 2. Multizone Thermodynamic Equilibrium Model

Current Multizone Thermodynamic Equilibrium Model only considers two dissociation reactions, i.e., water-gas reaction and carbon dioxide dissociation. As a large amount of hydrogen was used at experiments, the multizone model should consider the additional hydrogen dissociations. In this study, the reformer gas included 22.1% hydrogen. The hydrogen dissociation becomes important with more hydrogen involved in spite that it seemed no obvious impacts on present experimental results (see Appendix C for details). Depending on the temperature, pressure and extent of reaction, the hydrogen dissociation may include as many as 40 reactions with eight species involved: $H_2$, $O_2$, $H_2O$, OH, O, H, $HO_2$ and $H_2O_2$ [1]. The multizone model should consider some of the important dissociation reactions.

## 3. Analysis of Burning Velocity

As shown in the chapter two, the burning velocity is suggested to be corrected by the stretch rate through the Markstein equation [2, 3]:

$$S_u = S_{u,0} - LK \tag{5-1}$$

where,

$S_u$ is stretched laminar burning velocity;

$S_{u,0}$ is unstretched laminar burning velocity;

K is the stretch rate;

L is the Markstein length.

In spite of no big difference between stretched and unstretched burning velocities as shown in this study, the unstretched burning velocity provides more accurate and comparable value.

4. Effects of reformer gas

A theoretical model with chemical or thermodynamic effects of reformer gas is expected to analyze the burning velocity of methane/EGR/reformer gas mixture at elevated temperature and pressure. This study has investigated the effect by experiments and a theoretical model is welcome to verify the experimental results.

## REFERENCES:


1. Turns, S.R., *An Introduction to Combustion, Concepts and Applications*. 2nd edition ed. 2000.

2. Markstein, G.H., *Nonsteady flame propagation*. 1964: Pergamon.

3. Clavin, P., *Dynamic behavior of premixed flame fronts in laminar and turbulent flows*. Progress in Energy and Combustion Science, 1985. **11**(1): p. 1-59.

# APPENDIX A

# COMPARISON OF THERMAL EFFICIENCY AND ENERGY OF STEAM REFORMING AND PARTIAL OXIDATION

The thermal efficiency and thermal energy of steam reforming and partial oxidation are compared in this appendix. The thermal energy is referred as the lower heating value,

**NOMENCLATURE:**

| | |
|---|---|
| LHV | Lower heating value |
| M | Molar mass |
| PO | Partial oxidation |
| SR | Steam reforming |
| TE | Thermal Efficiency |

## A.1 DEFINITIONS AND DATA

Fuel: methane

Reform products: hydrogen, carbon monoxide

Thermal efficiency: the ratio of lower heating value (LHV) of reform products to lower heating value of methane (reactant)

(All data came from Heywood "*Internal combustion engine fundamentals*" (1988))

| | CO | $CH_4$ | $H_2$ |
|---|---|---|---|
| LHV (MJ/kg) | 10.1 | 50 | 120 |
| M (kg/kmol) | 28.011 | 16.043 | 2.016 |

## A.2 REACTION EQUATIONS

Steam Reforming $CH_4+H_2O=CO+3H_2$

Partial Oxidation $CH_4+\frac{1}{2}O_2=CO+2H_2$

## A.3 RESULTS AND CONCLUSIONS

**Table A-1** Thermal efficiency and thermal energy of steam reforming and partial oxidation

| Steam Reforming | | | Partial Oxidation | | |
|---|---|---|---|---|---|
| Thermal Efficiency | LHV (MJ) | | Thermal Efficiency | LHV (MJ) | |
| | Reactants | Products | | Reactants | Products |
| 1.25 | 802.2 | 1008 | 0.95 | 802.2 | 766.8 |

It is evident that the thermal efficiency of steam reforming is 1.3 times of that of partial oxidation. Meanwhile, the ratios of energy output to energy input in steam reforming and partial oxidation are 1.25 and 0.96, respectively. Therefore, steam reforming is better than partial oxidation in thermal efficiency and energy output.

# APPENDIX B
# EGR SIMULATION

The major components of EGR (exhaust gas recirculation) diluent are $CO_2$, $N_2$ and $H_2O$, which are the complete combustion products of stoichiometric hydrocarbon fuel/air mixtures. Since it was infeasible to add vapor or liquid water to an unheated combustion chamber, a mixture of $N_2$ and $CO_2$ was used to simulate the complete combustion products. Therefore, the specific heat and molar mass of the mixture of $N_2$ and $CO_2$ should be as close as possible to those of the complete combustion products. The chemical equations of stoichiometric combustion of methane and gasoline are:

$$CH_4 + 2\,(O_2 + 3.773\,N_2) \rightarrow CO_2 + 2\,H_2O + 7.546\,N_2$$

$$C_8H_{18} + 12.5\,(O_2 + 3.773\,N_2) \rightarrow 8\,CO_2 + 9\,H_2O + 47.1625\,N_2$$

A 81.5% $N_2$ and 18.5% $CO_2$ mixture was determined to have the closest specific heat to the EGR mixture. This mixture composition is different with mixtures with 86% $N_2$ and 14% $CO_2$ or 85% $N_2$ and 15% $CO_2$ used by other researchers [1, 2].

The specific heat capacity and molar mass of the combustion products of stoichiometric methane and gasoline and simulated EGR mixtures were calculated [3] for comparison. The molar mass of each mixture is shown in Table B-1. The Figure B-1 illustrates the specific heat capacity of all above mixtures. The Figure B-2 also illustrates the specific heat capacity of the simulated EGR mixtures and the dry combustion products of methane and gasoline, i.e., only $N_2$ and $CO_2$. The unburned gas temperature was considered approximately from 298 K to 580 K corresponding to the experimental initial temperature range from 298 K to 473 K. Hence, it is clear that the mixtures of 86% $N_2$ and 14% $CO_2$ or 85% $N_2$ and 15% $CO_2$ only simulate the $N_2$ and $CO_2$ blend

in the exhaust gas of gasoline combustion and ignore the big amount of water. But a mixture of 81.5% $N_2$ and 18.5% $CO_2$ has nearly the same specific heat capacity of the real "wet" exhaust gas of both gasoline and methane combustion. Hence, a mixture of 81.5% $N_2$ and 18.5% $CO_2$ was used in this study to simulate the EGR diluent.

**Table B-1** Calculation of molar mass of mixtures

| Mixtures | Products of methane combustion | Products of gasoline combustion | 81.5% $N_2$ + 18.5% $CO_2$ | 86% $N_2$ + 14% $CO_2$ |
|---|---|---|---|---|
| Molar mass (kg/kmol) | 27.63 | 32.97 | 30.97 | 30.25 |

## REFERENCES:


1. Elia, M., M. Ulinski, and M. Metghalchi, *Laminar burning velocity of methane-air-diluent mixtures.* Journal of Engineering for Gas Turbines and Power-Transactions of the Asme, 2001. **123**(1): p. 190-196.

2. Clarke, A., R. Stone, and P. Beckwith, *Measuring the laminar burning velocity of methane/diluent/air mixtures within a constant-volume combustion bomb in a microgravity environment.* Journal of the Institute of Energy, 1995. **68**(476): p. 130-136.

3. Cengel, Y.A. and M.A. Boles, *Thermodynamics: An Engineering Approach*. 3rd ed. 1998.

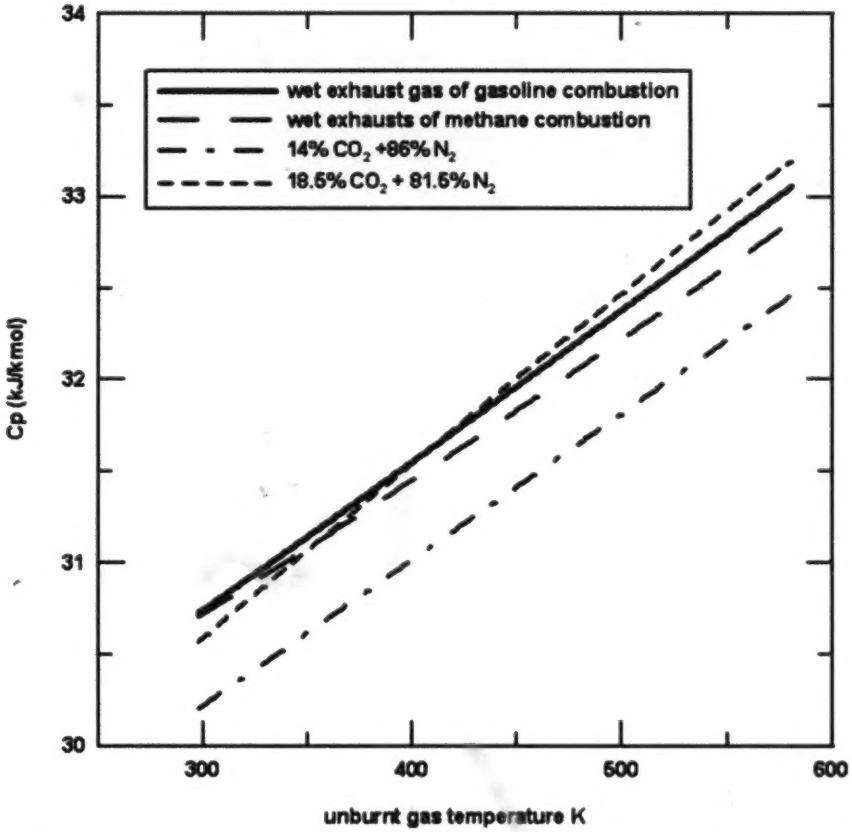


**Figure B-1** Comparison of specific heat capacity of simulated and wet exhaust gases

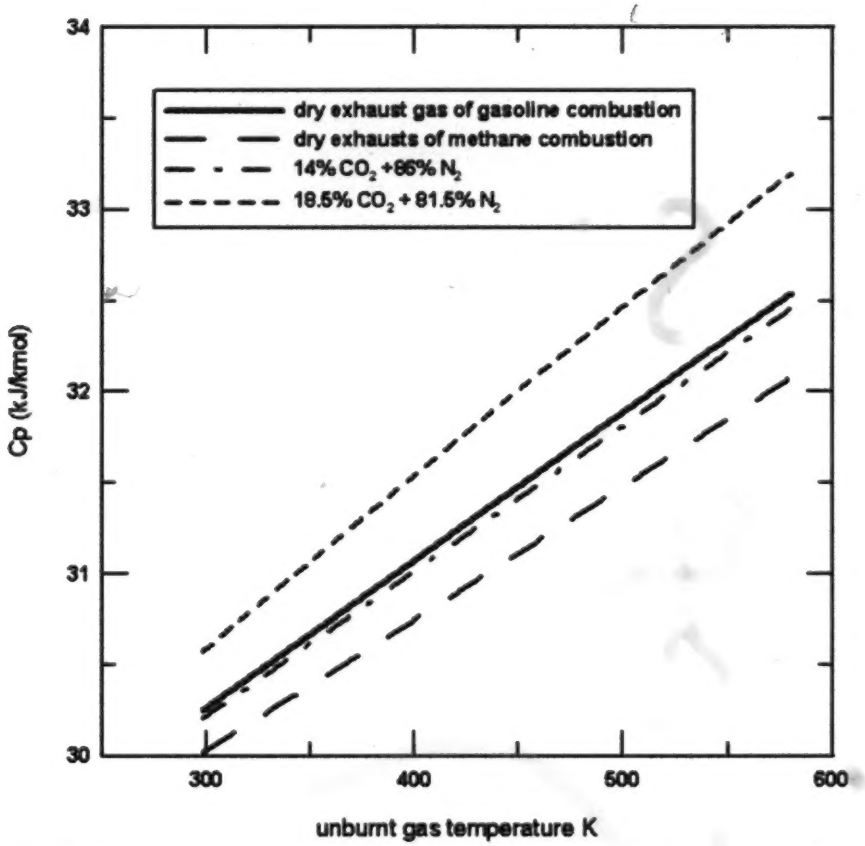


**Figure B-2** Comparison of specific heat capacity of simulated and dry exhaust gases

# APPENDIX C

# COMPARISON OF MULTI-ZONE MODEL AND STANJAN

**NOMENCLATURE:**

| | |
|---|---|
| M | molar mass |
| V | volume |
| U | internal energy |
| H | enthalpy |
| S | entropy |
| $T_i$ | initial temperature |
| $P_i$ | initial pressure |
| $T_u$ | unburnt mixture temperature |
| T | temperature after mixture burnt |
| $T_{flame}$ | flame temperature |

## C.1 INTRODUCTION

This appendix compares the results calculated from Multi-zone Thermodynamic Equilibrium Model and Stajan, respectively. Modien and Ting [1, 2] compared the results from two models before. More comparison is given in this appendix. Multi-zone model splits the combustion mixture into 1500 elements, and calculates the theoretical pressure, unburnt mixture temperature, burnt mixture temperature, burnt mixture mass faction, etc. of every element. The multi-zone model consists of several subroutines. Some results were evaluated by subroutines, while others were evaluated from main program. Stanjan [3] was set up as a standard. First of all, the properties of lean and stoichiometric methane are calculated; second, the properties of reformer gases, i.e., carbon

monoxide and hydrogen, are calculated; finally, the properties of methane with simulation EGR, carbon dioxide and nitrogen, are calculated.

## C.2 COMPARISON OF RESULTS

### I. INITIAL COMPOSITIONS AND CONDITIONS

| | $CH_4$ | $O_2$ | $N_2$ |
|---|---|---|---|
| composition | 0.075 | 0.1938 | 0.7312 |

$T_i$ = 297.65 K $P_i$ = 1 atm = 101.325 kPa Equivalence ratio = 0.77

Reactant properties (Stanjan): M= 27.888 kg/kmol

V= 8.7579e-1 m3/kg U=-2.9063e5 J/kg

H= -2.0189e5 J/kg S= 7.1653e3 J/kg-K

Molar mass of reactants (Multizone): M=27.889 kg/kmol

#### 1. Adiabatic Flame Temperature at Constant Volume Combustion

Multizone model: subroutine "Flame" can evaluate the flame temperature at constant pressure or constant volume, but now only the flame temperature at constant volume was calculated.

Stanjan: *Products**, and *Option 12, V and U same as last run.*

| | Stanjan | Multizone | error |
|---|---|---|---|
| $T_{flame}$ | 2335 K | 2344 K | 0.36% |

#### 2. Unburnt Gas Temperature

Mutizone: an arbitrary pressure $P_1$ = 1.0208 atm=103.4303 kPa.

Stanjan: *Products*, gas compositions $CH_4$, $O_2$ , and $N_2$, *Option 17, one of above at specified composition*, the same compositions with reactants, and *Option 6 specified P and S*, $P = P_1$, $S=S_{reactant}$ (isentropic compression).

| | Stanjan | Multizone | error |
|---|---|---|---|
| $T_u$ | 299.3 K | 299.5 K | 0.08% |

**3. Burnt Gas Temperature**

Multizone: an arbitrary pressure $P_1$ =1.0208 atm

Stanjan: *Products, Option 5, specified P and H*, P= $P_1$, and H=Hreactant

| | Stanjan | Multizone | error |
|---|---|---|---|
| T | 1953 K | 1965 K | 0.63% |

## II. INITIAL COMPOSITIONS AND CONDITIONS

| | $CH_4$ | $O_2$ | $N_2$ |
|---|---|---|---|
| composition | 0.095 | 0.1896 | 0.7154 |

$T_i$ = 294.15 K $P_i$ = 1 atm = 101.325 kPa Equivalence ratio =1.00

Reactant properties (Stanjan): M= 27.632 kg/kmol

V= 8.7351e-1 $m^3$/kg U=-3.5021e5 J/kg

H= -2.6171e5 J/kg S= 7.2217e3 J/kg-K

Molar mass of reactants (Multizone): M=27.633 kg/kmol

**1. Adiabatic Flame Temperature at Constant Volume Combustion**

Multizone model: subroutine "Flame" evaluated the flame temperature at constant volume.

Stanjan: *Products*, and *Option 12, V and U same as last run.*

| | Stanjan | Multizone | error |
|---|---|---|---|
| $T_{flame}$ | 2585 K | 2548 K | 1.4% |

**2. Unburnt Gas Temperature**

Mutizone: an arbitrary pressure $P_1$ = 1.00358 atm=101.688 kPa

Stanjan: *Products*, gas compositions $CH_4$, $O_2$, and $N_2$, *Option 17, one of above at specified composition*, the same compositions with reactants, and *Option 6 specified P and S*, $P = P_1$, $S=S_{reactant}$ (isentropic compression).

| | Stanjan | Multizone | error |
|---|---|---|---|
| $T_u$ | 294.3 K | 294.4 K | 0.004% |

**3. Burnt Gas Temperature**

Multizone: an arbitrary pressure $P_1$ =1.00358 atm

Stanjan: *Products, Option 5, specified P and H*, P= $P_1$, and H=Hreactant

| | Stanjan | Multizone | error |
|---|---|---|---|
| T | 2222 K | 2241 K | 0.86% |

## III. INITIAL COMPOSITIONS AND CONDITIONS

| | CO | $H_2$ | $O_2$ | $N_2$ |
|---|---|---|---|---|
| composition | 0.1 | 0.15 | 0.1571 | 0.5929 |

$T_i$ = 296.15 K $P_i$ = 1 atm = 101.325 kPa Equivalence ratio =0.8

Reactant properties (Stanjan): M= 24.74 kg/kmol

V= 9.8176e-1 $m^3$/kg U= -5.4881e5 J/kg

H= -4.4934e5 J/kg S= 7.8463e3 J/kg-K

Molar mass of reactants (Multizone): M=24.7412 kg/kmol

**1. Adiabatic Flame Temperature at Constant Volume Combustion**

Multizone model: subroutine "Flame" evaluated the flame temperature at constant volume.

Stanjan: *Products*, and *Option 12, V and U same as last run.*

| | Stanjan | Multizone | error |
|---|---|---|---|
| $T_{flame}$ | 2551K | 2536 K | 0.57% |

**2. Unburnt Gas Temperature**

Mutizone: an arbitrary pressure $P_1$ = 1.582 atm = 160.30 kPa

Stanjan: *Products*, gas compositions CO, $H_2$, $O_2$, and $N_2$, *Option 17, one of above at specified composition*, the same compositions with reactants, and *Option 6 specified P and S*, $P = P_1$, $S=S_{reactant}$ (isentropic compression).

| | Stanjan | Multizone | error |
|---|---|---|---|
| $T_u$ | 337.2 K | 336.7 K | 0.16% |

**3. Burnt Gas Temperature**

Multizone: an arbitrary pressure $P_1$ = 1.582 atm = 160.30 kPa

Stanjan: *Products, Option 5, specified P and H*, $P= P_1$, and H=Hreactant

| | Stanjan | Multizone | error |
|---|---|---|---|
| T | 2202 K | 2257 K | 2.5% |

As $P_2$ = 101.4767 kPa

| | Stanjan | Multizone | error |
|---|---|---|---|
| T | 2195 K | 2223 K | 1.2% |

## IV. INITIAL COMPOSITIONS AND CONDITIONS

| | $CH_4$ | $CO_2$ | $N_2$ | Air |
|---|---|---|---|---|
| composition | 0.0912 | 0.0344 | 0.0056 | 0.8688 |

$T_i$ = 297.15 K $P_i$ = 1 atm = 101.325 kPa Equivalence ratio =1.00

Reactant properties (Stanjan): M= 28.197 kg/kmol

V= 8.6472e-1 $m^3$/kg U= -8.1093e5 J/kg

H= -7.2331e5 J/kg S= 7.1493e3 J/kg-K

Molar mass of reactants (Multizone): M= 28.1988 kg/kmol

### 1. Adiabatic Flame Temperature at Constant Volume Combustion

Multizone model: subroutine "Flame" evaluated the flame temperature at constant volume.

Stanjan: *Products*, and *Option 12, V and U same as last run.*

| | Stanjan | Multizone | error |
|---|---|---|---|
| $T_{flame}$ | 2497K | 2462 K | 1.39% |

### 2. Unburnt Gas Temperature

Mutizone: an arbitrary pressure $P_1$ = 1.0217 atm = 103.5264 kPa

Stanjan: *Products*, gas compositions $CH_4$, $O_2$, and $N_2$, *Option 17, one of above at specified composition*, the same compositions with reactants, and *Option 6 specified P and S*, $P = P_1$, $S=S_{reactant}$ (isentropic compression).

| | Stanjan | Multizone | error |
|---|---|---|---|
| $T_u$ | 298.7 K | 298.5 K | 0.064% |

**3. Burnt Gas Temperature**

Multizone: an arbitrary pressure $P_1$ = 1.0217 atm

Stanjan: *Products, Option 5, specified P and H*, P= $P_1$, and H=Hreactant

| | Stanjan | Multizone | error |
|---|---|---|---|
| T | 2147 K | 2168 K | 0.98% |

## C.3 CONCLUSION

It is clear that Multi-zone model calculates the correct molar mass of reactants. Furthermore, the molar mass of reactants in the model is related to equivalence ratio, so it proves that the equivalence ratio calculated in model is correct too. The difference of unburnt mixture temperature between the model and Stanjan is slight, less than 1%. Multi-zone model only considers two dissociation reactions in combustion process, i.e.; carbon dioxide dissociation and water-gas reaction. Therefore, six gas species are represented as products, viz. $CO_2$, CO, $N_2$, $H_2$, $O_2$, and $H_2O$. In contrast, all gas species are considered as products in Stanjan. Even though the species of products are different, the error of adiabatic flame temperatures at constant volume is less than 1.5%, and the maximum error of burnt mixture temperatures is 2.5%. In summary, the multi-zone model is reliable and accurate.

* Except special noted, all gas species in Jannaf file are chosen for products.

## REFERENCES:


1. Modien, R.M., *The effects of enhanced ignition systems and turbulence on flame development*, in *Department of Mechanical Engineering,.*. 1991, University of Alberta.: Edmonton.

2. Ting, D.S.-K. and M.D. Checkel, *The effects of turbulence on spark-ignited, ultra lean, premixed methane-air flame growth in a combustion chamber.* Society of Automotive Engineers, SAE paper, 1995. **952410**.

3. Reynolds, W.C., *The element potentials method for chemical equilibrium analysis: implementation in the interactive program STANJAN.* 1986, Department of Mechanical Engineering, Stanford University.

# APPENDIX D
# ERROR ANALYSIS

The measured burning velocities of methane/air and methane/40% EGR/53% reformer gas mixtures at 5 atm are in reasonable agreement at most temperature range except 473 K as compared with other results. The burning velocity at 473 K is surprisingly high (see figure 4-14 and 4-21 for comparison). The reasons have been thoroughly investigated. The experiments on above two mixtures were repeated a few times to check the reproducibility. The standard deviation of the data at 473 K is as high as 2.08 cm/s, but the standard deviation of mean is only 0.69 cm/s as considering a large number of data. Since each experimental series was carried out by the same experimental method and mixtures except various initial temperature, it is unreasonable to question the sudden "burning velocity jump" at 473 K to the experimental method or mixtures. Hence, experimental method and mixtures are undoubtable at the 473 K. On the other hand, a certain percent of reformer gas retains the burning velocity at the full range of initial temperatures at 1 atm. In other words, the percent of reformer gas is temperature independent. The burning velocities of methane/air mixtures and methane/40% EGR/53% reformer gas mixtures agree well at full range of temperature between 298 K to 473 K. It indicates that unacceptably high burning velocity at 473 K is not caused by the properties of gas mixtures. Therefore, the focus was switched to the experimental instrument. Eventually, the problem was linked to the Omega PX800-2KSV pressure transducer used at the elevated pressure and temperature. It was found that the temperature of the pressure transducer was over the operating temperature range as the combustion chamber was heated to 473 K. Evidently, the pressure transducer did not have an accurate measurement after a long time over-range explosion (about 5~8 minutes from mixture filling to stabilization).

In order to correct the "too high" burning velocity at 473 K, two pressure calibrations were carried out in order to find the temperature compensation. The sensitivity drift [1] which reflects the temperature effect on a pressure transducer was determined by two calibration tests. In one test a series of pressures was recorded as the evacuated combustion chamber was heated up to 473 K. In the other test another series of pressures was recorded as the combustion chamber at room atmospheric pressure was heated up to 473 K again. Therefore, a pressure calibration at a certain temperature was able to be evaluated by the equation D-1.

$$sensitivity\ drift = \frac{dP_{eva} - dP_{atm}}{dV_{eva} - dV_{atm}} \qquad \text{(D-1)}$$

where,

P is pressure in Pascal;

V is voltage in V;

*eva* is evacuated condition and *atm* is atmospheric condition.

The sensitivity drift at various temperature was then determined by the pressure calibrations from the above equation. It decreased slightly with elevated temperature. The new sensitivity drift at 473 K was applied to the measured pressure trace and burning velocity. Unfortunately, the burning velocity was only slightly changed by the new sensitivity (typically 1 cm/s difference) and unable to return to the reasonable range. Hence, the unacceptable data of burning velocities at 473 K and 5 atm were ignored in later analysis.

## REFERENCE:

1. Doebelin, E.O., *Measurement Systems: Application and Design*. 3rd ed. 1983.

# APPENDIX E
# BURNING VELOCITY

All measured burning velocity data in this study are displayed from the table E-1 to E-5. Table E-1 shows the burning velocities of methane/EGR mixtures at elevated pressure and 298 K. Table E-2 shows the burning velocities of methane/EGR mixtures at 1 atm. Table E-3 shows the burning velocities of methane/EGR/reformer gas mixtures at 1 atm. Table E-4 gives the burning velocities at 5 atm and from 298 K to 423 K. Table E-5 gives the inaccurate burning velocity at 5 atm and 473 K.

**NOMENCLATURE:**

$T_i$: initial temperature

RG: reformer gas

**Table E-1** Burning velocity of methane/EGR mixtures at elevated pressure and 298 K

| EGR % | No. | Initial Pressure (atm) | | | |
|---|---|---|---|---|---|
| | | 2 | 3 | 4 | 5 |
| 0 | 1 | 28.7 | 24.8 | 20.0 | 18.9 |
| | 2 | 29.0 | 24.8 | 21.9 | 18.8 |
| | 3 | 28.2 | 25.6 | 20.7 | 19.5 |
| | 4 | 29.1 | 25.4 | 22.0 | 19.9 |
| | 5 | - | - | 22.3 | 19.2 |
| 15 | 1 | 14.2 | 11.6 | 9.3 | 8.7 |
| | 2 | 14.2 | 11.2 | 9.8 | 8.7 |
| | 3 | 14.7 | 11.2 | 9.7 | 8.5 |
| | 4 | 14.0 | 11.1 | - | - |

**Table E-2** Burning velocity of methane/EGR mixtures at 1 atm

| $T_i$ K | No. | EGR % | | | | |
|---|---|---|---|---|---|---|
| | | 0 | 5 | 10 | 15 | 20 |
| 298 | 1 | 35.4 | 28.2 | 21.7 | 16.3 | 12.7 |
| | 2 | 34.7 | 28 | 21.8 | 16.9 | 12.7 |
| | 3 | 35.8 | 26.8 | 23 | 16.5 | 13.5 |
| 373 | 1 | 50 | 43.5 | 34.8 | 25 | 19.7 |
| | 2 | 50.1 | 43.5 | 34.2 | 25.7 | 21.3 |
| | 3 | 53.55 | 42.5 | 33.4 | 25.4 | 19.4 |
| | 4 | 54.3 | - | - | - | - |
| 423 | 1 | 64.6 | 57.5 | 43.5 | 34.3 | 26.7 |
| | 2 | 63 | 57.4 | 43.5 | 31.1 | 24.6 |
| | 3 | 64.3 | 57.7 | 42.5 | 32.8 | 25.8 |
| | 4 | 62.3 | - | - | - | - |
| 473 | 1 | 76.9 | 70.2 | 56.0 | 42.6 | 34.2 |
| | 2 | 76.8 | 72.0 | 56.2 | 41.1 | 34.5 |
| | 3 | 74.8 | 67.2 | 57.3 | 44.0 | 33.4 |
| | 4 | 75.6 | - | - | - | 33.4 |
| | 5 | 79.9 | - | - | - | 37.4 |

**Table E-3** Burning velocity of methane/EGR/RG mixtures at 1 atm

| $T_i$ K | No. | EGR+RG % | | | |
|---|---|---|---|---|---|
| | | 5+11 | 10+19 | 15+28 | 20+34 |
| 298 | 1 | 34.9 | 34.4 | 34.8 | 35.0 |
| | 2 | 35.6 | 35.7 | 34.5 | 35.1 |
| | 3 | 35.3 | 35.3 | 36.5 | 34.9 |
| 373 | 1 | 53.8 | 52.3 | 53.1 | 52.6 |
| | 2 | 51.4 | 52.5 | 52.0 | 51.9 |
| | 3 | 53.2 | 49.5 | 54.2 | 54.1 |
| 423 | 1 | 63 | 67.1 | 66.2 | 64.1 |
| | 2 | 66.1 | 64.2 | 66.3 | 65.2 |
| | 3 | 63.6 | 63.1 | 70.5 | 65.3 |
| 473 | 1 | 76.9 | 76.2 | 86.3 | 80.7 |
| | 2 | 77.9 | 77.5 | 78.7 | 75.8 |
| | 3 | 77.9 | 75.6 | 77.8 | 83.2 |
| | 4 | 74.3 | - | 80.0 | 80.8 |
| | 5 | - | - | 77.1 | 79.9 |
| | 6 | - | - | 77.8 | 77.9 |

**Table E-4** Burning velocity at 5 atm

| $T_i$ K | No. | EGR+RG % | |
|---|---|---|---|
| | | $0+0^{(1)}$ | $40+53^{(2)}$ |
| 298 | 1 | 18.9 | 17.7 |
| | 2 | 18.8 | 18.9 |
| | 3 | 19.5 | 18.8 |
| | 4 | 19.9 | 20.3 |
| | 5 | 19.2 | 20.4 |
| 373 | 1 | 29.7 | 31.9 |
| | 2 | 32.0 | 33.6 |
| | 3 | 29.4 | 33.5 |
| | 4 | - | 34.4 |
| | 5 | - | 34.3 |
| 423 | 1 | 38.5 | 42.6 |
| | 2 | 41.3 | 41.6 |
| | 3 | 41.9 | 42.3 |
| | 4 | 41.8 | 40.2 |
| | 5 | - | 42.7 |

**Table E-5** Inaccurate burning velocity at 5 atm and 473 K

| No. | EGR+RG % | |
|---|---|---|
| | 0+0[1] | 40+53[2] |
| 1 | 64.5 | 64.7 |
| 2 | 63.5 | 61 |
| 3 | 65.2 | 60.6 |
| 4 | 62.9 | 60.2 |
| 5 | 61.7 | 65.8 |
| 6 | 62.6 | 61.7 |
| 7 | 59.6 | 62.3 |

Note: data in table E-5 were not included in analysis of this study.

1. Stoichiometric methane/air mixture
2. Methane/40% EGR/53% reformer gas mixture

# APPENDIX F
# NITRIC OXIDE FORMATION

In order to theoretically analyze the effects of EGR and reformer gas on NO formation of methane/air mixtures, Stanjan was run as a constant-volume combustion with all dissociation reactions at experimental initial temperature, pressure and compositions. The flame temperature, peak combustion pressure and equilibrium concentration of each compositions were obtained. The equilibrium NO concentration and formation rate of NO were evaluated from the equilibrium condition assumption and extended Zeldovich mechanism. Table F-1 to F-4 display the flame temperature, peak combustion pressure, NO equilibrium concentration and NO formation rate of methane/EGR mixtures at 1 atm. Table F-5 to F-8 give the flame temperature, peak combustion pressure, NO equilibrium concentration and NO formation rate of methane/EGR/RG mixtures at 1 atm. Table F-9 to F-12 display the flame temperature, peak combustion pressure, NO equilibrium concentration and NO formation rate at 5 atm. RG is referred as reformer gas in this appendix.

**Table F-1** Flame temperature (K) of methane/EGR mixtures at 1 atm

| EGR % | initial temperature | | | |
|---|---|---|---|---|
| | 298 K | 373 K | 423 K | 473 K |
| 0 | 2586 | 2604 | 2616 | 2628 |
| 5 | 2519 | 2539 | 2553 | 2567 |
| 10 | 2446 | 2470 | 2486 | 2502 |
| 15 | 2369 | 2396 | 2414 | 2432 |
| 20 | 2288 | 2319 | 2339 | 2359 |

**Table F-2** Peak combustion pressure (kPa) of methane/EGR mixtures at 1 atm

| EGR % | initial temperature | | | |
|---|---|---|---|---|
| | 298 K | 373 K | 423 K | 473 K |
| 0 | 892 | 719 | 638 | 574 |
| 5 | 866 | 699 | 620 | 559 |
| 10 | 840 | 678 | 603 | 543 |
| 15 | 811 | 656 | 584 | 526 |
| 20 | 782 | 634 | 564 | 509 |

**Table F-3** NO equilibrium concentration (ppm) of methane/EGR mixtures at 1 atm

| EGR % | initial temperature | | | |
|---|---|---|---|---|
| | 298 K | 373 K | 423 K | 473 K |
| 0 | 4892 | 5330 | 5623 | 5919 |
| 5 | 4037 | 4461 | 4746 | 5036 |
| 10 | 3225 | 3625 | 3898 | 4178 |
| 15 | 2538 | 2902 | 3155 | 3416 |
| 20 | 1845 | 2169 | 2397 | 2636 |

**Table F-4** NO formation rate (ppm/sec) of methane/EGR mixtures at 1 atm

| EGR % | initial temperature | | | |
|---|---|---|---|---|
| | 298 K | 373 K | 423 K | 473 K |
| 0 | 2.36e6 | 2.66e6 | 2.91e6 | 3.21e6 |
| 5 | 1.08e6 | 1.28e6 | 1.44e6 | 1.63e6 |
| 10 | 4.43e5 | 5.56e5 | 6.5e5 | 7.63e5 |
| 15 | 1.62e5 | 2.18e5 | 2.66e5 | 3.24e5 |
| 20 | 5.06e4 | 7.41e4 | 9.52e4 | 1.22e5 |

**Table F-5** Flame temperature (K) of methane/EGR/RG mixtures at 1 atm

| EGR+RG % | initial temperature | | | |
|---|---|---|---|---|
| | 298 K | 373 K | 423 K | 473 K |
| 5+11 | 2532 | 2551 | 2565 | 2579 |
| 10+19 | 2470 | 2493 | 2508 | 2523 |
| 15+28 | 2405 | 2431 | 2448 | 2465 |
| 20+34 | 2331 | 2361 | 2380 | 2399 |

**Table F-6** Peak combustion pressure (kPa) of methane/EGR/RG mixtures at 1 atm

| EGR+RG % | initial temperature | | | |
|---|---|---|---|---|
| | 298 K | 373 K | 423 K | 473 K |
| 5+11 | 857 | 691 | 614 | 552 |
| 10+19 | 825 | 666 | 591 | 533 |
| 15+28 | 790 | 639 | 568 | 512 |
| 20+34 | 758 | 614 | 546 | 493 |

**Table F-7** NO equilibrium concentration (ppm) of methane/EGR/RG mixtures at 1 atm

| EGR+RG % | initial temperature | | | |
|---|---|---|---|---|
| | 298 K | 373 K | 423 K | 473 K |
| 5+11 | 4257 | 4685 | 4973 | 5265 |
| 10+19 | 3553 | 3965 | 4245 | 4529 |
| 15+28 | 2882 | 3271 | 3537 | 3811 |
| 20+34 | 2231 | 2586 | 2833 | 3088 |

**Table F-8** NO formation rate (ppm/sec) of methane/EGR/RG mixtures at 1 atm

| EGR+RG % | initial temperature | | | |
|---|---|---|---|---|
| | 298 K | 373 K | 423 K | 473 K |
| 5+11 | 1.26e6 | 1.48e6 | 1.66e6 | 1.87e6 |
| 10+19 | 5.97e5 | 7.35e5 | 8.5e5 | 9.85e5 |
| 15+28 | 2.57e5 | 3.36e5 | 4.03e5 | 4.83e5 |
| 20+34 | 9.37e4 | 1.32e5 | 1.65e5 | 2.05e5 |

**Table F-9** Flame temperature (K) of methane/EGR mixtures at 5 atm

| EGR+RG % | initial temperature | | | |
|---|---|---|---|---|
| | 298 K | 373 K | 423 K | 473 K |
| 0+0 (1) | 2648 | 2671 | 2687 | 2703 |
| 40+0 (2) | 1904 | 1952 | 1984 | 2016 |
| 40+53 | 1970 | 2018 | 2050 | 2082 |

**Table F-10** Peak combustion pressure (kPa) of methane/EGR mixtures at 5 atm

| EGR+RG % | initial temperature | | | |
|---|---|---|---|---|
| | 298 K | 373 K | 423 K | 473 K |
| 0+0 (1) | 4550 | 3672 | 3260 | 2936 |
| 40+0 (2) | 3240 | 2653 | 2387 | 2162 |
| 40+53 | 3089 | 2529 | 2266 | 2059 |

**Table F-11** NO equilibrium concentration (ppm) of methane/EGR mixtures at 5 atm

| EGR+RG % | initial temperature | | | |
|---|---|---|---|---|
| | 298 K | 373 K | 423 K | 473 K |
| 0+0 [1] | 4483 | 4968 | 5295 | 5628 |
| 40+0 [2] | 184 | 271 | 341 | 423 |
| 40+53 [3] | 352 | 471 | 565 | 672 |

**Table F-12** NO formation rate (ppm/sec) of methane/EGR mixtures at 5 atm

| EGR+RG % | initial temperature | | | |
|---|---|---|---|---|
| | 298 K | 373 K | 423 K | 473 K |
| 0+0 [1] | 8.09e6 | 9.64e6 | 1.09e7 | 1.24e7 |
| 40+0 [2] | 75 | 206 | 389 | 718 |
| 40+53 | 367 | 877 | 1535 | 2644 |

1. Stoichiometric methane/air mixture
2. Methane /40% EGR mixture
3. Methane/40% EGR/53% reformer gas mixture